ON DESIGN CONCEPT FOR FULL-DUPLEX BASED FLEXIBLE RADIO TRANSCEIVERS

Zhaowu Zhan

Number of Order 2014-ISAL-0102 Year 2014

THESIS

ON DESIGN CONCEPT FOR FULL-DUPLEX BASED FLEXIBLE RADIO TRANSCEIVERS

defended at

L'INSTITUT NATIONAL DES SCIENCES APPLIQUÉES DE LYON

for the degree of

Doctor of Philosophy

École Doctorale : ÉLECTRONIQUE, ÉLECTROTECHNIQUE ET AUTOMATIQUE

Spécialité : STIC SANTÉ

By

Zhaowu ZHAN

Defense on 16 December 2014

THESIS COMMITTEE

Andreas BURG	EPFL, Ass. Professor	Reviewer
Ioannis KRIKIDIS	University of Cyprus, Ass. Professor	Reviewer
Jean-François DIOURIS	Polytech Nantes, Professeur	Reviewer
Patrick ROSSON	Ingénieur R&D, CEA-Leti Grenoble	Examiner
Jean-Marie GORCE	INSA de Lyon, Professeur	Examiner
Guillaume VILLEMAUD	INSA de Lyon, Maître de Conférences, HDR	Director

This thesis was prepared at CITI Laboratory,
INSA de Lyon - INRIA Rhône-Alpes
Lyon - France - 2014

Abstract

The wireless medium is a shared and limited resource. Current wireless standards always share the medium with Half-Duplex principle: the transmission and reception of signals are done in two separate time slots or two different frequency bands. Besides, the transceiver can only transmit and receive one signal at a time.

This dissertation takes an alternate approach: Instead of sharing the medium with Half-Duplex principle, the entire licensed frequency band is shared for simultaneous transmission and reception, which we call Full-Duplex. Besides, the design concept for a wideband flexible radio transceiver can process two different types of signals at a time.

To reach this goal, we propose to use an active analog radio frequency (RF) self-interference cancellation (AARFSIC) method or a combination scheme of the AARFSIC and active digital self-interference cancellation in time domain (ADSICT) to cancel the strong self-interference (SI) induced by the Full-Duplex principle. Based on the Full-Duplex radio, we propose a flexible Full-Duplex Dual-Band (FDDB) OFDM radio transceiver by combining the Dual-Band RF front-end.

Building on these, we make three main contributions: We present an active self-interference cancellation (ASIC) scheme, which can cancel both the strong one-path and multi-path SI completely, based on the combination of the AARFSIC and DSICT. Next, we introduce the design and evaluation of a Full-Duplex OFDM radio, including analysis and qualification of the impact of the thermal noise and phase noise on the system performance. Finally, we develop an FDDB OFDM radio that can work on two separate spectrum fragments. In order to eliminate the impact of the I/Q imbalance on the FDDB radio, a simple but practical digital I/Q imbalance estimation and compensation method is presented. The system level simulation conducted with ADS and Matlab software shows that this method can efficiently compensate both high and low I/Q imbalance.

Key-words : Full-Duplex, Self-interference cancellation, OFDM, Full-Duplex Dual-Band, Flexible radio transceiver, I/Q imbalance.

Résumé

Le medium sans fil est une ressource partagée et limitée. Les normes sans fil actuelles partagent toujours le principe de partage du medium Half-Duplex: la transmission et la réception de signaux sont effectuées dans deux intervalles de temps distincts ou deux bandes de fréquences différentes. En outre, l'émetteur-récepteur ne peut émettre et recevoir qu'un signal à la fois.

Cette thèse suit une autre approche: au lieu de partager le support avec le principe de Half-Duplex, toute la bande de fréquence autorisée est partagé pour la transmission et la réception simultanée, approche qui est appelée Full-Duplex. Dès lors, on peut concevoir une architecture d'un émetteur-récepteur radio flexible à large bande pour traiter deux types de signaux différents à la fois.

Pour approcher cet objectif, nous utilisons une méthode de suppression active analogique de l'auto-interférence (AARFSIC) et l'annulation active numérique d'auto-interférence dans le domaine temporel (ADSICT) pour annuler la forte auto-interférence (SI) induite par le principe Full-Duplex. Basé sur la radio Full-Duplex, nous proposons un système flexible Dual-Band (FDDB) émetteur-récepteur radio OFDM Full-Duplex en la combinant avec un front-end RF double bande.

S'appuyant sur ces principes, nous exposons trois contributions principales: Nous présentons une technique d'annulation analogique de l'auto-interférence (ASIC), qui peut annuler complètement l'auto-interférence à trajet direct ou multi-trajets, basée sur la combinaison des méthodes AARFSIC et DSICT. Ensuite, nous présentons la conception et l'évaluation d'une radio OFDM Full-Duplex, y compris l'analyse et la qualification de l'impact du bruit thermique et du bruit de phase sur les performances du système. Enfin, nous développons une radio dual-bande FDDB OFDM qui peut fonctionner sur deux fragments de spectre séparés. Afin d'éliminer l'impact du déséquilibre I/Q sur la radio FDDB, une méthode d'estimation des déséquilibres I/Q et de compensation, simple mais efficace, est présentée. La simulation au niveau système menée avec ADS et Matlab montre que cette méthode peut effectivement compenser des déséquilibres I/Q aussi bien élevés que faibles.

Mots-clés : Full-Duplex, annulation auto-interférence, OFDM, Full-Duplex Dual-Bande, émetteur-récepteur radio flexible, dśquilibre I/Q.

To my beloved parents and sister.

To my beloved wife.

Acknowledgements

The research work for this PhD dissertation was carried out during the years 2011-2014 at the CITI Research Laboratory (INSA Lyon - INRIA), Lyon. This place has provided me good conditions and great atmospheres for scientific research. Moreover, the UT-INSA project financially supported by the China Scholarship Council (CSC) gives me this opportunity to study in INSA Lyon, France.

Furthermore, I would like to express my sincerely appreciates to many peoples. First of all, I would like to thank Dr. Guillaume Villemaud. My experience was enriched tremendously by having him as my advisor. From my first year at the CITI Lab, despite my unfamiliarity with scientific research and pool oral english, he always discussed with me with great patience. He teaches me how to do research, gives me valuable advice and provides me encouragement and support, which led to the valuable results of this dissertation.

I am very grateful to Prof. Jean-Marie Gorce, who is my dissertation director in the first two and half years. Although we had very limited several talks, his passions on the scientific research greatly impressed me. Besides, he gave me some excellent valuable advices on my future professional career.

In addition, I would like to thank Prof. Andrea Burg, Prof. Ioannis Krikidis and Prof. Jean-François Diouris for making effort to read and review this dissertation, as well as thank Patrick Rosson and Prof. Jean-Marie Gorce for accepting to examining this dissertation.

Finally, I would like to take this opportunity to thank my dear friends and colleagues for their kindness and help all these years.

Lyon, Oct. 21. 2014

Zhaowu Zhan

Contents

List of Tables

List of Figures

Acronyms

List of Acronyms

AABBSIC	Active Analog BaseBand Self-Interference Cancellation.
AARFSIC	Active Analog Radio Frequency Self-Interference Cancellation.
ADSIC	Active Digital Self-Interference Cancellation.
ASIC	Active Self-Interference Cancellation.
AWGN	Additive White Gaussian Noise.
BER	Bit Error Rate.
CSI	Channel State Information.
DFT	Discrete Fourier Transform.
DRR	Direct-path to Reflect-path Ratio.
DSIC	Digital Self-Interference Cancellation.
DSICF	Digital Self-Interference Cancellation in Frequency domain.
DSICT	Digital Self-Interference Cancellation in Time domain.
FDDB	Full-Duplex Dual-Band.
GI	Guard Interval.
IDFT	Inverse Discrete Fourier Transform.
INR	self-Interference-to-Noise Ratio.
LoS	Line-of-Sight.
LNA	Low Noise Amplifier.
LS	Least Square.
MIMO	Multiple-Input Multiple-Output.
MSE	Mean Square Error.
NLoS	Non-Line-of-Sight.
NMSE	Normalized Mean Square Error.
OFDM	Orthogonal Frequency Division Multiplexing.
PA	Power Amplifier.
PSIS	Passive Self-Interference Suppression.
SI	Self-Interference.
SIC	Self-Interference Cancellation.

1 Introduction

The radio transceiver is concerned with the transmission and reception of the digital data symbols across the wireless channel via an RF front-end. Therefore, the radio transceiver design should include the baseband system design and RF front-end design. For the flexible radio transceiver design, the radio front-end should be capable of processing different RF signals and the baseband system should have the abilities to separate and recover different data symbols belong to different demands.

1.1 Flexible Radio Transceivers

1.1.1 Overview

It has been more than one century sine the invention of the wireless radio transmission using electromagnetic wave. In 1893, Nikolai Tesla demonstrated the wireless radio communications in St. Louis, which implied the beginning of the radio development. From the first telegraph to the first wireline telephone and to the first wireless telephone, and even to the modern digital cellular mobile phones, the way of information transmissions and radio applications have been experiencing great changes. The wireless radios enable the information to be transfered far and wide. Wireless radio terminals are increasingly pervasive in our everyday life. Initial wireless systems

were designed and developed to support only voice signal. However, current and future wireless systems will more focus on the high data rate transmissions due to the extensive deployment of multimedia applications and looking forward to the internet by people. Therefore, current and future wireless networks need to be designed and developed not only to support voice but also to support the data and multimedia applications.

There are several broadband wireless standards currently, such as the third generation (3G), the fourth generation (4G) and wireless fidelity (WiFi) and so on, which support relative high throughput compared to the first generation analog wireless communication and the second generation (2G). However, all these technologies, even the latest 4G, can not meet the requirement of the high data rate to be faced in the future. Besides, one radio terminal should accommodate different wireless technologies to be compatible with different wireless standards. Therefore, the designs of radio transceivers are challenged by the high flexibility and reconfigurability constraints.

1.1.2 Cognitive Radios

In 1998, Joseph Mitola III proposed the concept of cognitive radio which was defined as an intelligent radio system [82]. Cognitive radios are required to have the both abilities to sense the surrounding spectral environment and flexibly adapt its transceiver parameters to optimize the radio link. However, finding a suitable radio front-end to realize a flexible wideband and agile radio transceiver is always a big challenge. Cognitive radio requires a novel radio frequency (RF) transceiver architecture to provide cognitive capability and reconfigurability [9]. A cognitive radio transceiver is composed of two main components: RF front-end and baseband processing system. In the RF front-end, the received signal is amplified, mixed and analog-to-digital converted (ADC). While in the baseband, the signal is modulated or demodulated. Each component should be reconfigured via control bus to adapt to the time-varying radio environment as shown in Fig. 1.1.

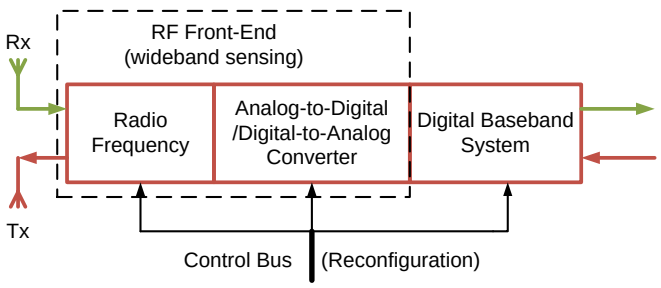

Figure 1.1: Block diagram of a general cognitive radio transceiver.

The cognitive radio transceiver should be equipped with a wideband RF front-end that is capable of sensing simultaneously over a wide frequency range. This capability is mainly related to the RF hardware, such as wideband antenna, power amplifier and adaptive filter [9]. A cognitive radio transceiver will receive signals from various radio terminals operating on different spectrum channels and at different power levels. Therefore, the RF front-end of a cognitive radio should have the capability of detecting a weak signal in a large dynamic range of frequency bands. This is a big challenge behind the design of the cognitive radio transceivers [29].

1.1.3 Multimode Radios

Various services demand a mobile terminal to support different wireless communication standards, so the integrated multi-standard wireless devices is required. In current wireless systems equipped with multi-standard functionality, the transceivers are mostly implemented by using separate RF front-end for each individual standard and sharing partially the analog baseband circuitry with the aid of a number of additional switchers. Although this approach could enable a radio terminal to accommodate various wireless standards, the increase in the hardware required to implement such a multi-standard radio transceiver increases the circuitry area, the cost as well as may increase the power consumption compared to the conventional single-standard radio transceiver implementation [53].

A radio which is multimode/multiband should work in multiple bands with few or no modifications. The block diagram of a multimode receiver [53] with an adaptive RF front-end, adaptive analog baseband circuitry and adaptive digital signal processing is illustrated in Fig. 1.2.

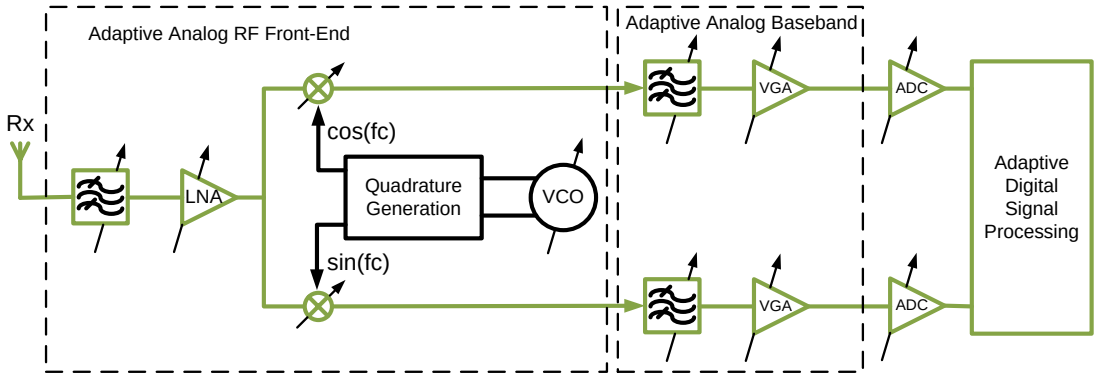

Figure 1.2: Block diagram of an adaptive multimode receiver.

Although this kind of multimode radio receiver can accommodate various wireless standards, it just can process one signal at a time.

1.1.4 Full-Duplex Radios

Full-Duplex is defined as a radio which can simultaneously transmit and receive signals over the same frequency band. Such a capability can be exploited to offer high efficiency of spectrum utilization, more efficient relaying, as well as more flexible medium access. Hence, Full-Duplex radio could show great potentialities for the future flexible radio transceiver design. Half-Duplex (i.e. FDD and TDD) is not only inefficient in the radio resource utilization but also in medium access. FDD, requiring paired-spectrum for uplink and downlink transmission, can not realize the flexible spectrum access. TDD, requiring different time slots for uplink and downlink connection, is inefficient in real time communications. While in the Full-Duplex mode meaning that one spectrum fragment can be used for both transmission and reception at a time, both of the demands of high efficiency of radio resource utilization and flexible access to medium can be met.

Besides, spectrum fragmentation will be compounded in the future 5G wireless network driven by the scarcity of spectrum [47], which can be enhanced by the Full-Duplex technique.

1.2 Context and Motivation

The physical layer is concerned with the transmission and the reception of digital information over the wireless channel via an RF front-end. Therefore, a general wireless communication system consists of a transmitter, a wireless channel and a receiver. The transmitter includes digital baseband system and transmitter RF front-end. The receiver includes receiver RF front-end and the correspondent digital baseband receiver system. Therefore, a general wireless system can be described as Fig. 1.3

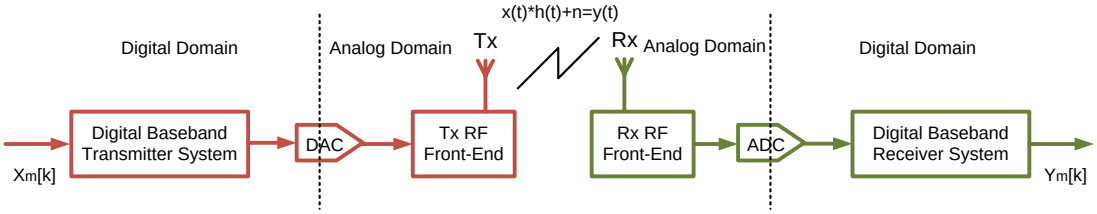

Figure 1.3: Block diagram of a general wireless communication system.

1.2.1 Digital Baseband Communications

The wireless revolution has resulted in ever increasing demands on high data rate over limited wireless spectrum, putting much more requirement of higher spectral

efficiency on the wireless systems. Therefore, the telecommunication engineers are always exploring the advanced physical layer techniques to approach this goal.

Multicarrier System

Orthogonal Frequency Division Multiplexing (OFDM) utilizes a large number of parallel and orthogonal narrow-band sub-carriers instead of a single wide-band carrier to transmit and receive informations. In details, OFDM divides a wideband frequency selective fading channel into an set of equivalent parallel narrowband frequency flat fading sub-channels. This division is achieved by splitting the input high-data stream into a number of substreams that are transmitted in parallel over the orthogonal sub-carriers. The sub-carriers are designed in order to have a minimum frequency space to maintain the orthogonality between different sub-channels and the adjacent signal spectra corresponding to different sub-carriers overlap with each other in frequency. Therefore, the available bandwidth is used more efficiently compared to a traditional single carrier system.

The basic diagram of a baseband OFDM transmitter is as shown in Fig. 1.4.

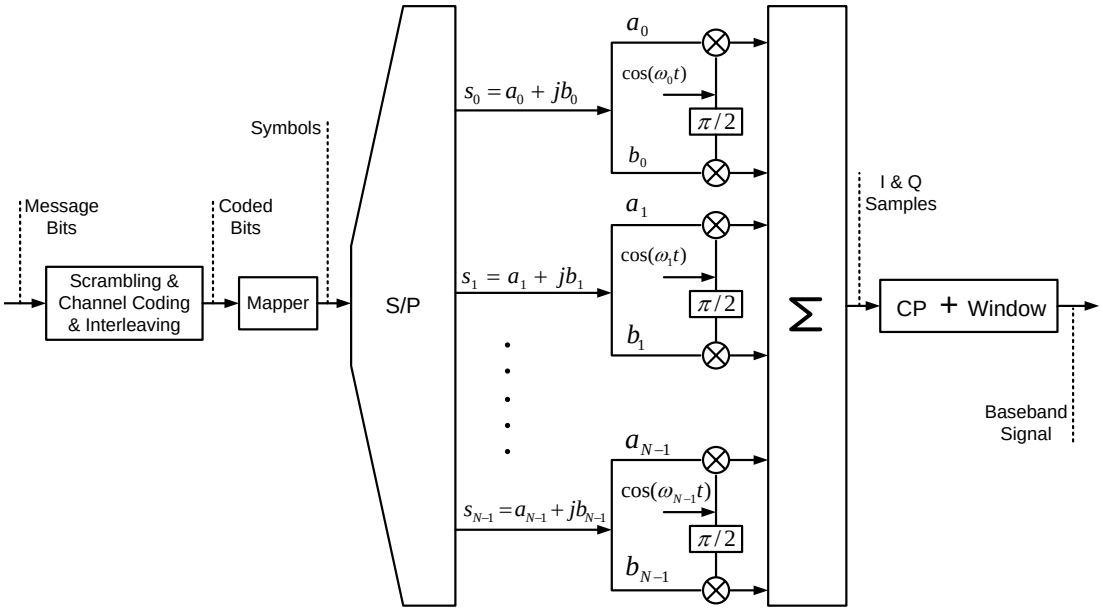

Figure 1.4: Basic diagram of an OFDM baseband transmitter.

At the transmitter, a message is first scrambled via multiplying it with a pseudo-random bit sequence in order to eliminate the unwanted regularity in the message that may confuse some PHY algorithm. Then, some form of forward error correction (FEC) is added to the scrambled message to protect against the channel-induced distortion. In order to make the FEC work more effectively, the transmitter optionally interleaves

the coded bits so that the adjacent coded bits will temporally non-adjacent to against the deep channel fading. Next, the transmitter uses the modulator or mapper to take groups of coded bits and maps them into complex baseband symbols for transmission by the RF front-end. The complex symbol $X[k] = a_k + \jmath b_k$ produced by the modulator will be converted into time-domain samples by using the Inverse Discrete Fourier Transform (IDFT), because the transmission hardwares operate only on time samples. The output of the IDFT are complex time-domain samples with real (I) and imaginary (Q) components. The I and Q components represent the two orthogonal dimensions along which informations could be transmitted via using electromagnetic waves.

Let $\{X[0], X[1], ..., X[N-1]\}$ be a block of N data symbols after the serial-to-parallel conversion. The k^{th} data symbol will be carried by the k^{th} sub-carrier. Then, the baseband time domain complex samples $x(n)$ can be obtained by IDFT of the symbol block as

$$\begin{aligned} x(n) &= \frac{1}{N}\sum_{k=0}^{N-1} X[k]e^{\jmath\omega_k n} \\ &\overset{\omega_k=\frac{2\pi k}{N}}{=} \frac{1}{N}\sum_{k=0}^{N-1} X[k]e^{\jmath\frac{2\pi kn}{N}}, n = 0, 1, ..., N-1, \end{aligned} \tag{1.1}$$

where the imaginary unit $\jmath = \sqrt{-1}$ and $\omega_k = \frac{2\pi k}{N}$.

After that, a guard interval (GI) is introduced to preserve the orthogonality of the sub-carriers and the independence of the adjacent OFDM symbols when the OFDM signal experiences a multi-path time-dispersive radio channel. The guard interval, usually using a cyclic prefix (CP), is the copy of the last part of the OFDM symbol. The duration of the GI, T_{guard} is chosen larger than the maximum excess delay of the multi-path radio channel. Because of the CP, the linear convolution of the transmitted symbols with the wireless channel is transformed to a circular convolution. Windowing is a well-known technique to reduce the power level of the side-lobes and thereby reduce the signal power out of band. In an OFDM system, the applied window must not influence the signal during its effective period [84].

These baseband I and Q samples obtained from above are then up-converted to the desired transmission frequency signal and transmitted over the air as analog waves by the RF front-end. The to be transmitted RF signal over the air could be expressed as

$$x_{RF}(t) = x(t)e^{\jmath 2\pi f_c t} \tag{1.2}$$

where $x(t)$ denotes the continuous baseband time-domain signal, f_c denotes the desired center carrier frequency. Over the multi-path fading channel $h(t)$, the received

RF signal can be expressed as

$$y_{RF}(t) = x(t)e^{j2\pi f_c t} * h(t) + w_{RF}(t) \tag{1.3}$$

where $w_{RF}(t)$ denotes the receiver thermal noise in the RF analog domain.

The basic block diagram of a baseband OFDM receiver is as shown in Fig. 1.5.

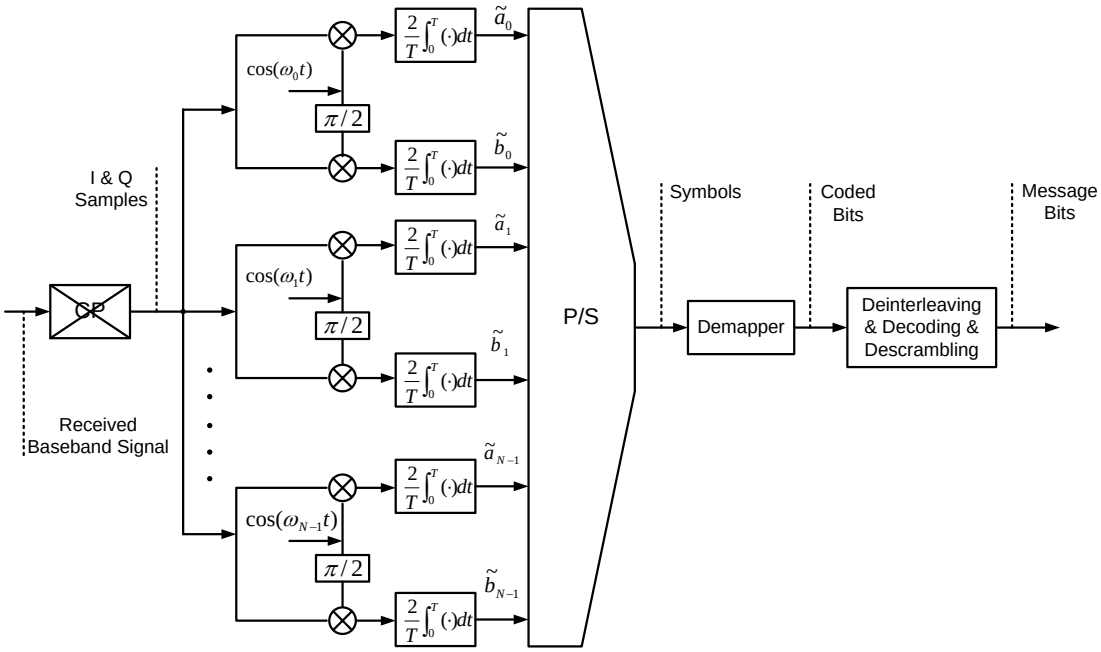

Figure 1.5: Basic block diagram of an OFDM baseband receiver.

At the receiver side, the RF signals received by the receive antenna is first down-converted to baseband continuous time-domain signal. Then, this continuous time-domain signal will be digitized via analog-to-digital converter (ADC). The obtained discrete time-domain signal will be further processed by the OFDM baseband receiver.

If the transceiver RF front-ends are assumed ideal, the received baseband equivalent signal $y(t)$ could be expressed as

$$y(t) = x(t) * h(t) + w(t) \tag{1.4}$$

where $w(t)$ denotes the receiver thermal noise in the continuous time domain. The demodulation of the OFDM signal should be performed by a bank of filters which are "matched" to the effective part of the OFDM symbol. Exact formulation of such a

bank of matched filters is as

$$\begin{aligned} Y[k] &= \frac{2}{T}\int_0^T y(t)e^{-\jmath\omega_k t}dt \\ &= \frac{2}{T}\int_0^T y(t)e^{-\jmath\frac{2\pi kt}{N}}dt \end{aligned} \tag{1.5}$$

Here, we obtained the complex symbol $Y[k] = \widetilde{a}_k + \jmath\widetilde{b}_k$ which is correspondent to the transmitted complex symbol $X[k] = a_k + \jmath b_k$.

In fact, because of the CP, the received equivalent baseband discrete time-domain signal can be represented in another way by

$$y(n) = x(n) \circledast h(n) + w(n) \tag{1.6}$$

where $\circledast$ denotes the circular convolution and $w(n)$ is the receiver thermal noise. After removing the CP, the received discrete time-domain signal is

$$y(n) = \sum_{k=0}^{N} X[k]H[k]e^{\jmath\frac{2\pi kn}{N}} + w(n) \tag{1.7}$$

where $H[k] = \sum_{n=0}^{N} h(n)e^{-\jmath\frac{2\pi kn}{N}}$ is the frequency domain expression of the wireless channel. Then, we can recover the frequency domain symbols by demodulating the received time domain OFDM symbol as

$$\begin{aligned} Y[k] &= \sum_{n=0}^{N} y(n)e^{-\jmath\frac{2\pi kn}{N}} \\ &= X[k]H[k] + W[k] \end{aligned} \tag{1.8}$$

Eq. (1.8) shows that OFDM transmission over a wireless frequency selective channel, as in (1.6), is equivalent to symbol transmission over N parallel sub-carrier channels.

If the transfer function of the k^{th} sub-carrier channel can be obtained as $\widetilde{H}[k]$, the transmitted complex symbol $X[k]$ can be recovered by one tap frequency-domain equalizer (FEQ) as

$$\begin{aligned} \widetilde{X}[k] &= \frac{Y[k]}{\widetilde{H}[k]} \\ &= \frac{H[k]}{\widetilde{H}[k]}X[k] + \frac{W[k]}{\widetilde{H}[k]} \end{aligned} \tag{1.9}$$

Then, the receiver baseband PHY undoes the various operations of the transmitter as shown in Fig. 1.5. After that, the transmitted bits message can be recovered.

Multiple Antenna System

Multi-Input Multi-Output (MIMO) is another promising technique for increasing the spectral efficiency. In MIMO wireless communications, the radio terminals employ multiple antennas at both the transmitter and the receiver to transmit multiple data streams concurrently in the same frequency band. The spectral efficiency can be improved and link reliability can be enhanced without requiring additional transmit power or bandwidth compared to that of the single-input single-output (SISO) system. The increased capacity is achieved by introducing additional spatial channels that are exploited by using the space-time coding.

A core idea in the MIMO system is the space-time signal processing in which time (the natural dimension of digital communications) is complemented with spatial dimension inherent in the use of multiple spatially distributed antennas. A key advantage of the MIMO system is the capability of making good use of multipaths to benefit the wireless transmissions. MIMO system provides a number of advantages over the single-antenna communication system. Sensitivity to fading is reduced by the spatial diversity provided by multiple spatial paths. Besides, array gain, diversity gain, spatial multiplexing gain, and interference reduction could be obtained by the use of MIMO systems [87]. With respect to a MIMO system with N_T transmit and N_R receive antennas, we can leverage these benefits briefly as following:

A. Array Gain

Array gain, obtained by coherently combining the signals at the receiver, could increase the average receive signal-to-noise ratio (SNR). This gain could be realized through the space-time signal processing at the transmitter or/and receiver. The transmit array gain requires the channel state information (CSI) to be available at the transmitter and the receive array gain requires the CSI to be available at the receiver. The final amount of array gain also depends on the number of transmit and receive antennas, i.e. N_T and N_R.

B. Diversity Gain

Over a wireless channel, the power of the received signal fluctuates randomly. Diversity is a well-known technique to combat fading. It relies on the fact that the signal is transmitted over multiple (ideally) independent fading paths in time, frequency, or space. Spatial diversity is preferred over time or frequency diversity as it does not require additional radio resource (time or bandwidth). The spatial diversity could be achieved in the absence of the CSI at the transmitter by using the space-time coding [10].

C. Spatial Multiplexing Gain

Without additional power or bandwidth expenditure, the MIMO system could offer a linear increase in the radio link capacity or data rate with the minimum number of antennas (min(N_T, N_R)). This gain, i.e. spatial multiplexing gain, is realized by transmitting independent signals from individual antennas. Each antenna of the receiver obtains a noisy superimposed of the transmitted signals. The receiver can reconstruct each of the original signals under conducive channel conditions such as rich scattering.

D. Interference Reduction

In wireless networks, cochannel interference arises due to that multiple users share time and frequency resources. In the MIMO system, the differentiation between the spatial signatures of the desired signal and the cochannel interference signal could be exploited to enhance the signals separation. Interference reduction (or avoidance) can be carried out by pre-coding when the CSI of the desired user is available at the transmitter.

When both the transmitter and receiver are equipped with multiple antennas as shown in Fig. 1.6, the pre-coding at the transmitter and post-processing at the receiver can be used to exploit the additional degree of freedom.

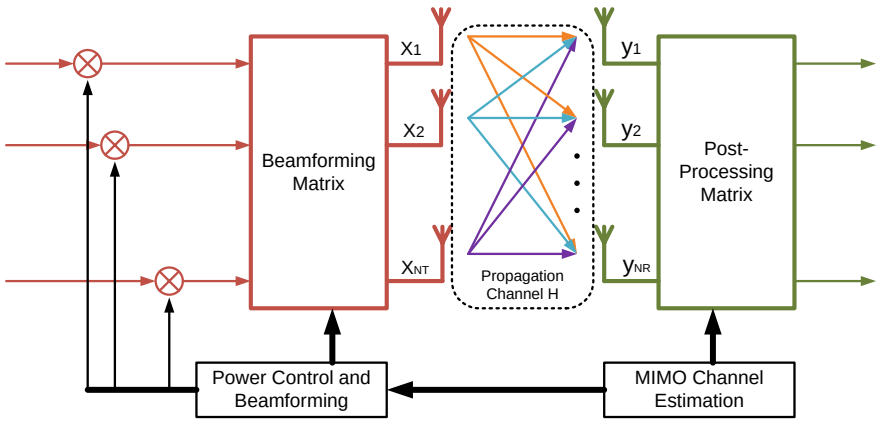

Figure 1.6: Basic block diagram of a MIMO baseband transceiver.

Considering a MIMO system with N_T transmit antennas and N_R receive antennas as shown in Fig. 1.6, the received $N_R \times 1$ symbol vector, $\mathbf{y} = [y_1, y_2, \cdots, y_{N_R}]^T$, can be expressed as

$$\mathbf{y} = \mathbf{H}\mathbf{x} + \mathbf{w} \tag{1.10}$$

where $\mathbf{x} = [x_1, x_2, \cdots, x_{N_T}]^T$ denotes the $N_T \times 1$ symbol vector to be simultaneously transmitted over the N_T transmit antennas, $\mathbf{H}$ is a $N_T \times N_R$-dimension complex channel matrix with each element $H_{n_r,n_t}, n_r \in [1, N_R]$ and $n_t \in [1, N_T]$, $\mathbf{w}$ represents the $N_R \times 1$ channel complex Gaussian noise with zero-mean and covariance $E[|\mathbf{w}|^2] = \delta_w^2 \mathbf{I}_{N_R}$. Therefore, each of the receive antennas obtains a signal which is a linear combination of all the transmitted signals, which could be expressed by

$$y_{n_r} = x_1 H_{n_r,1} + x_2 H_{n_r,2} + \cdots + x_{N_T} H_{n_r,N_T} + w_{n_r} \tag{1.11}$$

With full CSI available at both the transmitter and receiver, the knowledge of $\mathbf{H}$ could be exploited to design the beamforming scheme at the transmitter and the post-processing scheme at the receiver. If the rank of $\mathbf{H}$ is M ($M \leq min\{N_T, N_R\}$), it is possible to simultaneously transmit M individual symbols [25]. Let us decompose the MIMO channel matrix $\mathbf{H}$ by Singular-Value-Decomposition (SVD) as

$$\mathbf{H} = \mathbf{U}\mathbf{\Sigma}\mathbf{V}^H \tag{1.12}$$

where $\mathbf{U}$ and $\mathbf{V}$ are the $N_R \times N_R$ and $N_T \times N_T$ unitary matrices respectively, $\mathbf{\Sigma}$ is a $N_R \times N_T$ diagonal matrix which consists of singular values of $\mathbf{H}$ in a decreasing order. There are M nonzero singular values, represented by $\lambda_1 \geq \lambda_2 \geq \cdots \geq \lambda_M$, in $\mathbf{\Sigma}$ as the rank of the $\mathbf{H}$ is M. In the MIMO-SVD transmission [71], $\mathbf{V}$ is used for precoding or beamforming at the transmitter and $\mathbf{U}$ is employed for post-processing at the receiver. If we use $\{s_1, s_2, \cdots, s_M\}^T$ to denote the symbols to be transmitted and assume that the knowledge of $\mathbf{H}$ is available at the transmitter, the symbols can be precoded as

$$\mathbf{x} = \mathbf{V}\mathbf{s} \tag{1.13}$$

where $\mathbf{s} = [s_1, s_2, \cdots, s_M, 0, \cdots, 0]^T$ is a N_T-size symbol vector.

At the receiver, the SVD of $\mathbf{H}$ could be exploited to carry out the post-processing and further to separate the transmitted symbols $\mathbf{s}$. This can be achieved by employing $\mathbf{U}$ as the post-processing matrix as

$$\begin{aligned} \mathbf{z} &= \mathbf{U}^H \mathbf{y} \\ &= \mathbf{U}^H \mathbf{H}\mathbf{x} + \mathbf{w} \\ &= \mathbf{U}^H (\mathbf{U}\mathbf{\Sigma}\mathbf{V}^H)\mathbf{V}\mathbf{s} + \overline{\mathbf{w}} \\ &= \mathbf{\Sigma}\mathbf{s} + \overline{\mathbf{w}} \end{aligned} \tag{1.14}$$

where $\overline{\mathbf{w}} = \mathbf{U}^H \mathbf{w}$ is the equivalent noise vector with the same covariance as $\mathbf{w}$. As the

matrix $\mathbf{\Sigma}$ in Eq. (1.14) is a diagonal matrix, so the MIMO-SVD system could be equivalently regarded as M parallel single-input-single-output (SISO) systems as shown in Fig. 1.7.

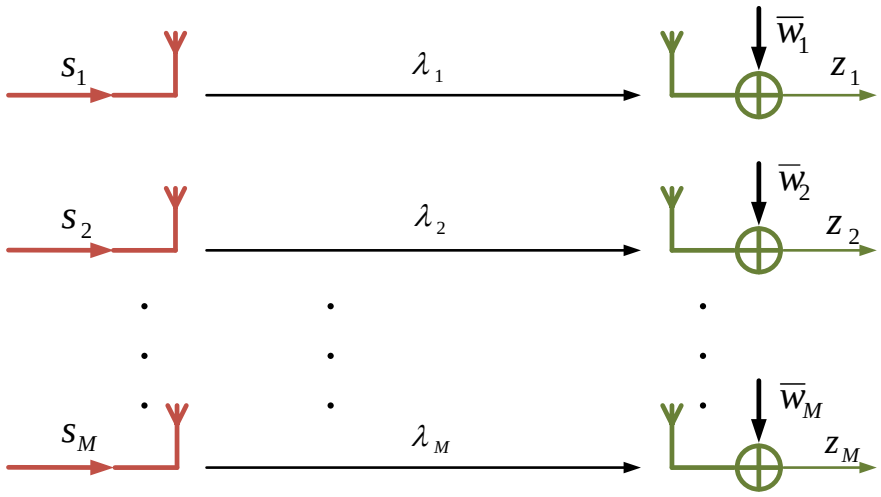

Figure 1.7: Equivalent parallel SISO channel of MIMO-SVD.

Therefore, the output of the m^{th} eigenvalue channel could be expressed as

$$z_m = \lambda_m s_m + \overline{w}_m, m = 1, 2, \cdots, M. \tag{1.15}$$

Based on the MIMO structure, let us take a linear precoding [107] as an example. In [107], the pre-coder consists of three separating processing blocks, i.e. orthogonal beam direction $\mathbf{U}_P$, per-beam power allocation $\mathbf{D}_P$ and input shaper $\mathbf{V}_P$. The SVD of the precoder matrix could be expressed as

$$\mathbf{P} = \mathbf{U}_P \mathbf{D}_P \mathbf{V}_P \tag{1.16}$$

To conserve the total transmit power, the precoder must satisfy

$$tr(\mathbf{P}\mathbf{P}^*) = 1 \tag{1.17}$$

That means the sum of the power over all beams is limited. However, the individual beam power can be allocated dynamically according to the beam quality or the design criterion.

In the MIMO-SVD system, the beam direction matrix $\mathbf{U}_P$ could be chosen as $\mathbf{V}$ of the wireless MIMO channel $\mathbf{H}$ and the per-beam power allocation matrix $\mathbf{D}_P$ can be determined according to the Water-Filling algorithm [34]. Then, the pre-coding structure could be illustrated as in Fig. 1.8.

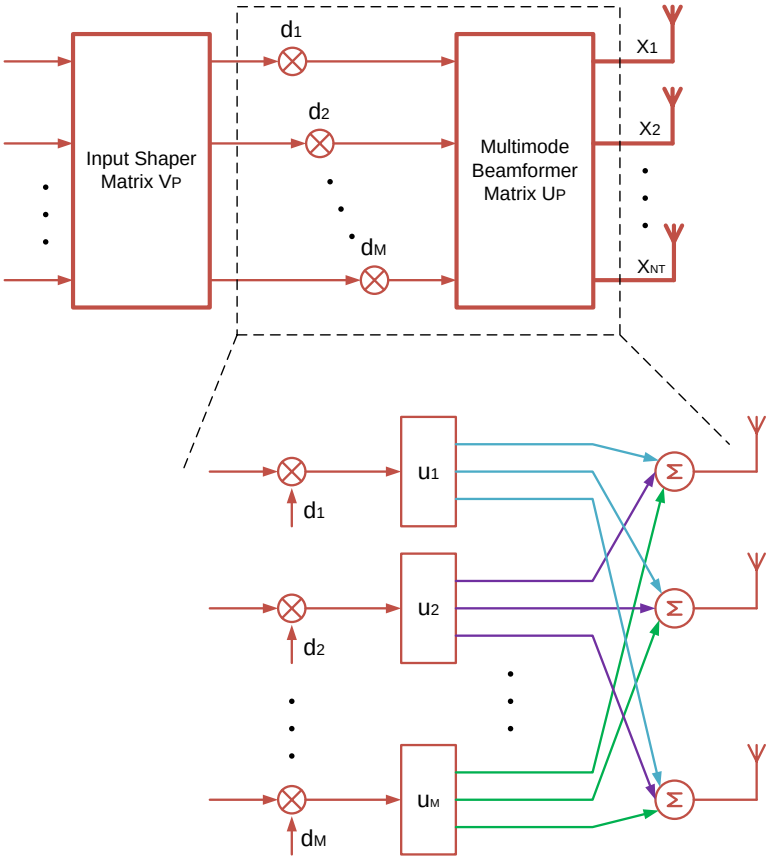

Figure 1.8: Structure of a linear pre-coder.

Generally, a pre-coder has two functions: (*i*) decoupling the input symbols into orthogonal spatial modes and direct different symbols to different directions; (*ii*) allocating power over these beams based on the channel state information at the transmitter (CSIT).

Multicarrier and Multiple Antenna System

MIMO-OFDM is a cooperative combination of the MIMO and OFDM, which can enhance the capacity and diversity and also can mitigate the detrimental effect due to the multipath fading. These benefits come from the advantages of the MIMO and OFDM individually.

OFDM is a block modulation scheme where a block of N symbols is modulated in parallel on N subcarriers as shown in Fig. 1.4, which can be implemented by using an IDFT. The time interval of an OFDM symbol is N times that of the single-carrier system when the system has the same bandwidth. In order to mitigate the inter symbol interference (ISI) induced by the time spread of the wireless multi-path channel, each

block of N symbols at the output of the IDFT is typically preceded by a CP or guard interval consisting of N_{guard} samples which is at least equal to the channel length. Under this condition, a linear convolution of the transmitted sequence and the channel becomes a circular convolution. Then, the ISI can be easily and completely eliminated. Moreover, the equalization of an OFDM receiver can be carried out by one tap equalizer in the frequency domain.

A MIMO system could take advantage of spatial diversity which is obtained by spatially separated antennas in a multi-path scattering environment [100] to enhance the system performance.

In most of radio environments, the wireless channel is a multi-path scattering channel which could degrade the reception performance of the conventional wireless techniques. Fortunately, OFDM can overcome the effect of various multi-path channel and MIMO could take advantage of multi-path scattering. Therefore, combining the techniques of the OFDM and MIMO to construct MIMO-OFDM system is a promising technique to provide high data rate wireless transmission in the harsh wireless environment.

We consider a MIMO-OFDM system based on the MIMO system with N_T transmit antennas and N_R and the OFDM system with N size IDFT/DFT as presented in the previous Subsection. The MIMO-OFDM baseband transmitter is illustrated as in Fig. 1.9 and the corresponding baseband receiver is as shown in Fig. 1.10.

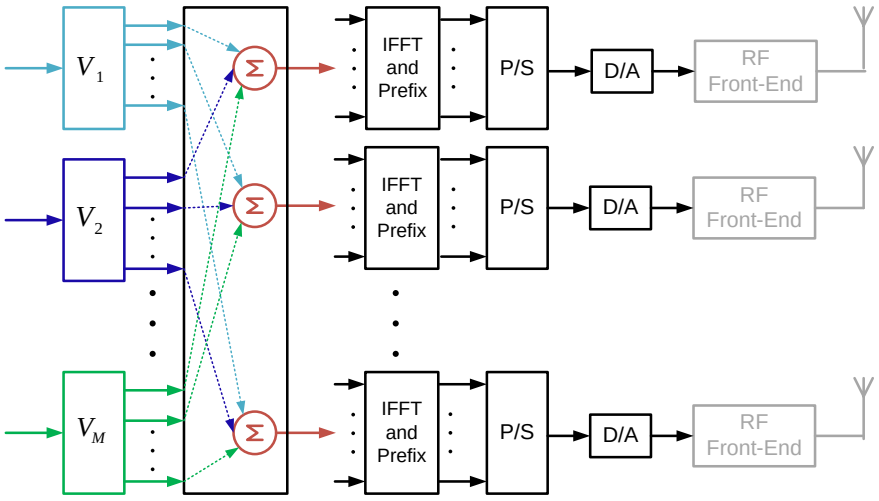

Figure 1.9: Illustration of a MIMO-OFDM transmitter.

Although the MIMO-OFDM based physical layers have greatly improved the capacity of radio link, the radio link capacity still can not meet the explosive rise of the data rate demand. Therefore, more advanced physical techniques and more flexible

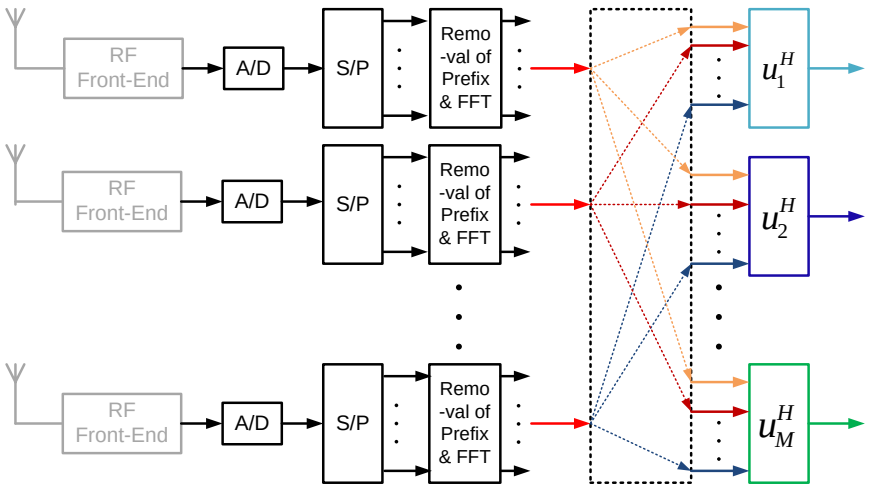

Figure 1.10: Illustration of a MIMO-OFDM receiver.

radio transceivers need to be developed to approach this goal. However, fully exploiting these gains comes, in general, at the cost of significantly increasing in signal-processing complexity, especially in the receiver.

Therefore, exploring a flexible and agile radio transceiver is great rewarding to provide high physical layer capacity for the future wireless network.

1.2.2 Transceiver RF Front-End

In the wireless system, the transmitter RF front-end is used to up-convert the analog baseband signal to the RF signal which is suitable for transmission over the wireless channel, while the receiver RF front-end is employed to down-convert the RF signal to the baseband signal. The receiver RF front-end always attracts more research attentions, because it is more closely related to signal reception and recovery. Generally, the traditional radio receivers are divided into Zero-IF receivers and Superheterodyne receivers which are correspondent to Zero-IF RF front-ends and superheterodyne RF front-ends respectively.

Zero-IF RF Front-End

In the Zero-IF or direct conversion RF front-end, the received RF signal is directly down-converted to the Zero-IF frequency [123] signal. A typical architecture of the Zero-IF RF front-end is as shown in Fig. 1.11. In this architecture, it is not necessary to require external high Q image rejection filter. Besides, a simple low pass filter (LPF) can be used to fulfill the channel selection.

Since the RF carrier and the local oscillator have the same center frequency, the

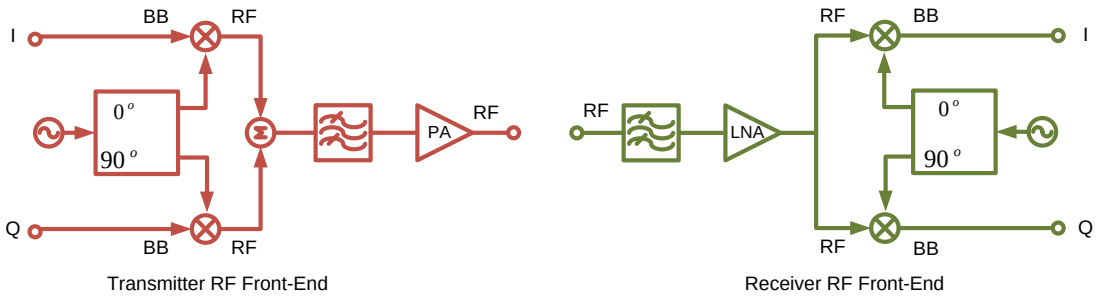

Figure 1.11: Simplified architecture of a direct conversion transmitter and receiver RF front-end.

biggest weakness of this architecture is that the local oscillator (LO) leakage to the mixer could result in self-mixing, which causes a time-varying direct conversion (DC) offset at the output of the mixer. Also, the Zero-IF RF front-end is sensitive to the I/Q imbalance. The gain and phase mismatch could significantly degrade the image rejection.

Superheterodyne RF Front-End

Armstrong proposed the superheterodyne receiver architecture in 1918 [16]. Most of the current radio transceivers still use similar approach for the frequency updown conversion with some refinements. Fig. 1.12 shows the block diagram of a superheterodyne RF front-end.

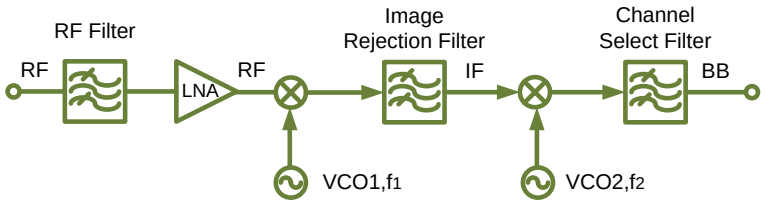

Figure 1.12: Simplified architecture of a superheterodyne RF front-end.

As we can see, the received RF signal is filtered by a RF band pass filter (BPF) first, then amplified by a low noise amplifier (LNA), after that down-converted to a intermediate frequency (IF) signal by using a mixer with carrier frequency f_1. After the image rejection filter, this IF signal is down-converted by another mixer with carrier frequency $f_2, (f_2 < f_1)$. The channel selecting filter selects the desired signal and output the desired baseband analog signal. The major advantages of this radio receiver based on the superheterodyne RF front-end are its high sensitivity, excellent selectivity and good image rejection. The major drawback of this radio receiver is that it requires high Q filters to fulfill the image rejection.

1.3 Contribution and Outline

This dissertation is part of research effort to:

- put the concept of Full-Duplex into practice
- develop an agile radio transceiver

for improving the spectral efficiency and providing high data rate for future wireless networks, like the *5G or cognitive radio networks*.

1.3.1 Contribution

The contributions of this dissertation to the research effort are threefolds:

I. Self-Interference Cancellation: With respect to the Full-Duplex OFDM wireless, the self-interference (SI) after the implementation of the active analog RF self-interference cancellation (AARFSIC) is still very strong. We dig deeply the characters of the residual SI and then propose an active digital self-interference cancellation in time domain (ADSICT) to eliminate it. The proposed ADSICT can bring down the residual SI to the noise floor.

II. Full-Duplex Wireless Radio: We design an in-band Full-Duplex OFDM radio node equipped with two antennas. The performance of the designed radio is evaluated by system level simulation and the impacts of the RF impairments (receiver thermal noise, phase noise in the local oscillator) on the Full-Duplex OFDM radio are qualified and then reduced or avoided.

III. Full-Duplex Dual-Band Wireless Radio: The flexible radio front-end based on the Full-Duplex radio and Dual-Band RF front-end is theoretically demonstrated and designed. The Full-Duplex Dual-Band OFDM (FDDB) radio transceiver based on the proposed RF front-end can simultaneously process two separate spectrum fragment signals. However, the I/Q imbalance significantly degrades the performance of the proposed radio transceiver. Therefore, we developed a suitable and advanced I/Q imbalance compensation method which could significantly eliminate the impact of the I/Q imbalance.

1.3.2 Thesis Outline

The outline of this dissertation is as follows:

Part I:

In this part, we present the Self-Interference Cancellation (SIC) schemes in details for the Full-Duplex wireless radio including the Chapter 2 and Chapter 3.

Chapter 2. gives the reviews about the state-of-the-art of the SIC schemes including antenna cancellation, passive self-interference suppression (PSIS) and active self-interference cancellation (ASIC). Besides, the key factors limiting the performance of the SIC are analyzed and studied.

Chapter 3. digs deeply the AARFSIC in the Full-Duplex OFDM wireless with one-path SI channel and multi-path SI channel, as well as finds the core problem limiting the capability of the SIC in the multi-path scenario. Then, the developed SIC which is based on the AARFSIC and ADSICT for the Full-Duplex OFDM wireless is presented.

Part II:

In this part, we present the design of a Full-Duplex OFDM wireless radio in details.

Chapter 4. gives the design and evaluation of an in-band two-antenna Full-Duplex OFDM wireless radio with one-path SI channel and multi-path SI channel. The impact of the Phase Noise on the Full-Duplex OFDM radio is qualified. Besides, the effect of the receiver Thermal Noise on the ASIC is elaborated and reduced.

Part III:

In this part, we present the design of a Full-Duplex Dual-Band (FDDB) wireless radio including Chapter 5.

Chapter 5. presents a FDDB radio based on the Full-Duplex radio and Dual-Band RF front-end at first. Then, the design of a FDDB OFDM radio transceiver is given. After that, a simple but practical I/Q imbalance estimation and compensation method based on the frequency-flat-fading behaviors of the SI channel is proposed. Finally, the proposed FDDB OFDM radio and the developed I/Q imbalance mitigation algorithm are evaluated by system level simulation.

Part IV:

In this part, we present the conclusions and future outlook of this dissertation.

Chapter 6. gives the conclusion and the future outlook.

1.4 Related Publications

Related Publications

Chapter 3 revises the related publications [116, 117].

Chapter 4 revises the related publications [116, 117, 118].

Chapter 5 revises the related publications [119, 120, 121].

Part I

Self-Interference Cancellation in Full-Duplex Wireless

2

State-of-the-Art of the Self-Interference Cancellation

Full-Duplex is a promising technique for supporting simultaneous transmission and reception at the same radio frequency band. Therefore, Full-Duplex wireless radio has emerged as an attractive solution to improve the efficiency of the spectrum utilization and to enhance the flexibility of radio transceivers. However, a key challenge behind the Full-Duplex is how to manage or cancel the so called self-interference (SI) induced by the leakage of its own transmission to the desired reception to a tolerable level.

In order to overcome the strong SI faced by the Full-Duplex wireless radio system, lots of efforts have been devoted to handle the strong SI. The researchers at the University of Waterloo [60, 61], Stanford University [30], NEC Lab and Princeton University [17, 83] propose interference nulling or canceling from the perspective of antennas. The researchers at Rice University [41] study the passive self-interference suppression (PSIS) including directional isolation, absorptive shielding and cross polarization. Besides, [19, 30, 39, 55, 56, 72, 95] focus on the active self-interference cancellation (ASIC). In this Chapter, these three schemes (antenna cancellation, PSIS and ASIC) are presented in details. Furthermore, the factors limiting the performance of the ASIC are introduced.

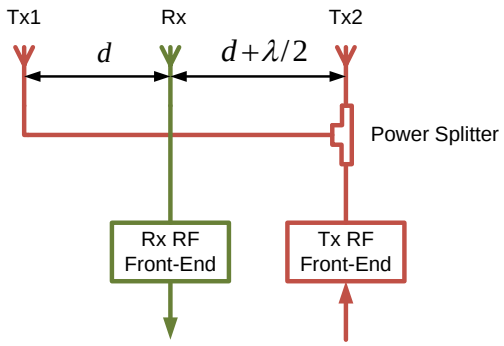

Figure 2.1: The block diagram of the SAC.

2.1 Antenna Cancellation

Antenna cancellation is a SIC method that employs multiple antennas to make the RF signals add destructively at the receiver antenna, or to obtain an inverse version of the received RF signal by internal phase shifting by 180^o and then subtract it at the RF part. There are mainly two antenna cancellation schemes, which will be presented in details in the following.

2.1.1 Antenna Cancellation based on $\lambda/2$ Spacing

In the Stanford Antenna Cancellation (SAC) [30], the Full-Duplex radio node employs three antennas, among which two antennas are used for transmission and the other one is used for reception. Besides, the radio node is equipped with two RF front-ends. One is used for up-converting the baseband transmit signal to the radio frequency (RF) signal. The other one is used for down-converting the received RF signal to the baseband analog signal. In order to make the two received RF signals from its own two transmit antennas add destructively, the receive antenna is placed such that the distance from the two transmit antennas to the receive antenna differs by half of the wavelength of the center carrier frequency. Fig. 2.1 shows the block diagram of the SAC. Let $x(t)$ be the unit power baseband transmit signal, P_{t1} and P_{t2} be the transmit power of the two signals from the two transmit antennas respectively, L_1 and L_2 denote the attenuations experienced by the two transmit signals before arriving at the receive antenna, d_1 and d_2 represent the distance from the two transmit antennas to the receive antenna respectively. The residual SI signal after the interference nulling, i.e. SAC, $r_{\mathsf{SAC}_{res}}(t)$, is given by

$$r_{\mathsf{SAC}_{res}}(t) = \sqrt{P_{t1}}\sqrt{L_1}x(t)e^{\jmath 2\pi f_c(t+\frac{d_1}{c})} + \sqrt{P_{t2}}\sqrt{L_2}x(t)e^{\jmath 2\pi f_c(t+\frac{d_2}{c})} \tag{2.1}$$

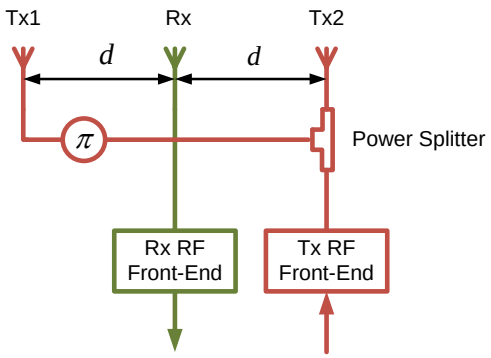

Figure 2.2: Block diagram of the Transmit Antenna Cancellation.

where f_c denotes the center carrier frequency and c is the speed of light. If $d_2 = d_1 + \frac{\lambda}{2}$, where λ is the wavelength of the carrier frequency f_c, these two signals add destructively and hence the SI signals can be nulled.

The experimental results in [30] show that this antenna cancellation could achieve 30dB of interference cancellation. However, this scheme could only be used for narrow-band signals because of its high dependency on the wavelength.

2.1.2 Antenna Cancellation based on Symmetry

Waterloo Antenna Cancellation based on Symmetry

The Waterloo Antenna Cancellation (WAC) [60] is based on the symmetric placement of the antennas. The block diagram of the WAC is as shown in Fig. 2.2. The two transmit antennas are placed symmetrically relative to the receive antenna. The signal from the transmit antenna-1 (Tx1) is phase shifted internally by a fixed π phase shifter. Then, the received residual SI signal, $r_{\mathrm{WAC}_{res}}$, after the WAC is represented by

$$r_{\mathrm{WAC}_{res}}(t) = \sqrt{P_{t1}}\sqrt{L_1}x(t)e^{\jmath[2\pi f_c(t+\frac{d}{c})+\pi]} + \sqrt{P_{t2}}\sqrt{L_2}x(t)e^{\jmath 2\pi f_c(t+\frac{d}{c})} \tag{2.2}$$

The two copies of the signal add π out of phase could null each other. This scheme uses the fixed π phase shifter instead of offsetting the distance by $\frac{\lambda}{2}$ to obtain the inverse version of the other signal. The experimental results in [17, 83] show that the WAC could achieve 22 to 30dB of SIC.

NEC-Princeton Antenna Cancellation based on Symmetry

The NEC-Princeton Antenna Cancellation (NEC-PAC) is also based on the symmetric placement of the antennas. Based on the architecture, the NEC-PAC includes NEC-Princeton Transmit Antenna Cancellation (NEC-PTAC) and NEC-Princeton Receive

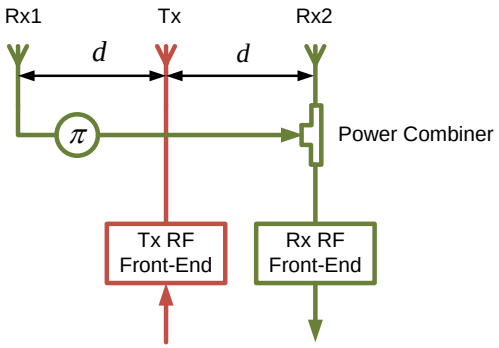

Figure 2.3: Block diagram of the Receive Antenna Cancellation.

Antenna Cancellation (NEC-PRAC).

NEC-PTAC: The block diagram of the NEC-PTAC scheme is similar to WAC, therefore be dropped here. The expression of the received residual SI, $r_{\text{NEC-PTAC}}$, after the NEC-PTAC is similar to Eq. (2.2).

NEC-PRAC: The block diagram of the NEC-PRAC scheme is as shown in Fig. 2.3. The two receive antennas are placed symmetrically relative to the transmit antenna. The signal received by the Rx1 is phase shifted internally by a fixed π phase shifter. After combining the two received signals by Rx1 and Rx2 at the power combiner, the residual SI, $r_{\text{NEC-PRAC}_{res}}(t)$, is expressed as

$$r_{\text{NEC-PRAC}_{res}}(t) = \sqrt{P_t}\sqrt{L_1}x(t)e^{j[2\pi f_c(t+\frac{d}{c})+\pi]} + \sqrt{P_t}\sqrt{L_2}x(t)e^{j2\pi f_c(t+\frac{d}{c})} \tag{2.3}$$

where P_t denotes the transmit power of the baseband signal $x(t)$. If $L_1 = L_2$, these two received RF signals could cancel each other by adding destructively.

NEC-PAC: The NEC-PAC is a cancellation method based on the NEC-PTAC and NEC-PRAC. The block diagram of the NEC-PAC is as shown in Fig. 2.4. Two Rx antennas are placed symmetrically on the perpendicular bisector of the two Tx antennas. The transmit signal from the Tx1 is phase shifted by π before emission. Each Rx will first receive the SI after the NEC-PTAC. Furthermore, the received residual SI by Rx1 is phase shifted by π via using a fixed π phase shifter before being combined with the other received residual SI signal. Therefore, the NEC-PAC includes two levels of SIC.

The residual SI received by the Rx1 after the NEC-PTAC is

$$r_{Rx1,\text{NEC-PTAC}_{res}}(t) = \sqrt{P_{t1}}\sqrt{L_{11}}x(t)e^{j[2\pi f_c(t+\frac{d_{11}}{c})+\pi]} + \sqrt{P_{t2}}\sqrt{L_{12}}x(t)e^{j2\pi f_c(t+\frac{d_{12}}{c})} \tag{2.4}$$

where L_{11} and L_{12} denotes the path fading loss from Tx1 and Tx2 to Rx1 respectively, d_{11} represents the distance between Tx1 and Rx1 and d_{12} represents the distance between Tx2 and Rx1.

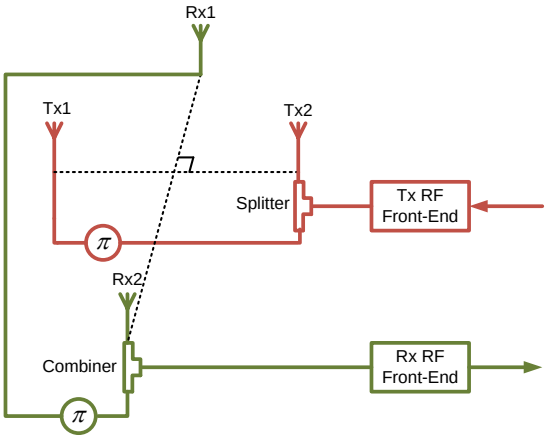

Figure 2.4: Block diagram of the NEC-PAC.

The residual SI received by the Rx2 after the NEC-PTAC is

$$r_{Rx2,\text{NEC-PTAC}_{res}}(t) = \sqrt{P_{t1}}\sqrt{L_{21}}x(t)e^{\jmath[2\pi f_c(t+\frac{d_{21}}{c})+\pi]} + \sqrt{P_{t2}}\sqrt{L_{22}}x(t)e^{\jmath 2\pi f_c(t+\frac{d_{22}}{c})} \quad (2.5)$$

where L_{21} and L_{22} denotes the path fading loss from Tx1 and Tx2 to Rx2 respectively, d_{21} represents the distance between Tx1 and Rx2 and d_{22} represents the distance between Tx2 and Rx2.

The residual SI, $r_{\text{NEC-PAC}_{res}}(t)$, after the two levels of SIC (NEC-PTAC and NEC-PRAC) can be given by

$$r_{\text{NEC-PAC}_{res}}(t) = r_{Rx1,\text{NEC-PTAC}_{res}}(t)e^{\jmath\pi} + r_{Rx2,\text{NEC-PTAC}_{res}}(t) \quad (2.6)$$

[17] experimentally demonstrates that the PAC could provide up to 45dB of SIC in a wireless environment with few multiple reflecting paths.

In fact, the schemes of the WAC, SAC and NEC-PAC are based on the principle of interference nulling which has high requirement on symmetries: power symmetry, placement symmetry of antennas, fading loss symmetry and channel symmetry. The first two symmetries can be guaranteed, because power allocation and placement of the antennas can be implemented exactly. However, the channel symmetry is dependent on the wireless environment. If in an anechoic chamber, which means the SI channel is a line-of-sight (LoS) path channel, the demand of channel symmetry can be met. While if in a chamber with rich reflections, the channel symmetry may not hold for the strong non-line-of-sight (NLoS) components. That is why antenna cancellation could achieve more SIC in the wireless environment with few reflectors as stated in [17, 83].

Another antenna cancellation technique proposed in [104] has been experimentally demonstrated by [42]. The experimental results show that this antenna cancellation based on the combination of null-steering beamforming and antenna polarization diversity could achieve up to 66dB of SIC but still in an anechoic chamber.

2.2 Passive Self-Interference Suppression

The basic principle of the PSIS is to use the electromagnetic isolation techniques to reduce the power of the leaked signal from its own transmission to the receiver. The PSIS includes antenna separation, directional antenna, absorptive shielding and antenna polarization. Antenna separation is one of the simplest ways of PSIS, which could result in around 40dB of the SI suppression when the antennas are separated by 30 centimeters. Directional antenna could result in $36 \sim 38$dB of SI suppression depending on the configuration [41]. Absorptive shielding can provide up to 25dB absorption [41]. Antenna polarization in the near-field wireless communications could achieve 10dB of SI isolation [17].

2.3 Active Self-Interference Cancellation

ASIC is a method to exploit the knowledge of its own transmission and emulate the over-the-air SI channel to craft a cancellation signal and then subtract it in the receiver chain. The classical radio receiver and potential placement of the SIC is as shown in Fig. 2.5. Based on the SIC being implemented before or after the Analog-to-Digital Converter (ADC), the ASIC is classified as Active Analog Self-Interference Cancellation (AASIC) and Active Digital Self-Interference Cancellation (ADSIC).

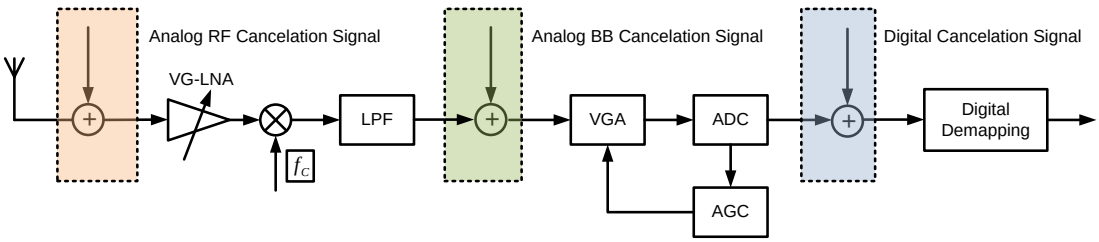

Figure 2.5: Classical radio receiver with possible SIC placements.

2.3.1 Active Analog Self-Interference Cancellation

As the name suggests, the AASIC is the active cancellation scheme performed in the analog domain before the received signal passing through the ADC. Based on the SIC being carried out in the RF domain or Base Band (BB) domain, the AASIC is divided into Active Analog RF Self-interference Cancellation (AARFSIC) and Active Analog Baseband Self-Interference Cancellation (AABBSIC) which are as shown in Fig. 2.5.

Active Analog RF Self-Interference Cancellation

Currently, there are mainly two types of AARFSIC which are proposed respectively by Stanford [24, 54, 55] and Rice [37, 38, 39, 40, 95].

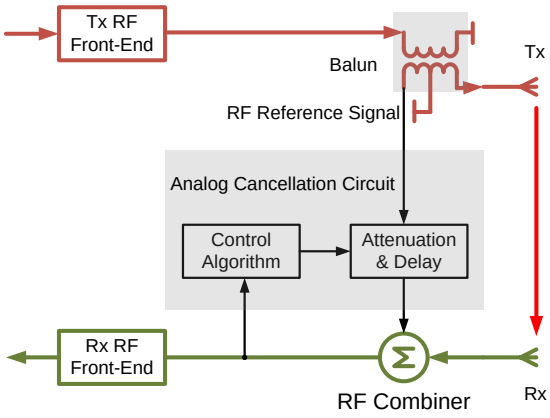

Figure 2.6: Simplified block diagram of Stanford AARFSIC.

Stanford AARFSIC: The structure of the Stanford AARFSIC is as shown in Fig. 2.6. Balun is utilized to obtain the inverse version of the transmitted signal which can be used as the reference signal to cancel the SI. The Received Signal Strength Indicator (RSSI) or other control algorithm is used to adjust the attenuations and delays which emulating the over-the-air SI channel. The residual SI signal, $r_{\mathrm{SAARFSIC}_{res}}(t)$, after the Stanford AARFSIC can be represented by

$$r_{\mathrm{SAARFSIC}_{res}}(t) = \sqrt{P_t}\sqrt{L_1}x(t)e^{j2\pi f_c t} * h_{si}(t) - \alpha_s\sqrt{P_t}\sqrt{L_2}x(t)e^{j2\pi f_c t} * \widetilde{h}_{si}(t) \quad (2.7)$$

where $h_{si}(t)$ denotes the impulse response of the wireless SI channel, α_s represents power split ratio by the Balun to the reference signal, $\sqrt{L_2}$ denotes the large scale fading factor which can be adjusted to meet $\sqrt{P_t}\sqrt{L_1} = \alpha_s\sqrt{P_t}\sqrt{L_2}$. $\widetilde{h}_{si}(t)$, denoting the emulated SI channel $h_{si}(t)$, is implemented by an analog cancellation circuit which is comprised of a certain number of fixed delays and variable attenuators. The experimental results show that the Stanford AARFSIC [55] could achieve $40 \sim 45$dB of SI

reduction for a 10MHz WiFi signal.

Rice AARFSIC: The Full-Duplex radio node knows what it has transmitted and what it will transmit, and also it is quite easy for a Full-Duplex radio node to obtain the estimated coefficients of the wireless SI channel. Besides, OFDM technique converts a frequency selective fading channel into lots of parallel frequency flat fading subcarrier channels which could help implement the SIC in each subcarrier channel. Based on these, the Rice AARFSIC utilizes an auxiliary transmitter chain to craft the RF cancellation signal as shown in Fig. 2.7 to carry out the SIC.

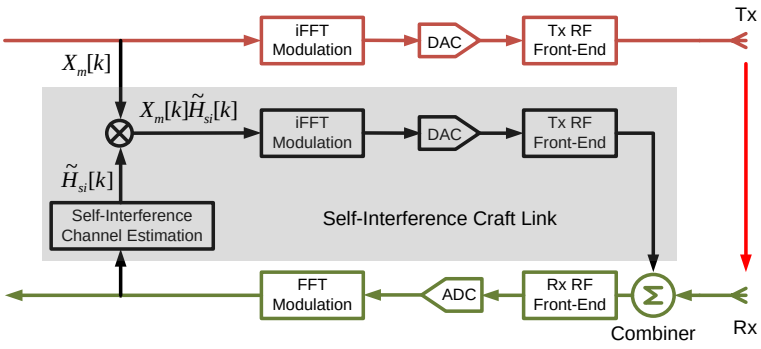

Figure 2.7: Simplified block diagram of Rice AARFSIC.

The residual SI, $r_{\mathsf{RAARFSIC}_{res}}(t)$, after the Rice AARFSIC can be expressed by

$$\begin{aligned} r_{\mathsf{RAARFSIC}_{res}}(t) &= \sqrt{P_{t1}}\sqrt{L_1}x(t)e^{\jmath 2\pi f_c t} * h_{si}(t) \\ &\quad -\sqrt{P_{t2}}\sqrt{L_2}\mathsf{DAC}\left\{\mathsf{CP}\left\{\mathsf{IDFT}\left\{X_m[k]\widetilde{H}_{si}[k]\right\}\right\}\right\}e^{\jmath 2\pi f_c t} \end{aligned} \tag{2.8}$$

where $\widetilde{H}_{si}[k]$ represents the estimated coefficients in the frequency domain of the SI channel $h_{si}(t)$, $\mathsf{IDFT}\{\chi_m[k]\} \triangleq \frac{1}{N}\sum_{k=-\frac{N}{2}}^{\frac{N}{2}-1}\chi_m[k]e^{\jmath 2\pi\Delta f k n}$ in which N denotes the total number of sub-carriers and Δf denotes the subcarrier space, CP denotes the operation of the adding of a cyclic prefix for the OFDM symbol, i.e. $\mathsf{CP}\{\chi_m(n), n \in [1, N]\} \triangleq \chi_m^T(n), n \in [1, N + N_{CP}]$ where N_{CP} represents the length of the cyclic prefix, DAC means the operation of converting the digital signal to the analog signal, i.e. $\mathsf{DAC}\{\chi_m^T(n)\} \triangleq \chi_m^T(t)$. Specifically, the transmit baseband analog signal $x(t)$ here should be expressed as $x(t) = \mathsf{DAC}\{\mathsf{CP}\{\mathsf{IDFT}\{X_m[k]\}\}\}$. The experimental results [38] show that this AARFSIC could achieve $\sim$ 31dB of SIC.

Except for the Stanford AARFSIC and the Rice AARFSIC, the literatures [19, 43, 45, 65, 69, 81, 106, 108, 114] are also devoted to the cancellation or isolation of the SI at the RF domain. Askar *et al.* [19] report 45 $\sim$ 50dB of SIC for one-antenna Full-Duplex by using the AARFSIC scheme which is similar to the approach in [39]. Gholian *et al.* [43] propose a cluster canceler which has important advantages over the uniform

canceler as presented in [24], which is based on the demonstrated result that the cluster canceler can emulate the multi-path SI more accurately than the uniform canceler do. He *et al*. [45] study the impact of amplitude and phase estimation errors of Line-of-Sight (LoS) components on the AARFSIC method which is similar to the approach in [24]. Kolodziej *et al*. [65] present an adaptive RF canceler, configured as four RF taps whose amplitude and phase weights are tuned by dithered linear search algorithm, which could contribute to 30dB of SIC. Krier *et al*. [69] introduce a Full-Duplex transceiver with an auxiliary transmitter used for crafting a RF cancellation signal, which is similar to the approach in [38], however this scheme crafts the baseband cancellation signal by using adaptive filtering in the digital time domain. McMichael *et al*. [81] present a novel convex problem about tuning the attenuation and phase offset of a multiple tap SI canceler, which could achieve 65dB average cancellation for the reflectors within 1.75 meters and at least 40dB average cancellation for the additional reflectors far away. Liempd *et al*. [106] propose two RF SIC schemes which could realize more than 50dB of suppression to the direct Tx-to-Rx leakage path for one-antenna Full-Duplex. Wang *et al*. [108] present a RF SIC method, which is similar to the scheme in [24], by using an adaptive least mean square (ALMS) algorithm to tune the amplitude and phase values. Yang *et al*. [114] present a RF SIC circuit controlled by a real time optimization algorithm, which could achieve more than 50dB of SIC.

Active Analog BB Self-Interference Cancellation

Although the antenna separation and AARFSIC could significantly reduce the received SI, even up to $30 \sim 60$dB of SIC, the residual SI is still strong enough to mask the weak desired signal from the distant radio node. Furthermore, the ADC has a very limited dynamic range (DR) which is defined as the ratio of the largest possible output (full-scale voltage) to the smallest possible output (the least significant bit or quantum voltage). When the dynamic range is exceeded, the quantization noise of the converter could bury the weaker signal, which can be shown as in Fig. 2.8. The DR(dB) can be expressed as [86]

$$\mathrm{DR}(dB) = 6.02 \times n_{ADC} + 1.76dB \tag{2.9}$$

where n_{ADC}, determining the resolution $N = 2^{n_{ADC}}$, is the number of bits of the ADC/DAC. As for a A/D converter with $n_{ADC} = 10$ bits, the precision is $\frac{1}{1024}$ of the full scale of the analog signal. Typically, n_{ADC} could be chosen as $8 \sim 24$. 14-bit ADC

could provide around 86dB of dynamic range. Therefore, the residual SI after the antenna separation and RF cancellation is not strong enough to saturate the ADC. However, the stronger residual SI occupies the whole dynamic range of the ADC, which means the residual interference signal takes all n_{ADC} bits for quantization. While for the desired signal which is still much weaker than the residual SI, it just takes a few bits of ADC for quantization. How many bits will be taken by the desired signal for quantizing depends on the gap between the residual SI and the desired signals. The bigger the gap, the fewer bits will be occupied by the signal of interest. Therefore, it is very necessary to further cancel the residual SI as much as possible before it going through the ADC.

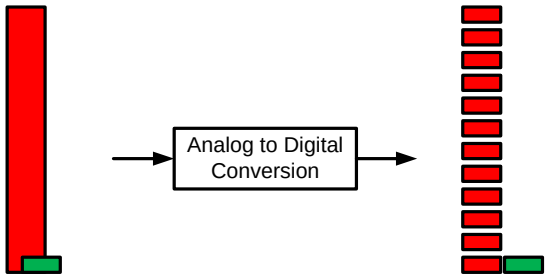

Figure 2.8: Illustration of the digitization of the mixed signals including the SI and the desired signal by ADC.

In the analog baseband domain, just after the RF front-end, the AABBSIC can be implemented as in [58, 59], in which 10dB more of SIC can be achieved by the AABBSIC after the current implementation of AARFSIC. The transmitted analog baseband signal $x(t)$ is known, so the AABBSIC can be implemented as shown in Fig. 2.9 if the time domain estimate of the SI channel can be obtained. Generally, the residual SI after the AABBSIC, $r_{\mathsf{AABBSIC}_{res}}(t)$, could be expressed as

$$\begin{aligned} r_{\mathsf{AABBSIC}_{res}}(t) &= [x(t)e^{\jmath(2\pi f_c t+\phi_t)} * h_{si}(t)]e^{-\jmath(2\pi f_c t+\phi_r)} - x(t) * \widetilde{h}_{si}(t) \\ &= x(t)e^{\jmath(\phi_t-\phi_r)} * h_{si}(t) - x(t) * \widetilde{h}_{si}(t) \\ &= x(t) * h_{si}(t)[e^{\jmath(\phi_t-\phi_r)} - 1] + x(t) * [h_{si}(t) - \widetilde{h}_{si}(t)] \\ &= x(t) * h_{si}(t)[e^{\jmath(\phi_t-\phi_r)} - 1] + x(t) * \Delta h_{si}(t) \end{aligned} \tag{2.10}$$

where $x(t)$ is the transmit baseband analog signal, ϕ_t and ϕ_r are the transmitter phase offset and the receiver phase offset respectively and $\widetilde{h}_{si}(t)$ is the estimate of the over-the-air SI channel $h_{si}(t)$. As it can be seen from the Eq. (2.10), the SI can be completely mitigated if the phase difference $(\phi_t - \phi_r)$ between the transmitter and receiver is zero and perfect channel estimate, i.e. $\widetilde{h}_{si}(t) = h_{si}(t)$, could be obtained.

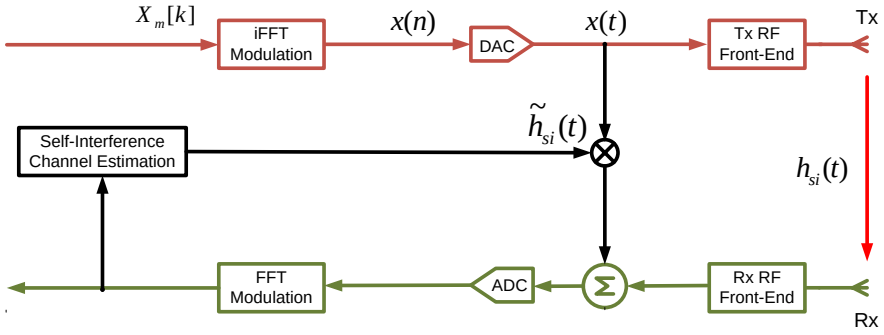

Figure 2.9: Simplified block diagram of AABBSIC.

2.3.2 Active Digital Self-Interference Cancellation

Although lots of efforts have been devoted to PSIS, AARFSIC and AABBSIC, the residual SI is still much stronger than the signal of interest. ADSIC aims to clean out the cancelable residual SI in the digital domain after the PSIS and AASIC. In the OFDM based Full-Duplex wireless, the ADSIC could be classified into active digital self-interference cancellation in time domain (ADSICT) and active digital self-interference cancellation in frequency domain (ADSICF) depending on where the SIC is implemented. A general ADSIC architecture including ADSICT and ADSICF is as shown in Fig. 2.10.

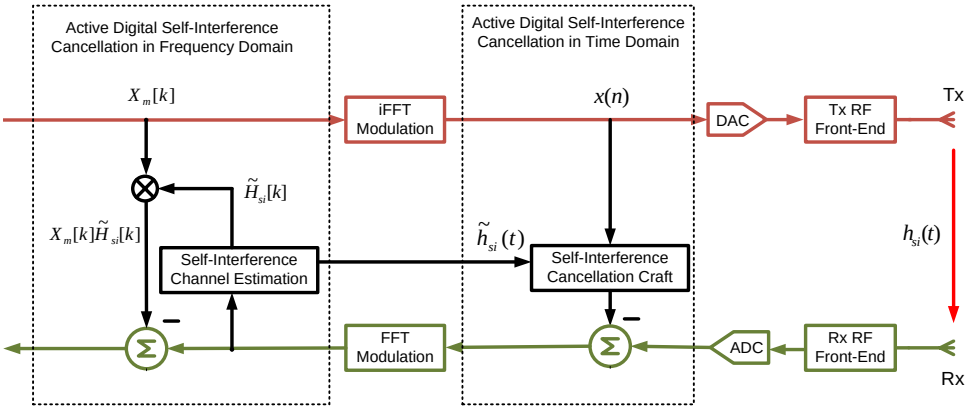

Figure 2.10: General block diagram of ADSIC.

Active Digital Self-Interference Cancellation in Time Domain

In fact, the knowledge of the transmitted discrete time domain signal, $x(n)$, is available at the receiver chain of the Full-Duplex radio node. Therefore, if we can obtain the coefficients of the equivalent discrete baseband SI channel, the SIC can be implemented in the discrete time domain as shown in Fig. 2.10. After the ADSICT, the residual SI,

$r_{\mathsf{ADSICT}_{res}}(n)$, could be expressed as

$$\begin{aligned} r_{\mathsf{ADSICT}_{res}}(n) &= \mathsf{ADC}\left\{\{[\mathsf{DAC}\{x(n)\}e^{\jmath(2\pi f_c t+\phi_t)}] * h_{si}(t)\}e^{-\jmath(2\pi f_c t+\phi_r)}\right\} - x(n) \circledast \widetilde{h}_{si}(n) \\ &= x(n) \circledast h_{si}(n)e^{\jmath(\phi_t-\phi_r)} - x(n) \circledast \widetilde{h}_{si}(n) \\ &= x(n) \circledast h_{si}(n)[e^{\jmath(\phi_t-\phi_r)} - 1] + x(n) \circledast [h_{si}(n) - \widetilde{h}_{si}(n)] \\ &= x(n) \circledast h_{si}(n)[e^{\jmath\Delta\phi} - 1] + x(n) \circledast \Delta h_{si}(n) \end{aligned} \tag{2.11}$$

where $\mathsf{ADC}(\chi)$ and $\mathsf{DAC}(\chi)$ denote the perfect conversion of analog signal $\chi(t)$ to digital signal $\chi(n)$ and digital signal $\chi(n)$ to analog signal $\chi(t)$ respectively, $\widetilde{h}_{si}(n)$ represents the estimate of the equivalent baseband discrete SI channel $h_{si}(n)$, $\Delta\phi$ denotes the phase offset between the transmitter and receiver of the Full-Duplex radio node and $\Delta h_{si}(n)$ represents the SI channel estimation error.

As it can be seen from Eq. (2.11), the SI channel estimation error $\Delta h_{si}(n)$ and the RF impairments, such as phase noise or phase offset, in the RF front-end limit the capability of the ASIC.

Active Digital Self-Interference Cancellation in Frequency Domain

Most of the current DSIC [37, 39, 54, 55] are implemented in the frequency domain. This is because the OFDM technique divides a wideband frequency selective fading channel into lots of narrowband frequency flat fading channels and each coefficient of the narrowband subcarrier channel can be easily estimated by using the long training symbols. Therefore, it is possible to craft a cancellation signal and cancel the SI in each subcarrier channel.

Especially, in an ideal OFDM system, in which perfect time and frequency synchronization and perfect suppression of multipath by the GI are available, the subcarrier channel of the OFDM system could be considered as a parallel Additive White Gaussian Noise (AWGN) channel as shown in Fig. 2.11.

In this ideal scenario, after taking the transmit power P_t, path fading loss L_{si} and low noise amplifier P_{LNA} into account to the signal model, the output of each subcarrier channel could be represented by

$$\begin{aligned} Y_{m,si}[k] &= \sqrt{P_t}\sqrt{L_{si}}\sqrt{P_{\mathsf{LNA}}}X_m[k]H_{si}[k] + w[k] \\ &= A_{si}X_m[k]H_{si}[k] + w[k] \end{aligned} \tag{2.12}$$

where $A_{si} \triangleq \sqrt{P_t}\sqrt{L_{si}}\sqrt{P_{\mathsf{LNA}}}$ denotes the amplitude of the received SI signal.

From Eq. (2.12), the SI signal in each subcarrier channel can be canceled if the A_{si} and $H_{si}[k]$ could be obtained as the transmit symbols $X_m[k], k \in [1, N], m \in [1, \infty]$

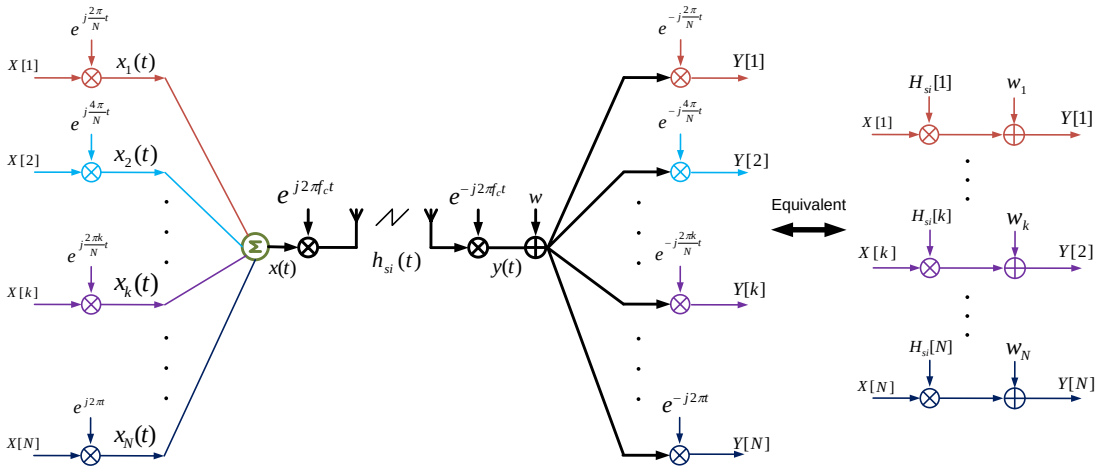

Figure 2.11: Perfectly synchronized OFDM system can be viewed as a set of parallel Gaussian sub-carrier channels.

are known. This enlightens us that the SIC can also be implemented in the digital frequency domain. However, the ideal received signal model (2.12) can not be used in the practical system design, because practical transceiver RF front-ends always prevent the received signal from the ideal scenario. The details of the ADSICF is shown as in Fig. 2.10. Then, a more practical residual SI, $R_{\mathsf{ADSICF}_{res}}[k]$, in the frequency domain after the ADSICF can be modeled as

$$\begin{aligned} R_{\mathsf{ADSICF}_{res}}[k] &= \mathsf{DFT}\left\{\mathsf{ADC}\left\{[A_{si}\mathsf{DAC}\left\{\mathsf{IDFT}\{X_m[k]\}\right\}e^{\jmath(2\pi f_c t+\phi_t)} * h_{si}(t)]e^{-\jmath(2\pi f_c t+\phi_r)}\right\}\right\} \\ &\quad -\widetilde{A}_{si}X_m[k]\widetilde{H}_{si}[k] \\ &\overset{2(a)}{=} A_{si}X_m[k]H_{si}[k]e^{\jmath(\phi_t-\phi_r)} - \widetilde{A}_{si}X_m[k]\widetilde{H}_{si}[k] \\ &= A_{si}X_m[k]H_{si}[k][e^{\jmath(\phi_t-\phi_r)}-1] + X_m[k](A_{si}H_{si}[k]-\widetilde{A}_{si}\widetilde{H}_{si}[k]) \end{aligned} \tag{2.13}$$

where DFT is the inverse operation of the IDFT and $\widetilde{A}_{si}$ is the estimation of the A_{si}. $2(a)$ holds because the DAC and ADC are assumed perfect.

2.4 Key Factors Limiting the Self-Interference Cancellation

From the studies above, we can find that any factors leading to the phase mismatch and magnitude mismatch between the SI radio link and the cancellation link will significantly limit the capability of the ASIC. Lots of works [26, 94, 118, 119, 121] have

demonstrated that the RF impairments, such as phase noise [94], thermal noise [118], I/Q imbalance and non-linearity of the power amplifier, are the factors limiting the SIC. Besides, the multiple reflecting paths of the wireless SI channel are also the main factor that limits the SIC [41, 116]. [41] has shown that the multi-path could significantly limit the PSIS, and [116] has demonstrated and described in details that the multi-path also significantly influences the ASIC.

2.4.1 RF Impairments

Phase Noise

Phase noise is one of the key factors that limits the ASIC by causing the phase mismatch between the SI radio link and the cancellation radio link [5, 90, 93, 94, 97, 101]. In fact, phase noise could affect all kinds of ASIC including the AARFSIC, AABBSIC, ADSICT and ADSICF. [93, 94] are the first studies demonstrating that the phase noise in the local oscillator is the bottleneck for the ASIC. [97] studies the effect of the phase noise on the ADSIC in the Full-Duplex OFDM wireless and gives a closed-form expression of the ADSIC performance with the oscillator's 3dB coherence bandwidth.

With respect to the AARFSIC, the influence of the phase noise could be modeled as

$$\begin{aligned} r_{RF}^{\text{AARFSIC}}(t) &= x_{BB}(t)e^{\jmath 2\pi f_c t}e^{\jmath\phi_1^t} * h_{si}^{RF}(t) - x_{BB}(t)e^{\jmath 2\pi f_c t}e^{\jmath\phi_2^t} * \tilde{h}_{si}^{RF}(t) \\ &\overset{2(b)}{=} x_{BB}(t)e^{\jmath 2\pi f_c t}e^{\jmath\phi_2^t} * h_{si}^{RF}(t)[e^{\jmath\Delta\phi^t} - 1] \\ &\overset{2(c)}{\approx} x_{BB}(t)e^{\jmath 2\pi f_c t}e^{\jmath\phi_2^t} * h_{si}^{RF}(t)\jmath\Delta\phi^t \end{aligned} \tag{2.14}$$

where $x_{BB}(t)$ denotes the to be transmitted analog baseband signal, ϕ_1^t and ϕ_2^t represent the whole phase of SI radio link and the cancellation radio link and $\phi_1^t = \phi_2^t + \Delta\phi^t$, and $h_{si}^{RF}(t)$ denotes the radio frequency wireless SI channel. $2(b)$ holds under the condition that the channel state information (CSI) of the SI channel can be obtained perfectly. $2(c)$ holds true because of the phase offset $\Delta\phi^t \to 0$.

With respect to AABBSIC, the impact of phase noise could be represented by

$$\begin{aligned} r_{BB}^{\text{AABBSIC}}(t) &= x_{BB}(t)e^{\jmath\phi_1^t} * h_{si}^{BB}(t) - x_{BB}(t)e^{\jmath\phi_2^t} * \tilde{h}_{si}^{BB}(t) \\ &= x_{BB}(t)e^{\jmath\phi_2^t} * h_{si}^{BB}(t)[e^{\jmath\Delta\phi^t} - 1] \\ &\overset{2(d)}{\approx} x_{BB}(t)e^{\jmath\phi_2^t} * h_{si}^{BB}(t)\jmath\Delta\phi^t \end{aligned} \tag{2.15}$$

where $h_{si}^{BB}(t)$ denotes the baseband continuous time domain SI channel. $2(d)$ holds true because of the phase offset $\Delta\phi^t \to 0$.

The signal model of the ADSIC with phase noise could be found in [5, 94, 97],

therefore be dropped here.

Thermal Noise

In fact, the thermal noise in the wireless communications includes the transmitter thermal noise and the receiver thermal noise. In the conventional wireless communications, the transmitter thermal noise experiences significantly path loss and arrive at the receiver with very low power level compared to the receiver thermal noise. Therefore, the transmitter thermal noise was not considered as an important RF impairment in the traditional Half-Duplex wireless communications. However, in Full-Duplex wireless, the transmitter thermal noise is another key factor limiting the SIC due to the fact that the transmitter thermal noise experiences very few power loss. The transmitter thermal noise affects the SIC by degrading the SI channel estimation and contributing to the residual SI as the receiver thermal noise does.

Transmitter Thermal Noise:
The authors in [19, 21, 50, 67] have modeled and studied the thermal noise induced by the transmitter. In [19], a passive cancellation approach was presented to suppress the transmitter thermal noise. In [50], a new analog-digital hybrid method was proposed to avoid the impact of the transmission noise.

Receiver Thermal Noise:
With respect to the receiver thermal noise, there is no literature dedicated to its impact on the SIC except for [118]. The receiver thermal noise affects the SIC performance in the form of worsening the SI channel estimation. For the Full-Duplex OFDM wireless, the estimate of the wireless SI channel could be expressed as [118]

$$\widetilde{H}_{si}[k] = H_{si}[k] + \underbrace{\frac{W[k]}{\sqrt{P_{si}}\sqrt{L_{si}}\sqrt{P_{\mathsf{LNA}}}T[k]}}_{\text{channel estimation error due to thermal noise}}, k \in [1, N_{nz}] \tag{2.16}$$

where $H_{si}[k]$ is the real SI channel, $W[k]$ denotes the receiver thermal noise, P_{si} represents the transmit power and L_{si} denotes the experienced path loss of the SI signal, $T_k, k \in [1, N_{nz}]$ represents the training symbols. The stronger the thermal noise, the worse channel estimation will be obtained and the more residual SI will occur.

I/Q Imbalance

The authors in [66, 76] consider the impact of the I/Q imbalance on the SIC performance and propose to use the ADSIC scheme to eliminate it. In [66], the received signal model after the antenna isolation and RF cancellation is formulated by a widely-linear

transformation of the original transmit data symbols. Then, a novel widely-linear ADSIC is proposed combining with the parameters estimation to suppress the impact of the I/Q imbalance on the Full-Duplex transceiver. In [76], the authors find that the I/Q imbalance is a key factor limiting the ADSIC and then they propose to use the signal at the output of the power amplifier to assist the DSIC for eliminating the effect of the I/Q imbalance.

Non-linearity of Power Amplifier

Non-linearity of the power amplifier is another significant factor limiting the precision of the ADSIC, which have been studied in [5, 14, 15, 61, 67, 76]. In fact, the power amplifier in the Full-Duplex radio transceiver includes the Hight Power Amplifier (HPA) at the transmitter and the LNA at the receiver. In [5], both the non-linearities of the HPA and LNA are studied and modeled in the received baseband digital signal and then a novel all-digital SIC scheme for the Full-Duplex system is proposed to suppress this RF impairment. [14, 15] modeled the SI signal corrupted by the non-linearity of the HPA in details, and then a novel ADSIC based on the SI model is presented. The author in [61] studies the impact of the non-linearity of HPA on the SIC and proposes to pre-weight in each OFDM tones to cancel the SI and further to suppress the non-linearity. In [76], the non-linearity of the HPA was avoided by using the signal from the output of the HPA to implement the SIC in digital time domain.

2.4.2 Multiple Paths of the Self-Interference Channel

Majority of the research works on the Full-Duplex wireless focuses on the impact of RF impairments on the performance of the ASIC [7, 8, 26, 94, 118]. We also find that the multiple reflecting paths significantly limit the SIC as well. [41] has demonstrated experimentally that the reflecting multi-path is the key factor limiting the PSIS. Passive methods, such as cross polarization antenna, antenna isolation, absorbing and so on, could only suppress the direct or main path of the SI. The residual SI caused by the reflecting paths is so high in the indoor environment that the Full-Duplex can not be putted into practice. For example, in a rich-reflector environment, the passive methods can only achieve 10dB of SIC. Besides, [116] discovers that the multiple paths also limit the ASIC. The AARFSIC [38, 40, 117] could efficiently eliminate the direct path of the SI. However, the residual SI caused by the reflecting multi-path is intolerable [116]. Therefore, more advanced SIC techniques are highly required to further cancel the residual multiple reflecting paths of the SI.

2.5 Conclusion and Discussion

In this Chapter, we summarize the antenna cancellation, AASIC and DSIC schemes in details. Antenna cancellation based on the specific placement of the antennas or the phase shifter can just cancel the direct path. The AARFSIC can further cancel the first path of the residual SI. For instance, if the SI channel consists of two paths: one direct path and one reflecting path, the antenna cancellation could eliminate the first path, and then the AARFSIC continues to cancel the second path. If the SI channel consists of more than two paths, antenna cancellation mitigates the direct path and AARFSIC cancels the second path and the remaining multiple paths left with the residual SI in the form of high peaks. DSICT can cancel the residual peaks completely in the digital time domain.

Here, we confront a question that why the AARFSIC just can cancel the direct path of the SI channel or the first path of the residual SI channel even with ideal transceiver RF front-ends and perfect SI channel estimation. In order to answer this question, we study deeply the AARFSIC and give the anatomy of the Full-Duplex OFDM wireless. We find that the residual SI occurs at the beginning of each OFDM symbol and the duration or the number of samples of the residual SI are determined by the time delay of the second path compared to the first path, which will be presented in details in Chapter 4.

3

Self-Interference Cancellation for Full-Duplex OFDM Wireless

Although the DSIC schemes have its own advantages in flexibility and simplification, the ADC at the receiver has a very limited dynamic range, hence it is better to cancel the strong SI as much as possible in the RF or analog domain. Therefore, in this Chapter, we first implement the AARFSIC to eliminate the direct path and part of the remaining paths of the SI. Then, we further propose to cancel the residual SI in the digital time domain by using DSICT.

Assumption: In order to highlight the fact that the strong SI could be canceled completely by combining the AARFSIC and the DSICT schemes, the transceiver RF front-ends are assumed ideal and the CSI of the SI channel can be obtained perfectly in the analysis system model.

3.1 AARFSIC for Full-Duplex OFDM Wireless

OFDM is a block modulation scheme where a block of N symbols is modulated in parallel on N subcarriers, which can be implemented by using an Inverse Discrete Fourier Transformation (IDFT). This enlightens us that the craft of cancellation signals

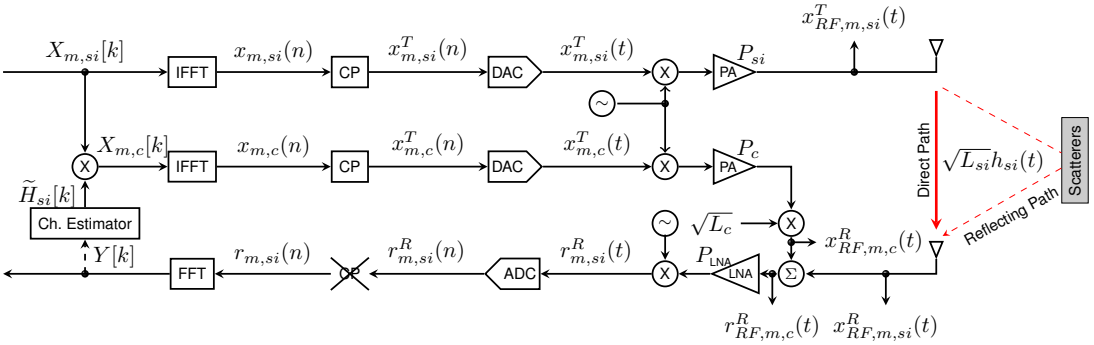

Figure 3.1: The block diagram of active analog RF self-interference cancellation.

can be carried out in each subcarrier channel and the SIC can be implemented in the analog RF domain, which we call AARFSIC (illustrated as in Fig. 3.1). In order to simplify the signal model, we just study the local Full-Duplex OFDM radio node, which means the Full-Duplex radio receiver just receives its own transmission.

Let $X_{m,si}[k], k \in [1, N]$ denotes the m^{th} symbol block which will be modulated by a N-size IDFT block. The output of the IDFT, $x_{m,si}(n), n \in [1, N]$, is corresponding to the m^{th} OFDM symbol. After inserting a N_{guard}-length cyclic prefix (CP), the new discrete time domain $(N + N_{\text{guard}})$-length OFDM symbol, $x^T_{m,si}(n), n \in [1, N + N_{\text{guard}}]$, will be converted to the analog signal, $x^T_{m,si}(t)$, by using a digital-to-analog converter (DAC). Then, the baseband analog signal, $x^T_{m,si}(t)$, is up-converted by using local oscillator with carrier frequency f_c and amplified by a High Power Amplifier (HPA) with power P_{si}, which yields the suitable transmit RF signal $x^T_{RF,m,si}(t) = \sqrt{P_{si}}x^T_{m,si}(t)e^{j2\pi f_c t}$. After emitted by the transmit antenna and going through the SI channel $\sqrt{L_{si}}h_{si}(t)$ where L_{si} denotes the path loss of the SI channel, the transmit RF signal $x^T_{RF,m,si}(t)$ is received as RF SI signal, $x^R_{RF,m,si}(t) = \sqrt{L_{si}}x^T_{RF,m,si}(t) * h_{si}(t)$, by its own receiver.

In order to implement the AARFSIC to cancel the RF SI, the estimated coefficients, $\widetilde{H}_{si}[k], k \in [1, N]$, of the SI channel $h_{si}(t)$ need to be obtained beforehand. With $\widetilde{H}_{si}[k], k \in [1, N]$ available, we craft an RF cancellation signal, $x^R_{RF,m,c}(t)$, in an auxiliary radio link. In this SI craft link, the m^{th} new symbol block, $X_{m,c}[k] = X_{m,si}[k]\widetilde{H}_{si}[k], k \in [1, N]$ instead of $X_{m,si}[k], k \in [1, N]$ is modulated by an IDFT block, which yields a discrete time domain OFDM symbol $x_{m,c}(n), n \in [1, N]$. After adding a N_{guard}-length CP, the m^{th} cancellation OFDM symbol, $x^T_{m,c}(n), n \in [1, N + N_{\text{guard}}]$, is obtained. DAC is used here to convert the discrete time domain OFDM symbol, $x^T_{m,c}(n)$, to continuous time domain OFDM signal, $x^T_{m,c}(t)$. Then, another RF front-end is used to up-convert and amplify this baseband signal to match the received RF SI. After the AARFSIC, the

residual RF SI, $r^R_{RF,m,si}(t)$, should be the difference between the received RF SI and the cancellation signal. The whole signal processing model of the AARFSIC could be expressed by

$$\begin{aligned} r^R_{RF,m,si}(t) &= x^R_{RF,m,si}(t) - x^R_{RF,m,c}(t) \\ &= \sqrt{P_{si}}\sqrt{L_{si}}\mathsf{DAC}\left\{\mathsf{CP}\{\mathsf{IDFT}\{X_{m,si}[k]\}\}\right\} e^{\jmath 2\pi f_c t} * h_{si}(t) \\ &\quad -\sqrt{P_c}\sqrt{L_c}\mathsf{DAC}\{\mathsf{CP}\{\mathsf{IDFT}\{X_{m,si}[k]\widetilde{H}_{si}[k]\}\}\}e^{\jmath 2\pi f_c t} \end{aligned} \tag{3.1}$$

where $\mathsf{IDFT}\{\chi[k]\} \triangleq \frac{1}{N}\sum_{k=-\frac{N}{2}}^{\frac{N}{2}-1}\chi[k]e^{-\jmath 2\pi\Delta f k n}$, in which Δf is the subcarrier space, $\mathsf{CP}\{\chi(n)\}$ represents the CP adding operation and $\mathsf{DAC}\{\chi(n)\} \triangleq \chi(t)$ where ideal DAC is assumed. Because of the *assumption*, it seems that the SI can be mitigated completely at the RF stage by using the AARFSIC if the emulating parameters can be obtained perfectly, i.e. $\sqrt{P_c}\sqrt{L_c} = \sqrt{P_{si}}\sqrt{L_{si}}$ and $\widetilde{H}_{si}[k] = H_{si}[k]$. However, our studies do not go into that direction as what we thought.

We can equivalently analyze and study the AARFSIC at the baseband because of the *assumption*. After digitizing the BB analog residual SI, $r^R_{m,si}(t)$, by using analog-to-digital converter (ADC), the baseband discrete-time-domain signal, $r^R_{m,si}(n)$, can be obtained as

$$\begin{aligned} r^R_{m,si}(n) &= \sqrt{P_{si}}\sqrt{L_{si}}\sqrt{P_{\mathsf{LNA}}}\mathsf{CP}\left\{\mathsf{IDFT}\{X_{m,si}[k]\}\right\} \otimes h_{si}(n) \\ &\quad -\sqrt{P_c}\sqrt{L_c}\sqrt{P_{\mathsf{LNA}}}\mathsf{CP}\left\{\mathsf{IDFT}\left\{X_{m,si}[k]\widetilde{H}_{si}[k]\right\}\right\} \end{aligned} \tag{3.2}$$

where P_{LNA} represents the amplified power level of the receiver LNA, $\otimes$ denotes circular convolution and $h_{si}(n)$ is the equivalent discrete baseband expression of the wireless SI channel $h_{si}(t)$.

Here comes the key question, if $\mathsf{CP}\{\mathsf{IDFT}\{X_{m,si}[k]\}\}\otimes h_{si}(n) = \mathsf{CP}\{\mathsf{IDFT}\{X_{m,si}[k]\widetilde{H}_{si}[k]\}\}$ for $n \in [1, N + N_{\mathsf{guard}}]$ holds even under the condition that we can obtain a perfect SI channel estimation? In order to answer this question, we study two scenarios: (i) AARFSIC for Full-Duplex OFDM wireless with one-path SI channel; (2) AARFSIC for Full-Duplex OFDM wireless with multi-path SI channel.

3.1.1 AARFSIC for One-Path Full-Duplex OFDM Wireless

In a two-antenna Full-Duplex wireless system, the power of the line-of-sight path dominates the SI channel due to the proximity between the transmit and receive antennas of the Full-Duplex radio node. Hence, it is reasonable to assume that the SI channel is one-path, which could be expressed by $h^S_{si}(n) = h_{si,0}\delta(n - n_0)$ where $h_{si,0}$ and n_0 represent the complex magnitude and delay of the wireless SI channel. The

frequency domain SI channel, $H_{si}^{S}[k]$, could be expressed as

$$\begin{aligned} H_{si}^{S}[k] &= \mathsf{DFT}\{h_{si}^{S}(n)\} \\ &= h_{si,0}e^{-\jmath 2\pi\Delta f k n_0}, k \in [1, N] \end{aligned} \tag{3.3}$$

Let $\widetilde{H}_{si}^{S}[k] = \widetilde{h}_{si,0}e^{-\jmath 2\pi\Delta f k \widetilde{n}_0}$, where $\widetilde{h}_{si,0}$ and $\widetilde{n}_0$ represent the estimate of the $h_{si,0}$ and n_0 respectively, denote the estimate of the real SI channel $H_{si}^{S}[k]$. Even for single-path SI channel, the delay could be from 0 to a large value, depending on system design. For example, when the SI channel is a short line-of-sight wireless channel, the delay n_0 should be 0. However, when the short line-of-sight path is suppressed completely by PSIS techniques or only one reflecting path exists, the delay n_0 should be at least 1, i.e. $n_0 \geq 1$.

$n_0 = 0$

When $\widetilde{n}_0 = n_0 = 0$ and after replacing $h_{si}(n)$ and $\widetilde{H}_{si}[k]$ in Eq. (3.2) by $h_{si,0}$ and $\widetilde{h}_{si,0}$ respectively, the residual SI, $r_{m,si}^{R}(n)$, could be expressed as

$$\begin{aligned} r_{m,si}^{R}(n) &= \sqrt{P_{si}}\sqrt{L_{si}}\sqrt{P_{\mathsf{LNA}}}x_{m,si}^{T}(n)h_{si,0} - \sqrt{P_c}\sqrt{L_c}\sqrt{P_{\mathsf{LNA}}}x_{m,si}^{T}(n)\widetilde{h}_{si,0} \\ &\overset{3(a)}{=} 0 \end{aligned} \tag{3.4}$$

$n_0 \geq 1$

When $n_0 \geq 1$, the received baseband SI signal in discrete time domain can be expressed as

$$\begin{aligned} x_{m,si}^{R}(n) &= \sqrt{P_{si}}\sqrt{L_{si}}\sqrt{P_{\mathsf{LNA}}}x_{m,si}^{T}(n) \otimes h_{m,si}^{S}(n) \\ &= \sqrt{P_{si}}\sqrt{L_{si}}\sqrt{P_{\mathsf{LNA}}}h_{si,0}x_{m,si}^{T}(n - n_0) \end{aligned} \tag{3.5}$$

While the baseband cancellation signal in discrete time domain can be derived and represented by

$$x_{m,c}^{T}(n) = \sqrt{P_c}\sqrt{L_c}\sqrt{P_{\mathsf{LNA}}}\widetilde{h}_{si,0}x_{m,si}^{T}(n) \tag{3.6}$$

Then, synchronizing the cancellation signal with the received SI signal via delaying $x_{m,c}^{T}(n)$ by $\widetilde{n}_0$, we can obtain the baseband cancellation signal at the receiver side as

$$x_{m,c}^{R}(n) = \sqrt{P_c}\sqrt{L_c}\sqrt{P_{\mathsf{LNA}}}\widetilde{h}_{si,0}x_{m,si}^{T}(n - \widetilde{n}_0) \tag{3.7}$$

The residual SI after the AARFSIC can be calculated as

$$\begin{aligned} r^R_{m,si}(n) &= x^R_{m,si}(n) - x^R_{m,c}(n) \\ &\overset{3(b)}{=} 0 \end{aligned} \tag{3.8}$$

$3(a)$ and $3(b)$ hold when perfect CSI of the SI channel can be obtained. That means the Eq. $\mathsf{CP}\{\mathsf{IDFT}\{X_{m,si}[k]\}\} \otimes \widetilde{h}_{si}(n) = \mathsf{CP}\{\mathsf{IDFT}\{X_{m,si}[k]\widetilde{H}_{si}[k]\}\}$ for $n \in [1, N + N_{\mathsf{guard}}]$ holds true when perfect SI channel estimation can be obtained. Therefore, the SI could be mitigated completely by using AARFSIC. However, when the SI channel estimation is influenced by the receiver thermal noise, the strong SI could only be brought down to the noise floor by AARFSIC [117, 118]. These study results are confined to anechoic Full-Duplex OFDM wireless.

3.1.2 AARFSIC for Multi-Path Full-Duplex OFDM Wireless

In a more general Full-Duplex wireless, the SI channel with high Ricean K factor [41] consists of one direct path and multiple reflecting paths. Let $h^M_{si}(n) = \sum_{\mathsf{n}_p^{si}=0}^{\mathsf{N}_p^{si}-1} h_{si,\mathsf{n}_p^{si}} \delta(n - n_{\mathsf{n}_p^{si}})$, where $h_{si,\mathsf{n}_p^{si}}$ and $n_{\mathsf{n}_p^{si}}$ represent the complex magnitude and delay of the $\mathsf{n}_p^{si th}$ path respectively, denote a N_p^{si}-path SI channel. The frequency domain SI channel, $H^M_{si}[k]$, could be expressed as

$$\begin{aligned} H^M_{si}[k] &= \mathsf{DFT}\{h^M_{si}(n)\} \\ &= \sum_{\mathsf{n}_p^{si}=0}^{\mathsf{N}_p^{si}-1} h_{si,\mathsf{n}_p^{si}} e^{-\jmath 2\pi \Delta f k n_{\mathsf{n}_p^{si}}}, k \in [1, N] \end{aligned} \tag{3.9}$$

Without loss of generality, we choose $\mathsf{N}_p^{si} = 2$, which means the SI channel is composed of one direct path and one reflecting path, to simplify the analysis of the signal model. Hence, the SI channel can be rewrote as $H^M_{si}[k] = h_{si,0} e^{-\jmath 2\pi \Delta f k n_0} + h_{si,1} e^{-\jmath 2\pi \Delta f k n_1}$. With the estimated CSI, $\widetilde{H}^M_{si}[k] = H^M_{si}[k]$, of the SI channel available, the RF cancellation signal, $x^R_{RF,m,c}(t) = \sqrt{P_c}\sqrt{L_c}\mathsf{DAC}\{\mathsf{CP}\{\mathsf{IDFT}\{X_{m,si}[k]\widetilde{H}^M_{si}[k]\}\}\}e^{\jmath 2\pi f_c t}$, could be crafted. Then, the AARFSIC can be implemented as in Eq. (3.1). This is the current AARFSIC implementation procedure even for the multi-path Full-Duplex OFDM wireless. However, the residual SI after this cancellation is still very strong, which can be as shown in Fig. 3.2. Fortunately, we can equivalently obtain and analyze the over-the-air SI signal and the cancellation signal in the discrete time domain when the transceiver RF front-ends are assumed ideal, which provides us the opportunity to insight the residual SI in discrete time domain.

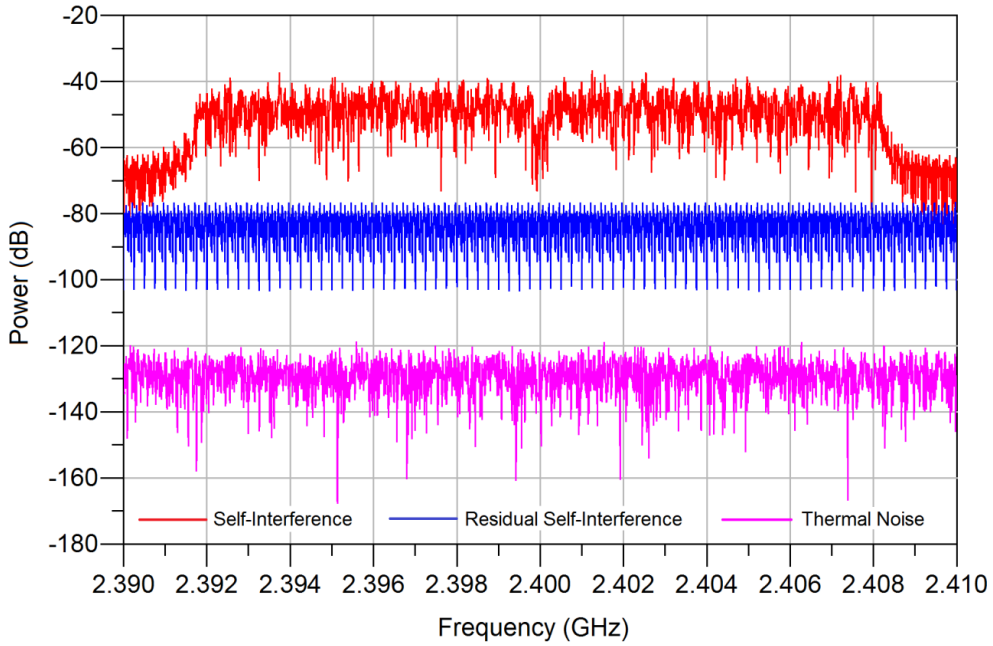

Figure 3.2: When the Full-Duplex OFDM wireless with multipath (here 2 paths SI wireless channel is considered, the second path has $50ns$ time delay and 20dB attenuation compared to the first path) SI channel, the AARFSIC has a very limited capability of SIC. As it is shown, the power of the strong SI at the antenna of the receiver is 80dB higher than the thermal noise. The AARFSIC can only achieve around 36dB SIC. Therefore, there is still 44dB residual SI.

Signal Model of the Received Self-Interference:

After experiencing the multipath SI channel, the received SI can be expressed as $x^R_{m,si}(n) = \sqrt{P_{si}}\sqrt{L_{si}}\sqrt{P_{\text{LNA}}}x^T_{m,si}(n) \otimes h^M_{si}(n)$. For simplifying the expression, we define $A_{si} \triangleq \sqrt{P_{si}}\sqrt{L_{si}}\sqrt{P_{\text{LNA}}}$. Then, the $m^{th}(m > 1)$ OFDM symbol of the received SI, $x^R_{m,si}(n)$, could be expressed in another form as

$$x^R_{m,si}(n) = \begin{cases} A_{si}[x^T_{m,si}(n)h_{si,0} + x^T_{m-1,si}(N + N_{\text{guard}} - n_1 + n)h_{si,1}], \text{for } n \in [1, n_1]; \\ A_{si}[x^T_{m,si}(n)h_{si,0} + x^T_{m,si}(n - n_1)h_{si,1}], \text{for } n \in [n_1 + 1, N + N_{\text{guard}}]. \end{cases} \tag{3.10}$$

Signal Model of the Crafted Cancellation Signal:

To craft a cancellation signal matching the SI, the AARFSIC utilizes a N-size IDFT to modulate the symbol block $X_{m,c}[k] = X_{m,si}[k]\widetilde{H}^M_{m,si}[k], k \in [1, N]$ where $\widetilde{H}^M_{si}[k] = \widetilde{h}_{si,0}e^{-\jmath 2\pi\Delta f k\tilde{n}_0} + \widetilde{h}_{si,1}e^{-\jmath 2\pi\Delta f k\tilde{n}_1}$ is the estimate of $H^M_{m,si}[k]$. The output of the IDFT

block can be expressed as a linear combination of the two-path OFDM symbols as

$$\begin{aligned} x_{m,c}(n) &= \mathsf{IDFT}\{X_{m,c}[k]\} \\ &= \widetilde{h}_{si,0}\mathsf{IDFT}\{X_{m,si}[k]e^{-\jmath 2\pi\Delta f k\widetilde{n}_0}\} + \widetilde{h}_{si,1}\mathsf{IDFT}\{X_{m,si}[k]e^{-\jmath 2\pi\Delta f k\widetilde{n}_1}\} \\ &= x^1_{m,c}(n) + x^2_{m,c}(n), n \in [1, N] \end{aligned} \tag{3.11}$$

where $x^1_{m,c}(n)$ and $x^2_{m,c}(n)$ denote the first path and the second path of the cancellation OFDM symbol respectively, which are corresponding to cancel the first path and the second path of the received SI OFDM symbols. Because of $\widetilde{n}_0 = n_0 = 0$, the first path OFDM symbol could be represented by

$$x^1_{m,c}(n) = x_{m,si}(n)\widetilde{h}_{si,0}, n \in [1, N] \tag{3.12}$$

While with respect to $x^2_{m,c}(n)$, which can be regarded as the m^{th} N-size OFDM symbol experiencing the second path of the SI channel with $\widetilde{n}_1$ delay, it can be expressed as

$$x^2_{m,c}(n) = \begin{cases} x_{m,si}(N - \widetilde{n}_1 + n)\widetilde{h}_{si,1}, \text{for } n \in [1, \widetilde{n}_1]; \\ x_{m,si}(n - \widetilde{n}_1)\widetilde{h}_{si,1}], \text{for } n \in [\widetilde{n}_1 + 1, N]. \end{cases} \tag{3.13}$$

Therefore, the m^{th} cancellation OFDM symbol, $x_{m,c}(n)$, could be rewritten as

$$\begin{aligned} x_{m,c}(n) &= x^1_{m,c}(n) + x^2_{m,c}(n), n \in [1, N] \\ &= \begin{cases} x_{m,si}(n)\widetilde{h}_{si,0} + x_{m,si}(N - \widetilde{n}_1 + n)\widetilde{h}_{si,1}, \text{for } n \in [1, \widetilde{n}_1]; \\ x_{m,si}(n)\widetilde{h}_{si,0} + x_{m,si}(n - \widetilde{n}_1)\widetilde{h}_{si,1}], \text{for } n \in [\widetilde{n}_1 + 1, N]. \end{cases} \end{aligned} \tag{3.14}$$

Then, the last N_{guard} samples of the OFDM symbol $x_{m,c}(n), n \in [1, N]$ are copied and placed at the beginning of this OFDM symbol, which yields the CP added OFDM symbol, $x^T_{m,c}(n)$.

The BB cancellation signal can be represented by $x^R_{m,c}(n) = \sqrt{P_c}\sqrt{L_c}\sqrt{P_{\mathsf{LNA}}}\mathsf{CP}\{\mathsf{IDFT}\{X_{m,si}[k]\widetilde{H}^M_{si}[k]\}\}$. Here, we define $A_c = \sqrt{P_c}\sqrt{L_c}\sqrt{P_{\mathsf{LNA}}}$. Then, the cancellation signal $x^R_{m,c}(n)$ can also be represented in another form as

$$x^R_{m,c}(n) = \begin{cases} A_c[x^T_{m,si}(n)\widetilde{h}_{si,0} + x^T_{m,si}(N - \widetilde{n}_1 + n)\widetilde{h}_{si,1}], \text{for } n \in [1, \widetilde{n}_1]; \\ A_c[x^T_{m,si}(n)\widetilde{h}_{si,0} + x^T_{m,si}(n - \widetilde{n}_1)\widetilde{h}_{si,1}], \text{for } n \in [\widetilde{n}_1 + 1, N + N_{\mathsf{guard}}]. \end{cases} \tag{3.15}$$

Comparing the Eq. (3.10) and (3.15), we can find that the equation $\mathsf{CP}\{\mathsf{IDFT}\{X_{m,si}[k]\} \otimes h_{si}(n)\} = \mathsf{CP}\{\mathsf{IDFT}\{X_{m,si}[k]\widetilde{H}_{si}[k]\}\}$ holds true for $n \in [n_1, N+N_{\mathsf{guard}}]$, while it no longer does for $n \in [1, n_1]$ even if the transceiver RF front-ends are ideal and perfect CSI of the SI channel can be obtained. Now, we find the real problem preventing the AARFSIC to

cancel the multi-path SI completely.

3.1.3 Characters of the Residual Self-Interference

As what we have presented above, the AARFSIC could bring down the strong SI to the noise floor for Full-Duplex OFDM wireless with one-path SI channel. However, for multi-path SI channel, the AARFSIC has very limited capability of SIC. Comparing Eq. (3.10) to (3.15), we find that the "non-zero" residual SI always occurs at the beginning of each OFDM symbol in the discrete time domain and the number of the "non-zero" samples is n_1 which represents the delay of the second path of the SI channel. When $A_{si} = A_c$ and $\widetilde{H}_{si}^{M}[k] = H_{si}^{M}[k]$, the residual SI of the $m^{th}(m > 1)$ OFDM symbol after the AARFSIC could be expressed as

$$\begin{aligned} r_{m,si}^{R}(n) &= x_{m,si}^{R}(n) - x_{m,c}^{R}(n) \\ &= \begin{cases} A_{si}h_{si,1}[x_{m-1,si}^{T}(N + N_{\text{guard}} - n_1 + n) \\ -x_{m,si}^{T}(N - n_1 + n)], n \in [1, n_1]; \\ 0, n \in [n_1 + 1, N + N_{\text{guard}}]. \end{cases} \end{aligned} \tag{3.16}$$

This shows that the first path SI is canceled completely and part of the second path remains as the residual SI. Besides, we can see that A_{si}, $h_{si,1}$ and n_1 are the factors that determine the power of the residual SI. The amount of dB of the SIC the AARFSIC can achieve even with ideal RF front-ends and perfect SI channel estimation is computed as

$$\begin{aligned} \alpha_{\text{AARFSIC}}(dB) &= \mathsf{E}\{|x_{m,si}^{R}(n)|^2\}_{dB} - \mathsf{E}\{|r_{m,si}^{R}(n)|^2\}_{dB} \\ &= \mathsf{dB}\Big[\frac{[\mathsf{E}\{|h_{si,0}|^2\} + \mathsf{E}\{|h_{si,1}|^2\}](N + N_{\text{guard}})}{2\mathsf{E}\{|h_{si,1}|^2\}n_1}\Big] \\ &\overset{3(c)}{\approx} \mathsf{dB}\Big[\frac{\mathsf{E}\{|h_{si,0}|^2\}(N + N_{\text{guard}})}{2\mathsf{E}\{|h_{si,1}|^2\}n_1}\Big] \end{aligned} \tag{3.17}$$

where $\mathsf{E}\{\chi(n)\}$ is defined as calculating the expectation of the variable $\chi(n)$. The approximation $(3(c))$ holds when the path gain of the second path is much smaller than that of the first path, i.e. $|h_{si,1}| \ll |h_{si,0}|$. As we can see in Eq. (3.17), the amount of SIC the AARFSIC can achieve is determined by the second path of the SI channel. Specifically, given the magnitude $h_{si,0}$ and $h_{si,1}$ are fixed, the larger the delay n_1, the less the amount of SIC the AARFSIC can achieve; when the delay $h_{si,0}$ and n_1 are fixed, the higher the magnitude $h_{si,1}$, the less amount of SIC the AARFSIC can achieve. When the worst scenario occurs in the practical wireless communications, $n_1 = N_{\text{guard}}$, $\alpha_{\text{AARFSIC}}(dB) = \mathsf{dB}\big[\frac{\mathsf{E}\{|h_{si,0}|^2\}\cdot(N+N_{\text{guard}})}{\mathsf{E}\{|h_{si,1}|^2\}\cdot 2N_{\text{guard}}}\big] = \mathsf{dB}\big[\frac{\mathsf{E}\{|h_{si,0}|^2\}}{\mathsf{E}\{|h_{si,1}|^2\}}\big] + 3.9794dB$, which means the

AARFSIC can only cancel 4dB more of SI except for the cancellation of the direct path. For instance, the AARFSIC can achieve 14dB of SIC when the second path has 10dB attenuation compared to the first path.

In order to demonstrate our theoretical analysis, we implement a waveform simulation constructed on the ADS (Advanced Design System, Agilent) and Matlab software. The co-simulation results match the theoretical analysis well, which is shown in Fig. 3.3. We define the power ratio of the direct-path to the reflect-path as $DRR \triangleq \frac{\mathsf{E}\{|h_{si,0}|^2\}}{\mathsf{E}\{|h_{si,1}|^2\}}$ here. We can find that the strength of the residual SI after the AARFSIC is de-

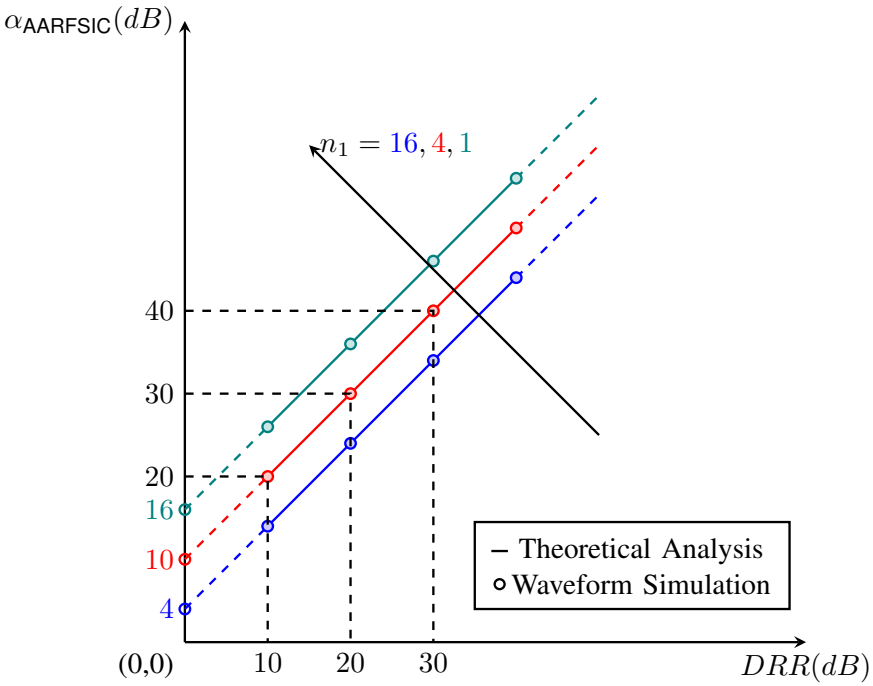

Figure 3.3: The amount of SIC by AARFSIC when the SI channel consists of a direct path and one reflecting path.

pendent on the wireless environments. In the indoor wireless environment, although the time delay is small, the second path experiences less path loss. Therefore, the AARFSIC has a very limited capability of SIC. As it is shown in Fig. 3.3, the AARFSIC can only achieve 26dB of SIC when the reflecting path has small delay ($n_1 = 1$) and small relative path loss ($DRR = 10$dB). While with respect to the outdoor with less reflecting path or anechoic chamber, although the reflecting paths have large time delay, they also experience larger path loss. In this scenario, the AARFSIC can achieve more SIC. For example, even with the largest delay $n_1 = N_{\mathsf{guard}} = 16$, if the reflecting path experiences large path loss, $DRR = 40$dB, the AARFSIC could achieve 44dB of SIC. Therefore, the strength of the reflecting paths have bigger influence on the capability

of the AARFSIC than that of the delay. Of course, the smaller the delay n_1 and the larger the power difference DRR, the greater amount of SIC the AARFSIC can achieve.

The study results above tell us that the SI can not be canceled completely by only using AARFSIC, because the reflecting paths have unexpected delay and unnegligible power strength compared to the direct path. The measurement-based characters of the residual SI after the AARFSIC has been studied in [11]. Therefore, further implementation of residual SIC is highly required.

3.2 Digital SIC in Time Domain

We discovered that the residual SI in the discrete time domain, $r^R_{m,si}(n)$, is closely related to the transmitted symbols, $x^T_{m,si}(n)$, which knowledge is available to the Full-Duplex radio node. Therefore, we propose to cancel the residual SI in the discrete time domain, which is as shown in Fig. 3.4. As we can see, the factor, $A_c = \sqrt{P_c}\sqrt{L_c}\sqrt{P_{\text{LNA}}}$ which is the estimate of the transmission factor $A_{si} = \sqrt{P_{si}}\sqrt{L_{si}}\sqrt{P_{\text{LNA}}}$, is required to implement the DSICT.

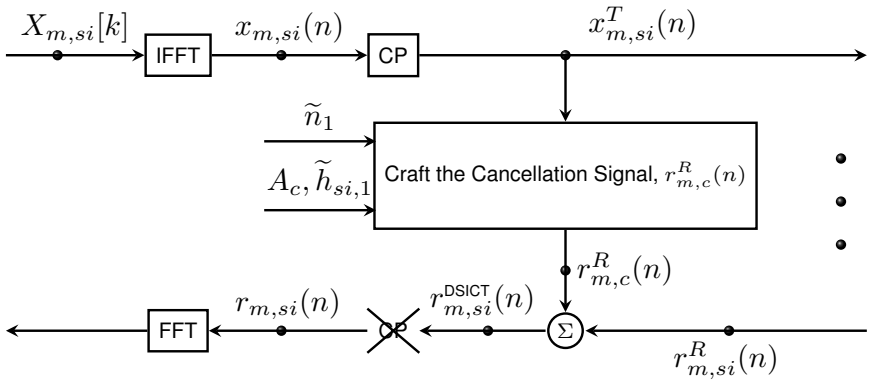

Figure 3.4: The block diagram of DSICT.

With A_c and the estimated $\widetilde{h}_{si,1}, \widetilde{n}_1 = n_1$ available, the baseband cancellation signal, $r^R_{m,c}(n)$, could be crafted as

$$r^R_{m,c}(n) = \begin{cases} A_c \widetilde{h}_{si,1}[x^T_{m-1,si}(N + N_{\text{guard}} - n_1 + n) - x^T_{m,si}(N - n_1 + n)], \text{for } n \in [1, n_1]; \\ 0, \text{for } n \in [n_1 + 1, N + N_{\text{guard}}]. \end{cases} \tag{3.18}$$

Then, the DSICT can be implemented as

$$\begin{aligned} r_{m,si}^{\mathsf{DSICT}}(n) &= r_{m,si}^{R}(n) - r_{m,c}^{R}(n) \\ &= \begin{cases} (A_{si}h_{si,1} - A_c\widetilde{h}_{si,1})[x_{m-1,si}^{T}(N + N_{\mathsf{guard}} - n_1 + n) \\ -x_{m,si}^{T}(N - n_1 + n)], \text{for } n \in [1, n_1]; \\ 0, \text{for } n \in [n_1 + 1, N + N_{\mathsf{guard}}]. \end{cases} \end{aligned} \tag{3.19}$$

where we can see that the residual SI can be eliminated completely by the proposed DSICT if the ideal estimate of A_{si} and $h_{si,1}$ can be obtained, i.e. $A_c = A_{si}$ and $\widetilde{h}_{si,1} = h_{si,1}$.

A perfect channel estimation is impossible in practical wireless communications, while it is possible to guarantee $A_c = A_{si}$. Then, the residual SI after DSICT can be modeled as

$$r_{m,si}^{\mathsf{DSICT}}(n) = \begin{cases} A_{si}\Delta h_{si,1}[x_{m-1,si}^{T}(N + N_{\mathsf{guard}} - n_1 + n) - x_{m,si}^{T}(N - n_1 + n)], \\ \text{for } n \in [1, n_1]; \\ 0, \text{for } n \in [n_1 + 1, N + N_{\mathsf{guard}}]. \end{cases} \tag{3.20}$$

where $\Delta h_{si,1} \triangleq h_{si,1} - \widetilde{h}_{si,1}$ denotes the estimate error of $h_{si,1}$.

The amount of SIC the DSICT achieves can be computed as

$$\begin{aligned} \alpha_{\mathsf{DSICT}}(dB) &= \mathsf{E}\{|r_{m,si}(n)|^2\}_{dB} - \mathsf{E}\{|r_{m,si}^{\mathsf{DSICT}}(n)|^2\}_{dB} \\ &= \mathsf{dB}[\frac{\mathsf{E}\{|h_{si,1}|^2\}}{\mathsf{E}\{|\Delta h_{si,1}|^2\}}] \end{aligned} \tag{3.21}$$

For the Full-Duplex OFDM wireless with two-path SI channel, the power of the residual SI after the AARFSIC and DSICT is closely related to the channel estimation of the second path. We can calculate the power of the residual SI after the ADSICT as

$$\begin{aligned} P_{\mathsf{ADSICT}}^{\mathsf{AARFSIC}} &= \mathsf{E}\{|r_{m,si}^{\mathsf{ADSICT}}(n)|^2\} \\ &= \mathsf{dB}[\frac{2n_1\mathsf{E}\{|A^R|^2\}\mathsf{E}\{|\Delta h_{si,1}|^2\}\mathsf{E}\{|x_{m,si}^{T}(n)|^2\}}{N + N_{\mathsf{guard}}}] \end{aligned} \tag{3.22}$$

Apparently, the residual SI after the AARFSIC can be mitigated completely by using ADSICT when the magnitude of the second path can be obtained perfectly.

3.3 Conclusion and Discussion

Finally, we would like to comment on the AARFSIC. AARFSIC is a simple but effective way to cancel the strong SI. However, the co-simulation results have demonstrated that the AARFSIC could bring down the single path SI to the noise level. In a multiple-reflector wireless environment, the AARFSIC could only eliminate the direct path and parts of the remaining multiple paths, which means that the AARFSIC has a very limited capability of SIC for the Full-Duplex OFDM wireless with multi-path SI channel. Therefore, ASIC after the AARFSIC is highly required to further cancel the residual SI. In this dissertation, a DSICT scheme is proposed to eliminate the residual SI. Although the wireless SI channel chosen for this analysis study is a two-path channel, the analysis model can be extended to multi-path SI channel scenario, e.g. $\mathsf{N}_p^{si} \geq 3$.

Part II

Full-Duplex OFDM Wireless Radios

4

Full-Duplex OFDM Radio Design

For wireless engineers, the strong SI made unthinkable the implementation of a real Full-Duplex system until the research articles [20, 30, 38, 39, 55, 95]. The authors combine the methods of passive and active SIC together to reduce the strength of the SI to a tolerable level, which enlightens us that the Full-Duplex wireless is actually feasible. More literatures on the SIC schemes can be found in Chapter 2.

In this Chapter, 20MHz in-band two-antenna Full-Duplex OFDM wireless systems with a one-path SI channel and a multi-path SI channel are studied respectively. (i) *Full-Duplex OFDM wireless with a one-path SI channel:* The SI channel between the transmit antenna and receive antenna is assumed to be a line-of-sight channel with one single dominant path. This assumption relies on the fact that the strength of the line-of-sight path dominates the power of the SI channel when the distance between the transmit antenna and receive antenna at the Full-Dull radio node is of few centimeters while the reflecting paths should be in meters, therefore considered as negligible in this first study. For the single path SI channel, the relatively simple AARFSIC can significantly reduce the SI to the noise level for the design of Full-Duplex OFDM wireless. However, this study is confined to the anechoic Full-Duplex OFDM wireless, like outdoor without multiple reflecting paths or anechoic chamber; (ii) *Full-Duplex OFDM wireless with a multi-path SI channel:* With respect to a more general and practical wireless scenario, the SI channel, including the direct path and multiple reflecting paths,

should be a multi-path fading channel with a high Ricean factor K. In order to cancel the multi-path SI signal, more taps in the analog cancellation circuit are needed to emulate the SI channel and then craft the cancellation signal [24] or a DSICT method is required to follow the AARFSIC to cancel the remaining multi-path SI [116]. The system designs are carried out on ADS and Matlab software. Most of the baseband systems and RF front-ends are modeled by using ADS and parts of the digital components, e.g. time synchronization and the DSICT scheme, are implemented on Matlab.

Before presenting in details our design and finds on the two-antenna Full-Duplex OFDM wireless, the summary of the state-of-art of the Full-Duplex OFDM wireless designs are given at first.

4.1 State-of-the-Art of the Full-Duplex Prototype

Up to date, the practical designs of the Full-Duplex wireless [23, 24, 30, 48, 55] have made it extremely feasible to implement a real Full-Duplex radio by using a combination of passive and active SIC techniques. Especially in [24], a point-to-point one-antenna Full-Duplex radio link is built by implementing the SIC schemes on the off-the-shelf radios. The authors use an extra analog cancellation circuit to emulate the strong paths of the SI channel and craft the RF cancellation signal. In the analog cancellation circuit, a certain number of taps, each with delay d_i and magnitude a_i, are utilized to match the strong SI paths which consist of the leaked path due to the imperfection of the circulator and the reflecting paths from the near-field region of the antenna. This AARFSIC combining with the circulator isolation which can contribute 15dB of SI isolation could achieve 72dB of SIC for a 20MHz OFDM signal and even for the transmitter thermal noise. After the AARFSIC, they propose a DSICF to cancel the residual SI including the leaked SI path through the circulator after the analog cancellation and the reflecting paths from the far-field region. This digital cancellation can bring down the residual SI to roughly 1dB higher than the noise floor of a Half-Duplex radio. They prototype the design by using the radio test equipment from Rohde and Schwarz and also on WARP radio boards. In [23], a near-ideal in-band Full-Duplex MIMO radio system is designed and implemented. They prototype a 3×3 Full-Duplex MIMO radio using the off-the-shelf WiFi radios.

Another practical design [38, 40] has formulated the experiment-based characterization of a Full-Duplex OFDM wireless system. The authors demonstrate that the amount of total ASIC decrease if the amount of PSIS increase, while the total amount of SIC increase if the amount of PSIS increase. They also found that the total amount of the active cancellation is not the linear addition of the amount of SIC by AASIC and

the amount of SIC by ADSIC individually. The total amount of ASIC is limited by the power of the received SI. This means the more amount of SIC the AASIC can achieve, the less ADSIC it can obtain, and vice versa. Obviously, it is not necessary to cascade an ADSIC to follow the AASIC if the SI is completely eliminated in the analog domain. Thus, the ADSIC is optional, because it can only cancel the residual SI related with the SI signal. Even after the implementation of antenna, analog and digital SIC, the power of the residual SI is still 15dB higher than the thermal noise floor. Based on this design, they prototype a two-antenna Full-Duplex OFDM radio based on the WARP radio.

The other practical design [21, 22] uses the AARFSIC which is similar to the scheme in [38, 39] to cancel the strong SI at the RF analog domain. Based on the AARFSIC, they prototype two Full-Duplex OFDM radios: (i) one-antenna Full-Duplex OFDM radio and (ii) two-antenna Full-Duplex OFDM radio, on the National Instruments FlexRIO device with two FlexRIO 5791R RF transceiver modules. In the one-antenna Full-Duplex OFDM wireless, a total 77dB of SIC can be achieved. The circulator could isolate up to 18dB and AARFSIC could achieve 37dB of cancellation. With a shared local oscillator between the transmitter and cancellation links, the AARFSIC could achieve an additional 12dB and up to 49dB of SIC. After the AARFSIC, the digital cancellation can not achieve any SIC due to the reason that at this point the residual SI is dominated by the transmitter noise and the SI channel estimation error. However, they can further suppress 10dB of SIC by using a genie suppression based on the fact that the residual SI closely related to the transmitted signal is cancelable. While in the two-antenna Full-Duplex OFDM wireless, a total 87dB of SIC can be achieved. 39dB of SIC is obtained by separating the transmit and receive antennas by 30cm for a signal at 2.4GHz ISM band. In this scenario, the AARFSIC can achieve 46dB of SIC and the digital cancellation can contribute 2dB of SIC respectively. However, the genie suppression can not cancel any SI, because the cancelable residual SI has been canceled completely.

For more system level designs of Full-Duplex wireless, please refer to [17, 33, 49, 61, 75, 88, 125].

4.2 General System Model of Full-Duplex OFDM Wireless

Before presenting the system design in details, a general system model of Full-Duplex OFDM wireless is given beforehand to help to have a comprehensive understanding.

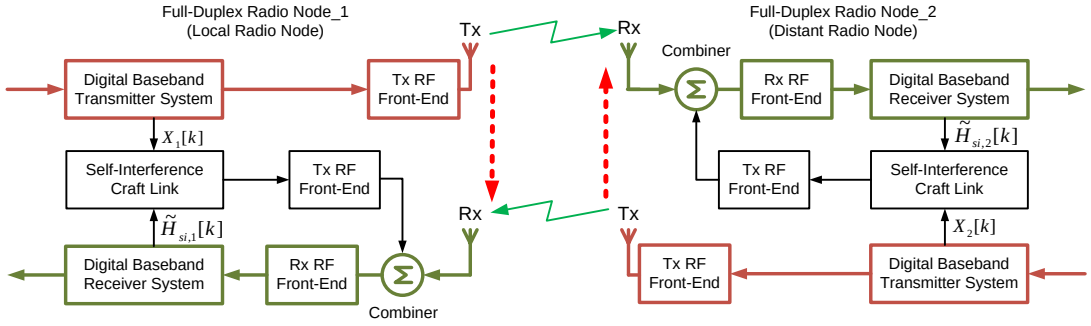

Figure 4.1: Block diagram of a Full-Duplex wireless transmission.

4.2.1 Signal Model

In Half-Duplex wireless system, the transceiver uses orthogonal radio resources for transmitting and receiving signals. While in Full-Duplex wireless system, the transceiver transmits and receives signals simultaneously on the same frequency. Fig. 4.1 shows the block diagram of a two-antenna Full-Duplex architecture. As this is a symmetric problem, we just study the Full-Duplex radio node-1, i.e. local radio node. The transmitted signal of the local radio node not only goes through the multi-path fading channel and arrives at the receive antenna of the distant radio node but also experiences the line-of-sight wireless channel and arrives at the receive antenna of the local radio node. Therefore, the received signal of each of these two radio nodes is composed of the signal of interest, the strong SI and the thermal noise. Then, the received signal of the local radio node without SIC can be expressed as

$$\begin{aligned} y(t) &= x^R_{RF}(t) + x^R_{RF,si}(t) + w(t) \\ &= \sqrt{P}\sqrt{L}x(t)e^{j2\pi f_c t} * h(t) + \underbrace{\sqrt{P_{si}}\sqrt{L_{si}}x_{si}(t)e^{j2\pi f_c t} * h_{si}(t)}_{\text{self-interference}} + w(t) \end{aligned} \quad (4.1)$$

where P and P_{si} denote the transmit power of the distant radio node and local radio node respectively, L and L_{si} represent the distant fading loss of the desired radio link and the SI radio link respectively, $x(t)$ and $x_{si}(t)$ are the transmitted signals from the distant radio node and the local radio node respectively, $h(t)$ and $h_{si}(t)$ denote the wireless fading channel of the intended radio link and the SI link, "$*$" denotes the convolution and $w(t)$, following the normal distribution $\mathcal{N}(0, \delta_n^2)$, represents the receiver thermal noise in the time domain.

Due to the proximity between the transmit antenna and receive antenna of the local radio node, L_{si} is much stronger than L. Therefore, the SI signal is much stronger than the signal of interest which relies on a reasonable assumption that the distant radio

node and the local radio node have the same transmit power level, i.e. $P = P_{si}$.

At the receiver side, the total received signal is scaled by the automatic gain controller (AGC) to the full dynamic range of ADC, and then it is digitized and quantized by the ADC. The stronger the SI is, the fewer useful information is included in the digital samples, because the number of the resolution bits of the ADC is limited. In order to reduce this strong SI signal for implementing a Full-Duplex radio, AASIC is required to be implemented before the ADC. The AASIC is largely dependent on the SI channel estimation, hence we discuss briefly the channel model at first.

4.2.2 Channel Model

In the indoor environment, the wireless channel between different nodes can be modeled as a typical indoor WLAN channel. Here, the indoor WLAN channel is assumed to be quasi-static. In other words, the channel condition is considered to be static during each transmit frame. The channel impulse response $h(t)$ can be expressed as

$$h(t) = \sum_{\mathsf{n}_p=0}^{\mathsf{N}_p-1} h_{\mathsf{n}_p}\delta(t-\tau_{\mathsf{n}_p}) \tag{4.2}$$

where N_p is the total number of propagation paths, h_{n_p} is the complex impulse response of the ${\mathsf{n}_p}^{th}$ path, t is the delay spread index and τ_{n_p} is the delay of the ${\mathsf{n}_p}^{th}$ path.

The characterization of the SI channel are quite different from that of the multi-path fading channel. As a consequence of the proximity between the transmit and receive antenna, the power of the line-of-sight path dominates the power of the SI channel. Therefore, the SI channel is assumed to be a one-path channel or a multi-path channel with high Ricean factor. The channel impulse response can be represented by

$$h_{si}(t) = \sum_{\mathsf{n}_p^{si}=0}^{\mathsf{N}_p^{si}-1} h_{si,\mathsf{n}_p^{si}}\delta(t-\tau_{si,\mathsf{n}_p^{si}}) \tag{4.3}$$

where $h_{si,\mathsf{n}_p^{si}}$ and $\tau_{si,\mathsf{n}_p^{si}}$ denote the complex impulse response and the delay of the ${\mathsf{n}_p^{si}}^{th}$ path of the SI channel, N_p^{si} represents the total number of the SI paths.

4.2.3 Channel Estimation

Typical channel estimation is either performed in the time domain to measure the channel impulse response or carried out in the frequency domain for estimating the

transfer function in the specific frequency. In order to construct the cancellation signal in each subcarrier channel, the channel estimation is carried out in the frequency domain here. Due to the maturity of IEEE 802.11g standard, we choose it as the PHY technique in this dissertation. In each frame of the IEEE 802.11g, the preamble consists of 10 identical short OFDM symbols each of length 16 and 2 identical long OFDM symbols each of length 64. Each long OFDM symbols is generated via IFFT of the $N_{nz} = 52$ known BPSK symbols $T[k], k \in [1, N_{nz}]$ and 12 nulls. The estimates of the coefficients of the N_{nz} subcarrier channels is carried out via dividing the received long OFDM symbols by the N_{nz} known symbols. The k^{th} subcarrier channel can be estimated as

$$\widetilde{H}[k] = \frac{Y[k]}{T[k]}, k \in [1, N_{nz}] \tag{4.4}$$

where $Y[k]$ denotes the received symbol carried by the k^{th} subcarrier in the frequency domain.

Even small error of the subcarrier channel estimation may cause a large residual SI. The researchers in [27] have studied the impact of the channel estimation error on the in-band Full-Duplex. In order to avoid the impact of the SI channel estimation errors induced by the signal of interest from the distant radio node, the long training symbols from different radio nodes are assigned on the orthogonal time slots for transmission. Therefore, the receive antenna just receives the long training symbol from its own transmission during the SI channel estimation. Then, the received long training symbols could be expressed as

$$Y_{si}^{LTS}[k] = \sqrt{P_{si}}\sqrt{L_{si}}\sqrt{P_{\mathsf{LNA}}}T[k]H_{si}[k] + W[k] \tag{4.5}$$

where $Y_{si}^{LTS}[k]$ denotes the received SI long training symbol carried by the k^{th} subcarrier, P_{LNA} represents the amplified power level of the receiver LNA, $H_{si}[k]$ is the real SI channel and $W[k]$ denotes frequency-domain expression of the receiver thermal noise $w(t)$.

Then, we can replace $Y[k]$ in Eq. (4.4) by Eq. (4.5) and normalize it as

$$\begin{aligned} \widetilde{H}_{si}[k] &= \frac{Y_{si}^{LTS}[k]}{\sqrt{P_{si}}\sqrt{L_{si}}\sqrt{P_{\mathsf{LNA}}}T[k]} \\ &= H_{si}[k] + \frac{W[k]}{\sqrt{P_{si}}\sqrt{L_{si}}\sqrt{P_{\mathsf{LNA}}}T[k]}, k \in [1, N_{nz}] \end{aligned} \tag{4.6}$$

After that, the implementation of the AARFSIC at the RF stage based on the estimate of the coefficient of each SI subcarrier channel can be carried out to design a Full-Duplex OFDM wireless system as following.

4.3 Full-Duplex OFDM Wireless with One-Path SI Channel

With respect to the Full-Duplex OFDM wireless with single-path SI channel, the strong SI could be brought down to the noise floor [117, 118] by only using AARFSIC when the transceiver RF front-ends are ideal. Therefore, it is not necessary to implement a digital SIC following the AARFSIC to cancel the residual SI.

Given that the wireless SI channel is a one-path one-delay channel, i.e. $\mathsf{N}_p^{si} = 1$, the SI channel model in Eq. (4.3) could be modified as $h_{si}^S(t) = h_{si,0}\delta(t - \tau_{si,0})$. After digitizing, the discrete-time-domain SI channel could be $h_{si}^S(n) = h_{si,0}\delta(n - n_{si,0})$. This channel model in the frequency domain could be expressed by $H_{si}^S[k] = h_{si,0}e^{-\jmath 2\pi\Delta f k n_{si,0}}$ as in (3.3).

4.3.1 Active Analog RF Self-Interference Cancellation

In the analysis signal model of the Full-Duplex OFDM wireless with AARFSIC, the RF front-ends of the transceivers are assumed to be ideal, i.e. the dynamic range of DAC/ADC is large enough, phase noise (PN) does not exist in the local oscillator and there is no I/Q imbalance. Transmit continuous baseband signal can be formulated by cascading the time domain OFDM symbols one by one. By up-converting this baseband signal, RF signal which is to be emitted from the transmit antenna is generated.

In practice, each OFDM symbol is generated by using an inverse DFT to modulate a symbol block. Let $X_{m,si}[k]$ denote the symbol, to be carried by the k^{th} subcarrier, of the m^{th} symbol block. Then, the m^{th} N-length OFDM symbol can be obtained as

$$\begin{aligned} x_{m,si}(n) &= \mathsf{IDFT}\left\{X_{m,si}[k]\right\} \\ &= \frac{1}{N}\sum_{k=-\frac{N}{2}}^{\frac{N}{2}-1} X_{m,si}[k]e^{\jmath 2\pi\Delta f k n}, n \in [1, N] \end{aligned} \tag{4.7}$$

After adding a CP to each original OFDM symbol and converting it to the continuous time domain signal by using a DAC, the m^{th} OFDM symbol could be expressed as

$$x_{m,si}^T(t) = \mathsf{DAC}\{\mathsf{CP}\{x_{m,si}(n)\}\}, (m-1)T \leq t < mT \tag{4.8}$$

where T is the time interval of each OFDM symbol. After cascading them one by one, the continuous time domain baseband SI signal $x_{si}(t)$ is generated.

In order to simplify the analysis of the signal model in Eq. (4.1), we just extract the

m^{th} OFDM symbol based signal as

$$\begin{aligned} y^S_m(t) &= x^R_{RF,m}(t) + x^{R,S}_{RF,m,si}(t) \\ &= \sqrt{P}\sqrt{L}x^T_m(t)e^{\jmath 2\pi f_c t} * h(t) + \underbrace{\sqrt{P_{si}}\sqrt{L_{si}}x^T_{m,si}(t)e^{\jmath 2\pi f_c t} * h^S_{si}(t)}_{\text{self-interference}} \\ &\quad + w(t), (m-1)T \le t < mT \end{aligned} \tag{4.9}$$

where $x^{R,S}_{RF,m,si}(t)$ denotes the received RF SI signal which experienced a single path SI channel. For simplifying the expression, $(m-1)T \le t < mT$ will be dropped in the following formulas.

The SI term in Eq. (4.9) is much stronger than the signal of interest. Therefore, canceling or eliminating the strong SI is the key first step for implementing a Full-Duplex OFDM radio. For combating the strong SI, we first craft the SI in the digital frequency domain and then carry out the SIC in the RF stage as presented in details in the developed SIC scheme for Full-Duplex OFDM wireless in the Chapter 3. The RF cancellation signal $x^{R,S}_{RF,m,c}(t)$, corresponding to the cancellation of the SI signal $x^{R,S}_{RF,m,si}(t)$ in Eq. (4.9), is constructed as

$$x^{R,S}_{RF,m,c}(t) = \sqrt{P_c}\sqrt{L_c}x^{C,S}_{m,c}(t)e^{\jmath 2\pi f_c t} \tag{4.10}$$

where P_c and L_c are the parameters chosen for matching the P_{si} and L_{si} respectively in the cancellation link. The baseband cancellation signal, $x^{C,S}_{m,c}(t)$, can be expressed as

$$x^{C,S}_{m,c}(t) = \mathsf{DAC}\{\mathsf{CP}\{x^S_{m,c}(n)\}\} \tag{4.11}$$

where $x^S_{m,c}(n) = \mathsf{IDFT}\{X_{m,si}[k]\widetilde{H}^S_{si}[k]\} = \frac{1}{N}\sum_{k=-\frac{N}{2}}^{\frac{N}{2}-1} X_{m,si}[k]\widetilde{H}^S_{si}[k]e^{\jmath 2\pi \Delta f k n}, n \in [1, N]$. After the SI channel estimation as in Eq. (4.6), the estimate of $H^S_{si}[k]$ could be as

$$\widetilde{H}^S_{si}[k] = \widetilde{h}_{si,0}e^{-\jmath 2\pi \Delta f k \tilde{n}_{si,0}} \tag{4.12}$$

where $\widetilde{h}_{si,0}$ and $\widetilde{n}_{si,0}$ are the estimate of $h_{si,0}$ and $n_{si,0}$.

With the SI channel estimation $\widetilde{H}^S_{si}[k]$ available, the baseband cancellation signal can be crafted as

$$\begin{aligned} x^S_{m,c}(n) &= \mathsf{IDFT}\{X_{m,si}[k]\widetilde{H}^S_{si}[k]\} \\ &= \widetilde{h}_{si,0}\mathsf{IDFT}\{X_{m,si}[k]e^{-\jmath 2\pi \Delta f k \tilde{n}_{si,0}}\} \\ &= \widetilde{h}_{si,0}x_{m,si}(n - \widetilde{n}_{si,0}) \end{aligned} \tag{4.13}$$

Then, the RF cancellation signal would be

$$\begin{aligned} x^{R,S}_{RF,m,c}(t) &= \sqrt{P_c}\sqrt{L_c}x^{C,S}_{m,c}(t)e^{\jmath 2\pi f_c t} \\ &= \sqrt{P_c}\sqrt{L_c}\mathsf{DAC}\{\mathsf{CP}\{x^{S}_{m,c}(n)\}\}e^{\jmath 2\pi f_c t} \\ &= \sqrt{P_c}\sqrt{L_c}\widetilde{h}_{si,0}\mathsf{DAC}\{\mathsf{CP}\{x_{m,si}(n-\widetilde{n}_{si,0})\}\}e^{\jmath 2\pi f_c t} \\ &= \sqrt{P_c}\sqrt{L_c}\widetilde{h}_{si,0}x^{T}_{m,si}(t-\widetilde{\tau}_{si,0})e^{\jmath 2\pi f_c t} \end{aligned} \tag{4.14}$$

The RF SI signal, after experiencing the wireless SI channel $h^{S}_{si}(t) = h_{si,0}\delta(t-\tau_{si,0})$, received by the local radio node can be represented by

$$x^{R,S}_{RF,m,si}(t) = \sqrt{P_{si}}\sqrt{L_{si}}h_{si,0}x^{T}_{m,si}(t-\tau_{si,0})e^{\jmath 2\pi f_c t} \tag{4.15}$$

Then, the residual RF SI, $r^{R,S}_{RF,m,si}(t)$, could be expressed by

$$\begin{aligned} r^{R,S}_{RF,m,si}(t) &= x^{R,S}_{RF,m,si}(t) - x^{R,S}_{RF,m,c}(t) \\ &= \sqrt{P_{si}}\sqrt{L_{si}}h_{si,0}x^{T}_{m,si}(t-\tau_{si,0})e^{\jmath 2\pi f_c t} \\ &\quad -\sqrt{P_c}\sqrt{L_c}\widetilde{h}_{si,0}x^{T}_{m,si}(t-\widetilde{\tau}_{si,0})e^{\jmath 2\pi f_c t} \end{aligned} \tag{4.16}$$

where we can find that the SI could be eliminated completely when the perfect channel estimation could be obtained. This could be demonstrated by the waveform simulation as in Fig. 4.2. Here, we define the power ratio of the received SI signal to the receiver thermal noise as INR. As it can be seen in Fig. 4.2 (a), when the INR=20dB, the residual SI after the AARFSIC is almost at the noise level. Even in Fig. 4.2 (b) (c), INR=40dB, INR=60dB, the residual SI signals after AARFSIC are also extremely close to the noise level. By comparison, the spectrum power of the received SI is much stronger than the residual SI. Therefore we can conclude that the strong SI can be significantly reduced to almost noise level by using the AARFSIC when the transceiver RF front-ends are ideal and the SI channel is a single path wireless channel. This conclusion can also be further confirmed by Fig. 4.3.

In Fig. 4.3, once INR$\geq$20dB, the SI can be brought down to the noise floor; while once INR$<$15dB, there is some unexpected residual SI. From INR=5dB to INR= 15dB, the higher the INR is, the less residual SI occurs. This is because the AARFSIC is largely dependent on the quality of the SI channel estimation. Once the INR is low, the accurate SI channel estimation can not be guaranteed, hence the AARFSIC can not perform the expected SIC. While once the INR is high enough, the SI channel can be estimated accurately, so the strong SI can be brought down to the noise level by the AARFSIC. However, even for INR=60dB, which means the CSI of the SI channel can be obtained accurately, there is still 3dB residual SI, which will be explained in the following.

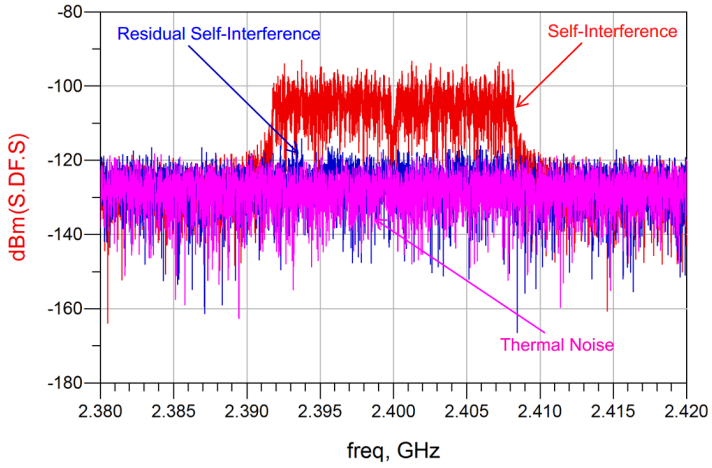

(a). INR=20dB

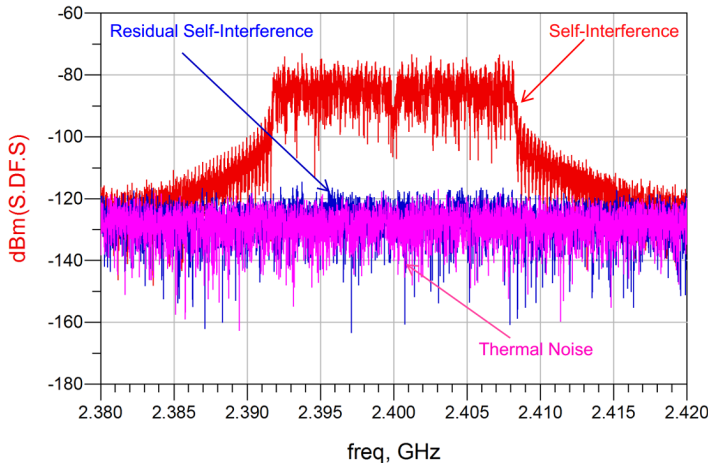

(b). INR=40dB

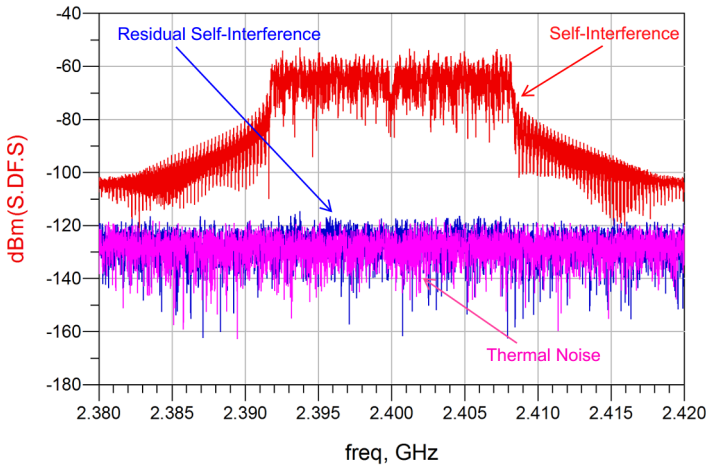

(c). INR=60dB

Figure 4.2: **One-path SI channel:** Comparison of the spectrum power (dBm) of the SI before and after the AARFSIC with different INR . (ADS simulation)

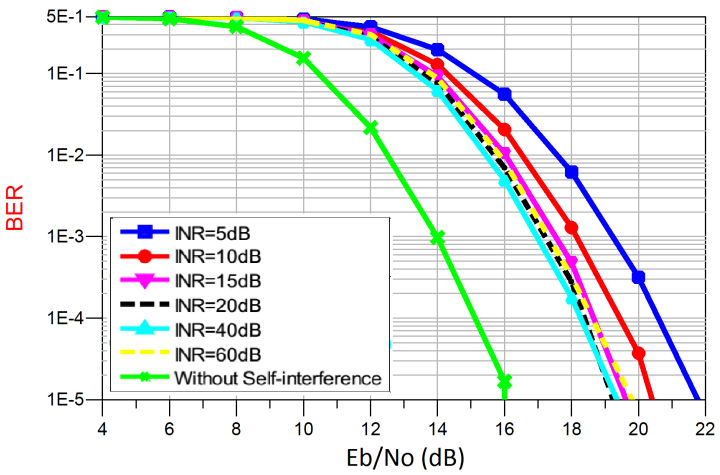

Figure 4.3: **One-path SI channel:** The BER performance comparison of the Full-Duplex OFDM wireless with different INR.

4.3.2 Effect and Mitigation of RF Impairments

The Full-Duplex OFDM wireless radio without any RF impairments has been studied above. However, RF impairments [26, 45, 66, 67, 91], such as thermal noise (including transmitter thermal noise and receiver thermal noise) and phase noise, always come with the radio front-end and degrade the radio receptions in the practical wireless communications. Hua et al. [50] have studied the transmission noise in Full-Duplex. In the following, we will analyze and study the effects of the receiver thermal noise and phase noise on the Full-Duplex OFDM wireless as well as how to mitigate it or avoid it.

Thermal Noise

In fact, the CSI of the SI channel can not be obtained perfectly, because the SI channel estimation is at least influenced by the receiver thermal noise. This could be explained by Eq. (4.6). The SI channel estimation error due to the receiver thermal noise will further limit the SIC capability of the AARFSIC, which can be explained by Eq. (4.16). However, how big is the impact caused by the thermal noise on the AARFSIC?

In order to qualify the impact of the receiver thermal noise on the Full-Duplex OFDM wireless, we study the signal model in the digital frequency domain equivalently. This holds depending on the assumption that the transceiver RF front-ends are ideal. After the residual SI behind the AARFSIC going through the LNA with amplified power level P_{LNA}. We can equivalently express the residual SI in the digital

frequency domain according to Eq. (4.16) as

$$\begin{aligned} R^{R,S}_{BB,m,si}[k] &= \sqrt{P_{si}}\sqrt{L_{si}}\sqrt{P_{\mathsf{LNA}}}H^{S}_{si}[k]X_{si,m}[k] - \sqrt{P_c}\sqrt{L_c}\sqrt{P_{\mathsf{LNA}}}\widetilde{H}^{S}_{si}[k]X_{si,m}[k] \\ &\overset{4(a)}{=} \sqrt{P_{si}}\sqrt{L_{si}}\sqrt{P_{\mathsf{LNA}}}X_{si,m}[k]\left[H^{S}_{si}[k] - \widetilde{H}^{S}_{si}[k]\right] \end{aligned} \tag{4.17}$$

where $4(a)$ holds when $P_{si}L_{si} = P_cL_c$.

After replacing the $\widetilde{H}^{S}_{si}[k]$ in Eq. (4.17) by (4.6), the residual SI can be rewritten as

$$R^{R,S}_{BB,m,si}[k] = -\frac{X_{m,si}[k]}{T[k]}W[k] \tag{4.18}$$

Because of the independence between $X_{m,si}[k]$, $T[k]$ and $W[k]$, the power of the residual SI could be calculated as

$$P_{rsi} = E[R^{R,S}_{BB,m,si}[k] \cdot R^{*R,S}_{BB,m,si}[k]] = \delta_n^2 \tag{4.19}$$

where we can see that the power of the residual SI due to the receiver thermal noise is δ^2 which represents the power of the receiver thermal noise. That means the residual SI caused by the receiver thermal noise can be regarded as another additive noise and it has the same power level as the receiver thermal noise.

In fact, the receiver thermal noise affects the SIC by the form of worsening the SI channel estimation. Hence, the power of the residual SI can be reduced by enhancing the quality of SI channel estimation. The *Normalized Mean Square Error* (NMSE) is used as the criteria to assess the performance of the SI channel estimation. The NMSE is defined as

$$NMSE = \frac{\sum_k |\widetilde{H}_{si}[k] - H_{si}[k]|^2}{\sum_k |H_{si}[k]|^2} \tag{4.20}$$

Instinctively, the higher the power ratio of the interference to the receiver thermal noise (INR) of the SI radio link is, the better quality of the SI channel estimation can be achieved. The estimated coefficients of each subcarrier channel of the SI link with or without the receiver thermal noise are obtained from the 36Mbps IEEE 802.11g channel estimator in the ADS software. Based on the obtained channel state information $H_{si}[k]$ and $\widetilde{H}_{si}[k]$, we draw the Fig. 4.4.

As it can be shown in Fig. 4.4, a 10dB increase in the INR makes almost 10dB decrease in the NMSE. However, for different INRs, the powers of the residual SI are always approximate to δ^2 when the power level of the long training signal is the same as that of the normal WiFi signals, which can be explained by Eq. (4.19). However, if there is a relative power difference between the long training signal and the rest of the

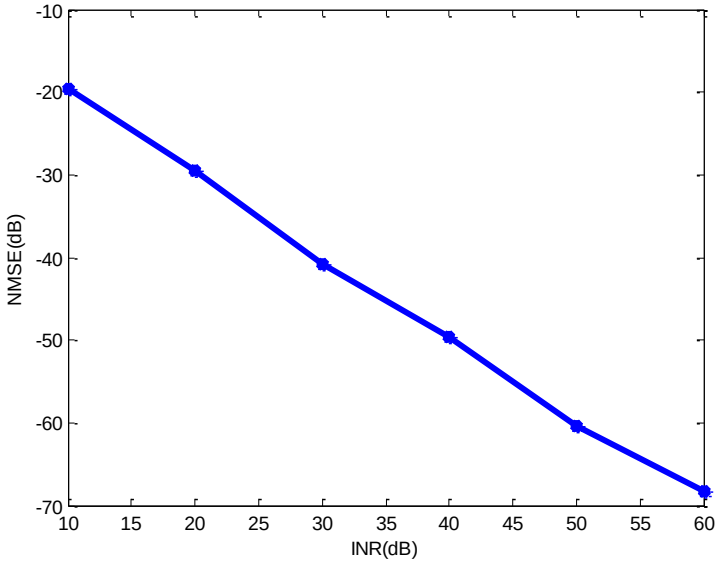

Figure 4.4: NMSE of the self-interference channel estimation vs. INR.

normal WiFi signal, the residual SI could be expressed as

$$\begin{aligned} R^{R,S}_{BB,m,si}[k] &= -\frac{\sqrt{P_{si}}X_{m,si}[k]}{\sqrt{P^{\text{LTS}}_{si}}T[k]}W[k] \\ &= -\frac{X_{m,si}[k]}{\alpha T[k]}W[k] \end{aligned} \tag{4.21}$$

where $\alpha \triangleq \frac{\sqrt{P^{\text{LTS}}_{si}}}{\sqrt{P_{si}}}$. Then, the power of the residual SI would be

$$P_{rsi} = \frac{\delta_n^2}{\alpha^2} \tag{4.22}$$

Depending on the value of α, the power of the residual SI can be expressed as

$$P_{rsi}\begin{cases} > \delta_n^2, & \text{if } \alpha < 1 \\ = \delta_n^2, & \text{if } \alpha = 1 \\ < \delta_n^2, & \text{if } \alpha > 1. \end{cases} \tag{4.23}$$

From the Eq. (4.23), we can get that the power of the residual SI equals δ_n^2 [117] when $\alpha = 1$ which means the long training symbols are transmitted with the same power level as the data symbols. This is a common scenario in current practical WiFi implementation. However, the residual SI can be reduced to under noise level by setting higher power level to the long training symbols than the power of the data symbols, namely $\alpha > 1$. Therefore, we propose to redesign the data packet as in Fig.

4.5.

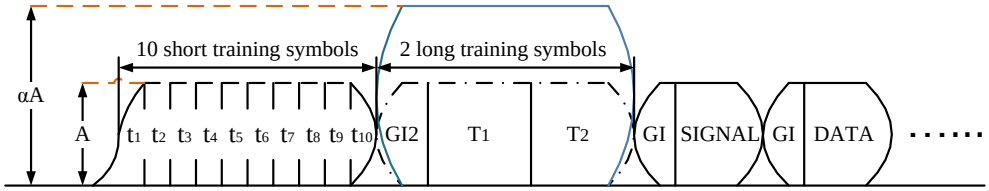

Figure 4.5: The structure of the redesigned data packet.

In order to demonstrate our theoretical analysis, a Full-Duplex OFDM radio link is built on the ADS (Advanced Design System, Agilent Tech.) and Matlab software. The transceiver RF front-ends and most of the baseband sub-systems are constructed with ADS and part of the digital signal processing is implemented on Matlab.

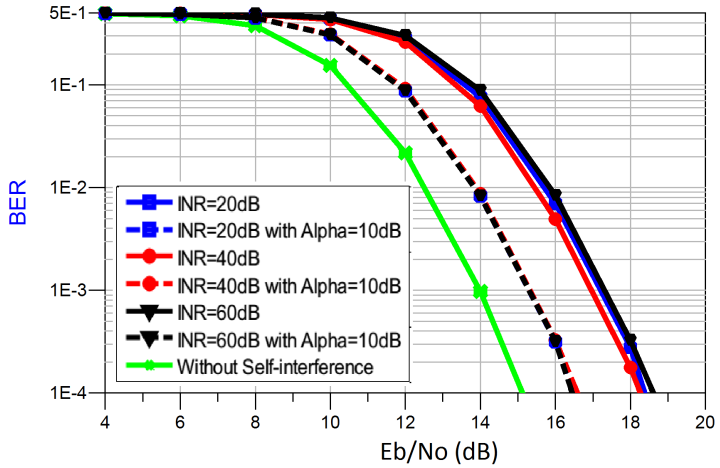

Figure 4.6: The BER comparison of the Full-Duplex wireless for different INRs.

As shown in Fig. 4.6, when the power putted on the long training symbols is equal to the power of the data symbols, i.e. $\alpha = 1$, the BER curves of the intended radio link with different power levels of the SI signals almost overlap with each other, and there is a 3dB gap between these BER curves and the BER curve of the radio link without SI. This can be explained by Eq. (4.23). The channel estimation error due to the receiver thermal noise causes another thermal noise (residual SI) to the distant radio link. However, after employing our power-difference-allocation method, there is just 1.5dB residual SI.

As it can be seen in Fig. 4.7, there are 5dB of residual SI when INR=5dB if $\alpha = 0$dB, which means there is no SI suppression by using the AARFSIC if $\alpha = 0$dB when INR is

low. This is because the SI channel estimation is not accurate enough to implement the AARFSIC for the Full-Duplex wireless when the INR is low. However, the residual SI can be reduced by the power-difference-allocation method. The residual SI is reduced by 2.5 dB via increasing the α from 0dB to 2.5dB; when α increase to 5dB, the residual SI is around 1.7dB. If we further increase α, the strength of the residual SI comes to 1.5dB.

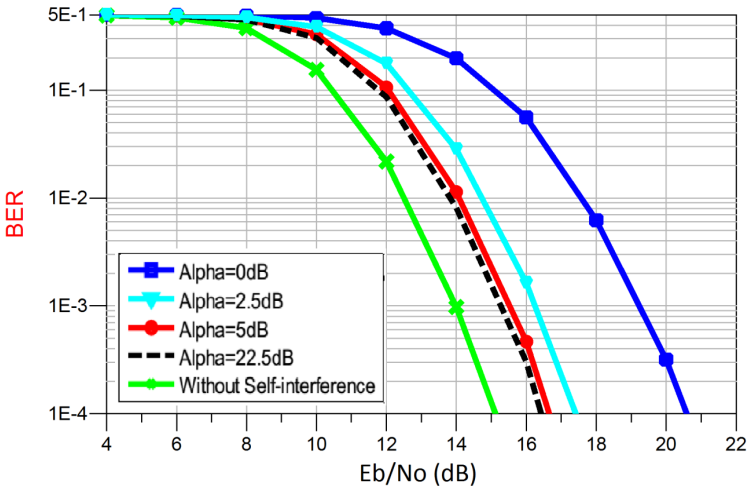

Figure 4.7: The BER of the Full-Duplex wireless for INR=5dB with different α.

Phase Noise

In the Full-Duplex OFDM wireless, the phase noise in the local oscillator is another important RF impairment, significantly limiting the capability of the SIC. For the Full-Duplex OFDM wireless system with AARFSIC as in Fig. 4.1, the mismatch between the SI signal and the cancellation signal caused by the phase noise in the local oscillator can be modeled as shown in Fig. 4.8.

As in Fig. 4.8, the signal model of the AARFSIC with phase noise can be expressed by

$$\begin{aligned} r_{RF,si}^{R,S}(t) &= x_{RF,si}^{R,S}(t) - x_{RF,c}^{R,S}(t) \\ &= \sqrt{P_{si}}\sqrt{L_{si}}x_{si}^{T}(t)e^{\jmath[2\pi f_c t+\phi_1]} * h_{si}^{S}(t) - \sqrt{P_c}\sqrt{L_c}x_c^{C,S}(t)e^{\jmath[2\pi f_c t+\phi_2]} \end{aligned} \tag{4.24}$$

where $x_{si}^{T}(t)$ denotes the baseband analog SI signal which will experience the single path SI channel $h_{si}^{S}(t)$, $x_c^{C,S}(t)$ represents the corresponding cancellation signal including the CSI of the single path SI channel and the data symbols, ϕ_1 and ϕ_2 denote

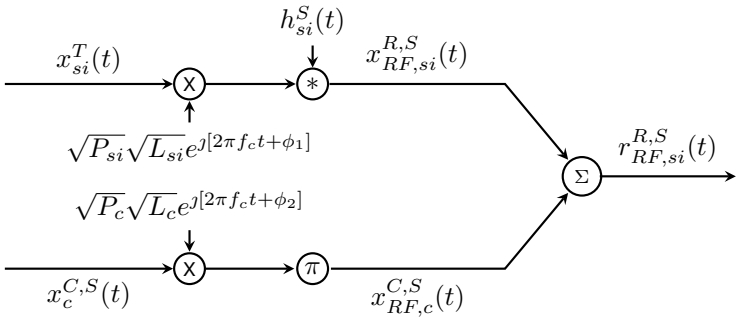

Figure 4.8: The analysis signal model of AARFSIC for the Full-Duplex wireless with phase noise.

the phase noise in the local oscillator of the SI radio link and the cancellation radio link respectively. For the Full-Duplex OFDM wireless with a single path SI channel, $x_c^{C,S}(t) = x_{si}^{T}(t) * h_{si}^{S}(t)$ can be met easily, which has been demonstrated in Chapter 2. To simplify the analysis signal model of the Full-Duplex OFDM wireless, we define $x_{si,c}(t) \triangleq x_{si}^{T}(t) * h_{si}^{S}(t) \triangleq x_c^{C,S}(t)$. Therefore, the Eq. (4.24) could be expressed as

$$\begin{aligned} r_{RF,si}(t) &= \sqrt{P_{si}}\sqrt{L_{si}}x_{si,c}(t)e^{\jmath(2\pi f_c t+\phi_1)} - \sqrt{P_c}\sqrt{L_c}x_{si,c}(t)e^{\jmath(2\pi f_c t+\phi_2)} \\ &\overset{4(b)}{=} \sqrt{P_{si}}\sqrt{L_{si}}x_{si,c}(t)e^{\jmath(2\pi f_c t+\phi_2)}[e^{\jmath(\phi_1-\phi_2)} - 1] \\ &\overset{4(c)}{=} \sqrt{P_{si}}\sqrt{L_{si}}x_{si,c}(t)e^{\jmath(2\pi f_c t+\phi_2)}(e^{\jmath\Delta\phi} - 1) \end{aligned} \tag{4.25}$$

where $4(b)$ holds when $P_{si}L_{si} = P_cL_c$ and $4(c)$ holds because of $\Delta\phi \triangleq \phi_1 - \phi_2$.

Then, the instantaneous power of the residual SI could be computed by

$$\begin{aligned} P_{rsi} &= r_{RF,rsi}(t)r_{RF,rsi}^{*}(t) \\ &= 2P_{si}L_{si}|x_{si,c}(t)|^2[1 - cos(\Delta\phi)] \\ &= 4P_{si}L_{si}|x_{si,c}(t)|^2 sin^2(\frac{\Delta\phi}{2}) \\ &\overset{4(d)}{\approx} P_{si}L_{si}|x_{si,c}(t)|^2\Delta\phi^2 \\ &= P_{si}^{R}\Delta\phi^2 \end{aligned} \tag{4.26}$$

where $P_{si}^{R} = P_{si}L_{si}|x_{si,c}(t)|^2$ denotes the power of the received SI without SIC. When $\Delta\phi = 0$, the instantaneous power of the residual SI, P_{rsi}, would be zero. While when $\Delta\phi \neq 0$, the residual SI occurs. $4(d)$ holds because $\Delta\phi \to 0$.

From Eq. (4.26), it is also can be found that the power of the residual SI is proportional to the power level of the received SI and the power level of the phase noise. The

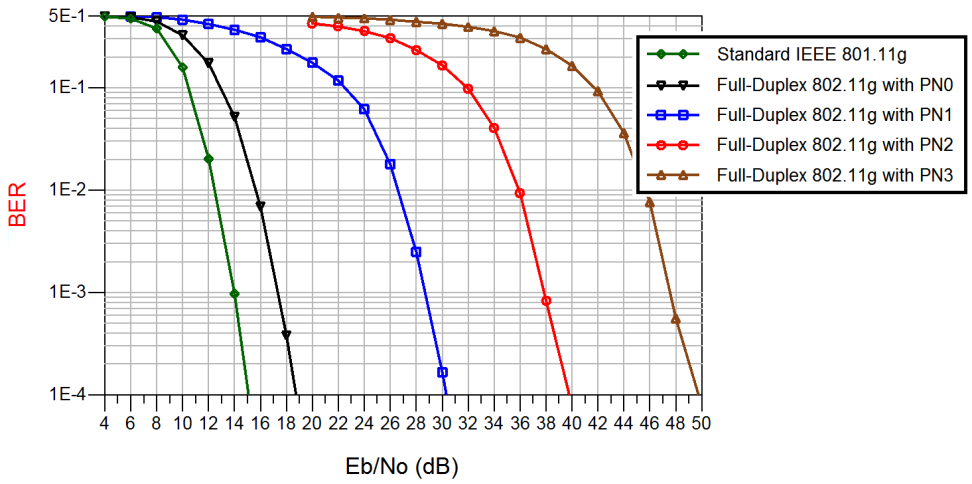

Figure 4.9: The BER performance comparison of the Full-Duplex 802.11g with different phase noise level.

Eq. (4.26) can be rewritten in another form as

$$P_{rsi}(dB) \approx P_{si}^{R}(dB) + \Delta\phi^{2}(dB) \tag{4.27}$$

where we can see that an XdB increase in the power level of the phase noise offset will cause an XdB increase in the power level of the residual SI. For instance, each 10dB increase in the power of the phase noise could induce a 10dB increase in the power of the residual SI, which is demonstrated by Fig. 4.9.

In this simulation of the Full-Duplex OFDM system conducted with ADS and Matlab, the INR= 60dB. The strength of the phase noise is setting as: PN0=0 means without phase noise; PN1 means 'PhaseNoiseData[1]="120 -75 300 -83 3000 -103 30000 -123 1200000 -155"' in ADS software; PN2 means 'PhaseNoiseData="120 -65 300 -73 3000 -93 30000 -113 1200000 -145"' in ADS software; PN3 means means 'PhaseNoiseData="120 -55 300 -63 3000 -83 30000 -103 1200000 -135"' in ADS software. As shown in Fig. 4.9. When a 10dB increase occurs in the strength of the phase noise from PN1 to PN2 and from PN2 to PN3, the BER curves shift to the right direction in each 10dB E_b/N_o, which means the residual SI increases by 10dB as the strength of phase noise increases by 10dB.

Here, the impact of the oscillator phase noise on the two-antenna Full-Duplex OFDM wireless is analyzed and qualified. With respect to the phase noise suppression for Full-Duplex OFDM wireless, [6] proposes to suppress the phase noise in time domain or in frequency domain.

[1]The expression of the PhaseNoiseData in ADS contains double values of offset frequency (Hz) and single sideband relative power level (dBc/Hz).

4.4 Full-Duplex OFDM Wireless with Multi-Path SI Channel

We have found that the AARFSIC could only achieve a very limited amount of SIC for the Full-Duplex OFDM wireless with a multi-path SI channel, even under the condition that the transceiver RF front-ends are ideal and the CSI of the SI channel can be obtained perfectly. In the indoor reflecting environment, the AARFSIC can achieve no more than 40dB of SIC, which order of magnitude was also confirmed by [38]. Therefore, a digital SIC is quite necessary to further cancel the residual SI. When the SI channel is modeled as a multi-path wireless channel, i.e. $\mathsf{N}_p^{si} > 1$, the SI channel model Eq. (4.3) could be modified as $h_{si}^M(t) = \sum_{\mathsf{n}_p^{si}}^{\mathsf{N}_p^{si}-1} h_{si,\mathsf{n}_p^{si}} \delta(t - \tau_{si,\mathsf{n}_p^{si}})$. After digitizing, the discrete time domain channel will be $h_{si}^M(n) = \sum_{\mathsf{n}_p^{si}=0}^{\mathsf{N}_p^{si}-1} h_{si,\mathsf{n}_p^{si}} \delta(n - n_{si,\mathsf{n}_p^{si}})$. This channel in the frequency domain can be expressed by $H_{si}^M[k] = \sum_{\mathsf{n}_p^{si}=0}^{\mathsf{N}_p^{si}-1} h_{si,\mathsf{n}_p^{si}} e^{-\jmath 2\pi \Delta f k n_{si,\mathsf{n}_p^{si}}}$ as in (3.9).

In order to overcome the strong SI for the Full-Duplex OFDM wireless with a multi-path SI channel, we will combine the AARFSIC and the DSICT as presented in Chapter 3.

4.4.1 Active Analog RF Self-Interference Cancellation

For the Full-Duplex OFDM wireless with a multi-path SI channel, the general received signal model can be constructed as that of the Full-Duplex OFDM wireless with a one-path SI channel as

$$\begin{aligned} y_m^M(t) &= x_{RF,m}^R(t) + x_{RF,m,si}^{R,M}(t) \\ &= \sqrt{P}\sqrt{L} x_m^T(t) e^{\jmath 2\pi f_c t} * h(t) + \underbrace{\sqrt{P_{si}}\sqrt{L_{si}} x_{m,si}^T(t) e^{\jmath 2\pi f_c t} * h_{si}^M(t)}_{\text{self-interference}} \\ &\quad + w(t) \end{aligned} \tag{4.28}$$

The SI term in Eq. (4.28) is so strong that it can saturate the receiver chain. Therefore, we first craft the SI signal in the digital frequency domain and carry out the SIC in the RF stage as presented in details in the developed SIC for Full-Duplex OFDM wireless in the Chapter 3. The RF cancellation signal, $x_{RF,m,c}^{R,M}(t)$ corresponding to cancel the SI $x_{RF,m,si}^{R,M}(t)$ in Eq. (4.28), is constructed as

$$x_{RF,m,c}^{R,M}(t) = \sqrt{P_c}\sqrt{L_c} x_{m,c}^{C,M}(t) e^{\jmath 2\pi f_c t} \tag{4.29}$$

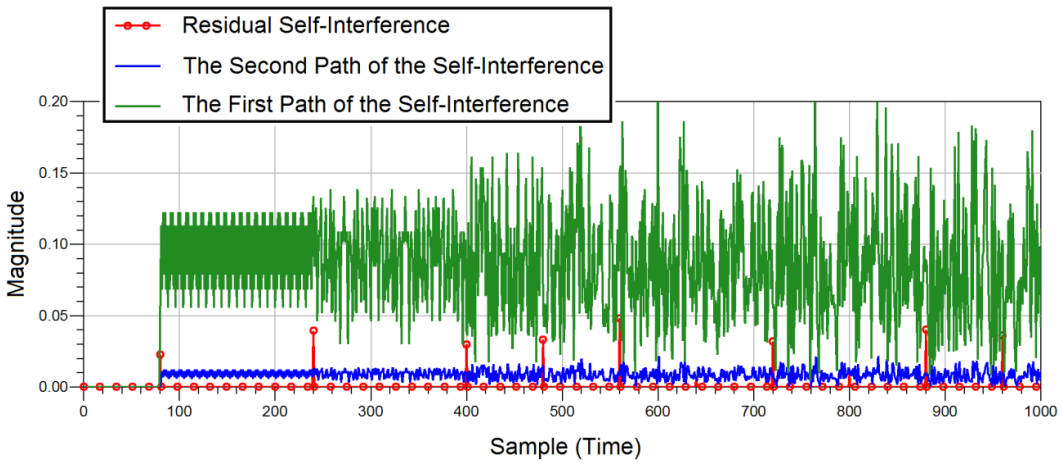

Figure 4.10: Magnitude measurement of the received signals before and after the AARFSIC. The received signals consist of the direct-path signal and another reflecting-path signal when the two-path SI channel is used here. The reflecting path has $50ns$ delay and 20dB attenuation compared to the direct path. (Note: For the wireless system with 20MHz bandwidth, $50ns$ means one sampled point. Hence, $50ns$ delay in continuous time domain represents one sampled point delay in discrete time domain.)

where the baseband cancellation signal, $x_{m,c}^{C,M}(t)$, can be expressed as

$$x_{m,c}^{C,M}(t) = \mathsf{DAC}\{\mathsf{CP}\{x_{m,c}^{M}(n)\}\} \tag{4.30}$$

where $x_{m,c}^{M}(n) = \mathsf{IDFT}\{X_{m,si}[k]\widetilde{H}_{si}^{M}[k]\} = \frac{1}{N}\sum_{k=-\frac{N}{2}}^{\frac{N}{2}-1} X_{m,si}[k]\widetilde{H}_{si}^{M}[k]e^{\jmath 2\pi\Delta fkn}, n \in [1, N]$.

After the AARFSIC, we can obtain the residual RF SI, $r_{RF,m,si}^{R,M}(t)$, as

$$\begin{aligned} r_{RF,m,si}^{R,M}(t) &= x_{RF,m,si}^{R,M}(t) - x_{RF,m,c}^{R,M}(t) \\ &= \sqrt{P_{si}}\sqrt{L_{si}}e^{\jmath 2\pi f_c t}[x_{m,si}^{T}(t) * h_{si}^{M}(t) - x_{m,c}^{C,M}(t)] \end{aligned} \tag{4.31}$$

If $r_{RF,m,si}^{R,M}(t) = 0$, i.e. $x_{m,si}^{T}(t) * h_{si}^{M}(t) = x_{m,c}^{C,M}(t)$, the strong SI could be canceled completely by the AARFSIC. However, our waveform simulations have shown that $r_{RF,m,si}^{R,M}(t) \neq 0$, which means the strong SI in the Full-Duplex OFDM wireless with multi-path SI channel can not be canceled completely by using the AARFSIC. This result can also be demonstrated by the waveform simulation as in Fig. 4.10.

As we can see from the Fig. 4.10, except that some peaks occurs at certain time points, the strong SI can be canceled efficiently by using the AARFSIC. However, the magnitudes of the residual peaks are higher than that of the reflecting path (almost two times). Therefore, the received signal samples from the distant radio node at these certain time points will be masked by the unexpected peaks. That is why we got

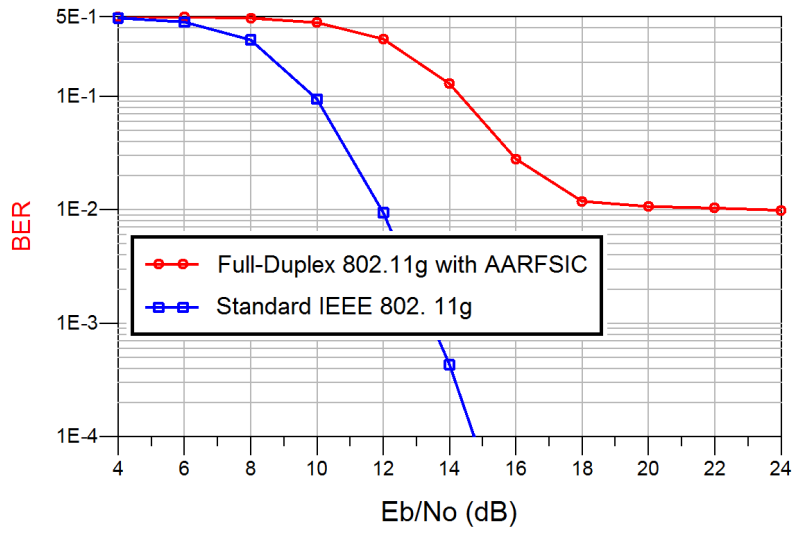

Figure 4.11: **Multi-path SI channel:** The BER performance of the Full-Duplex IEEE 802.11g with the AARFSIC for multi-path SIC. When $E_b/N_0 \leq 16$dB, the BER performance is determined by the receiver thermal noise. However, when $E_b/N_0 > 16$dB, the BER performance begin to be mainly determined by the residual peaks after the AARFSIC.

a BER curve with around 10^{-2} floor as shown in Fig. 4.11. Therefore, we can conclude that the AARFSIC could eliminate the first path completely and can cancel only part of the multiple reflecting paths. The uncanceled peaks could significantly degrade the performance of the system reception. If the SI is even much stronger, the whole Full-Duplex system will be destroyed completely.

Therefore, the strong SI in the Full-Duplex OFDM wireless with a multi-path SI channel can not be canceled completely by only using the AARFSIC even under the assumptions that the transceiver RF front-ends are ideal and the CSI of the SI channel can be obtained perfectly. Fortunately, we find that the multiple-reflecting-paths is the key factor limiting the capability of the AARFSIC and the residual high peaks could be eliminated in the discrete time domain, which has been theoretically analyzed and demonstrated in simulation in Chapter **??**. In order to mitigate the residual peaks, we will further implement a digital SIC in the time domain in the following.

4.4.2 Digital Self-Interference Cancellation in Time Domain

As it has been presented in Sec. 4.4.1, the AARFSIC has a very limited capability of SIC for the Full-Duplex OFDM wireless with a multi-path SI channel. The residual SI signal performs as a number of high peaks which will affect the reception of the signal of interest. In the following , we will develop a DSICT to cancel this residual SI.

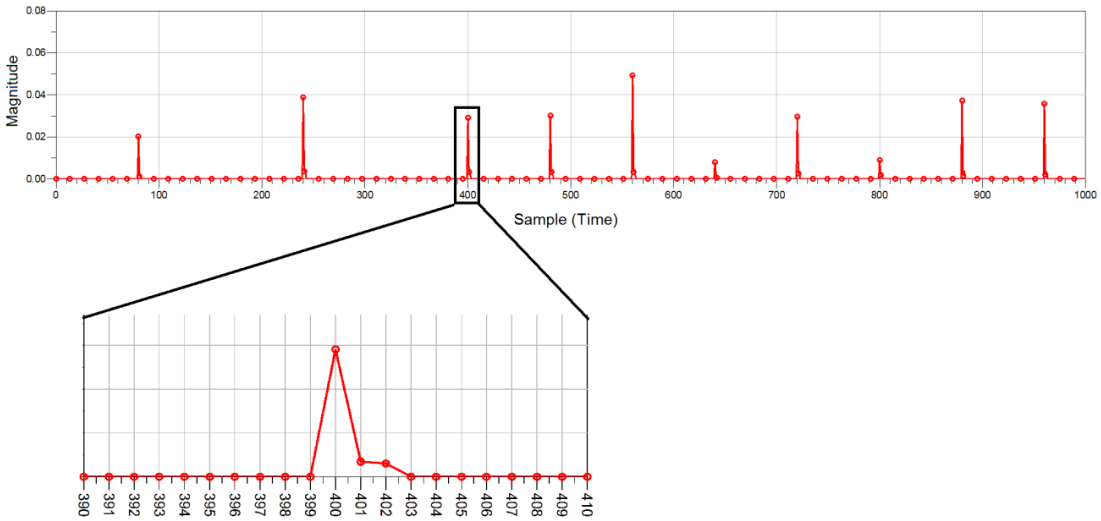

Figure 4.12: **The residual peaks after the AARFSIC**. In this waveform simulation, the number of the paths of the SI channel is $\mathsf{N}_p^{si} = 3$. The second path has 20dB attenuation and 50ns delay compared to the direct path. The third path has 40dB attenuation and $150ns$ delay compared to the direct path. Therefore, there are three non-zeros points. The first point is caused by the combination of the second path and the third path. The second point and the third point are caused by the third path.

In order to highlight the fact that the residual SI can be canceled by the DSICT from a theoretical perspective, we still make the assumption that the transceiver RF front-ends are ideal and the CSI of the SI channel can be obtained perfectly. Hence, the equivalent baseband expression of the residual SI, $r_{m,si}^{R,M}(n)$, after the receiver LNA and according to the Eq. (4.31), could be represented by

$$r_{m,si}^{R,M}(n) \quad = \quad \sqrt{P_{si}}\sqrt{L_{si}}\sqrt{P_{\mathsf{LNA}}}[x_{m,si}^{T}(n) \otimes h_{si}^{M}(n) - \mathsf{CP}\{x_{m,c}^{M}(n)\}] \tag{4.32}$$

Because the residual RF SI, $r_{RF,m,si}^{R,M}(t)$, is not zero, hence the equivalent residual baseband SI $r_{m,si}^{R,M}(n), n \in [1, +\propto]$ are not alway zeros, which can also be shown as in Fig. 4.12. As it has been presented above, the residual peaks are caused by the multiple reflecting paths. While the number of the residual points is determined by the maximum delay of the nontrivial multi-path components. The bigger the maximum delay of the multi-path components is, the bigger number of the high peaks will occur in each of the OFDM symbols. For instance, when the maximum delay of the multi-path components is $150ns$, there will be 3 high peaks occur.

In the following, we will figure out where exactly the high peaks occurs and how the multiple reflecting paths cause the residual SI. In order to achieve this goal, the

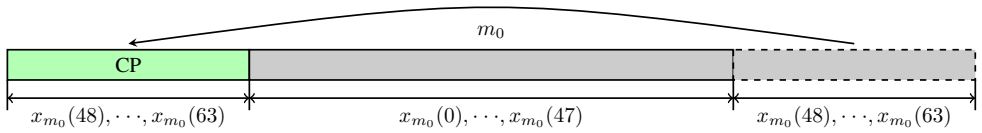

Figure 4.13: General structure of the m_0^{th} generated OFDM symbol, $x_{m_0}^T(n), n \in [1, N + N_{CP}]$, in IEEE 802.11g.

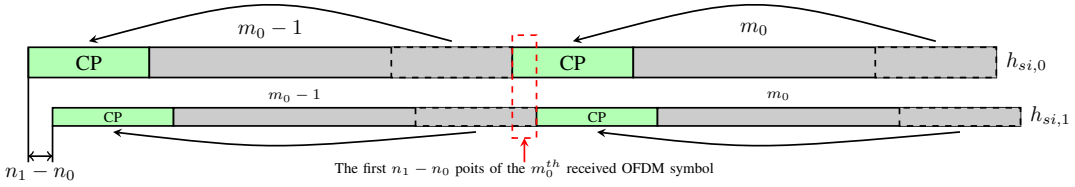

Figure 4.14: General structure of the received OFDM symbol in IEEE 802.11g.

details of the OFDM signal model are required. OFDM based IEEE 802.11g transmission is chosen as the physical layer in this dissertation. Hence, the generated OFDM symbol by IFFT could be shown as in Fig. 4.13, which could also be expressed as $x_{m_0}^T(n) = \mathsf{CP}\{x_{m_0}(n)\}$ where $x_{m_0}(n) = \mathsf{IFFT}\{X_{m_0}[k]\}$. After experiencing a multi-path SI channel $h_{si}^M(n)$, the received OFDM symbol could be as shown in Fig. 4.14, where we just take a SI channel with two paths as an example and the delay of the first path is zero, i.e. $n_0 = 0$. Therefore, for the m_0^{th} received OFDM symbol, the term $x_{m_0,si}^T(n) \otimes h_{si}^M(n)$ in Eq. (4.32) could be expressed by

$$x_{m_0,si}^T(n) \otimes h_{si}^M(n) = \begin{cases} x_{m_0,si}^T(n)h_{si,0} + x_{m_0-1,si}^T(n - n_1 + N + N_{CP})h_{si,1}, \\ \text{for } n \in [1, n_1]; \\ x_{m_0,si}^T(n)h_{si,0} + x_{m_0,si}^T(n - n_1)h_{si,1}, \\ \text{for } n \in [n_1 + 1, N + N_{CP}]. \end{cases} \tag{4.33}$$

While for the m_0^{th} cancellation OFDM symbol without CP, $x_{m_0,c}^M(n)$, it could be represented by

$$x_{m_0,c}^M(n) = \begin{cases} x_{m_0,si}(n)h_{si,0} + x_{m_0,si}(n - n_1 + N)h_{si,1}, \text{for } n \in [1, n_1]; \\ x_{m_0,si}(n)h_{si,0} + x_{m_0,si}(n - n_1)h_{si,1}, \text{for } n \in [n_1 + 1, N]. \end{cases} \tag{4.34}$$

After adding a N_{CP}-length CP, the m_0^{th} cancellation OFDM symbol, $\mathsf{CP}\{x_{m_0,c}^M(n)\}$

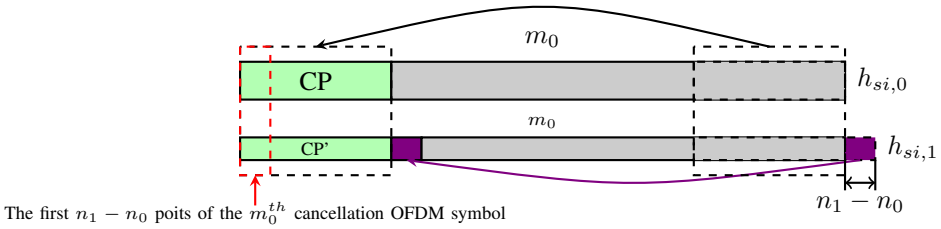

Figure 4.15: The structure of the crafted cancellation OFDM symbol.

in Eq. (4.32) could be expressed by

$$\mathsf{CP}\{x^M_{m_0,c}(n)\} = \begin{cases} x^T_{m_0,si}(n)h_{si,0} + x^T_{m_0,si}(n-n_1+N)h_{si,1}, \\ \text{for } n \in [1, n_1]; \\ x^T_{m_0,si}(n)h_{si,0} + x^T_{m_0,si}(n-n_1)(n)h_{si,1}, \\ \text{for } n \in [n_1+1, N+N_{CP}]. \end{cases} \tag{4.35}$$

where the m_0^{th} cancellation OFDM symbol is as shown in Fig. 4.15

Comparing the Eq. (4.33) and Eq. (4.35), or the Fig. 4.14 and the Fig. 4.15, we can find that the residual SI occurs at the beginning of each of the OFDM symbols and the length of the residual SI is determined by the maximum delay of the SI channel. Therefore, when the maximum time delay of the multiple reflecting paths is zero, i.e. $n_1 - n_0 = 0$, the residual SI should be zero, which comes to the case of the AARFSIC for the Full-Duplex OFDM wireless with a one-path SI channel. However, in a more practical wireless communications, the SI channel should be a multi-path fading channel with a high Ricean factor K, which means $n_1 - n_0 \geq 1$. Hence, the SI in the Full-Duplex OFDM wireless can not be canceled completely by only using the AARFSIC. Fortunately, we also find that the residual SI after the AARFSIC is cancelable.

For the m_0^{th} OFDM symbol, the residual SI (peaks) could be expressed as

$$x^T_{m_0,si}(n) \otimes h^M_{si}(n) - \mathsf{CP}\{x^M_{m_0,c}(n)\} = \begin{cases} [x^T_{m_0-1,si}(n-n_1+N+N_{CP}) - \\ x^T_{m_0,si}(n-n_1+N)]h_{si,1}, \text{for } n \in [1, n_1]; \\ 0, \text{for } n \in [n_1+1, N+N_{CP}]. \end{cases} \tag{4.36}$$

Therefore, if we can obtain an estimate of the magnitude, $h_{si,1}$, of the second path, the residual SI could be further canceled, which relies on the fact that the Full-Duplex radio node knows its own transmit symbols, $x^T_{m_0,si}(n)$. Let $\widetilde{h}_{si,1}$ denotes the estimate

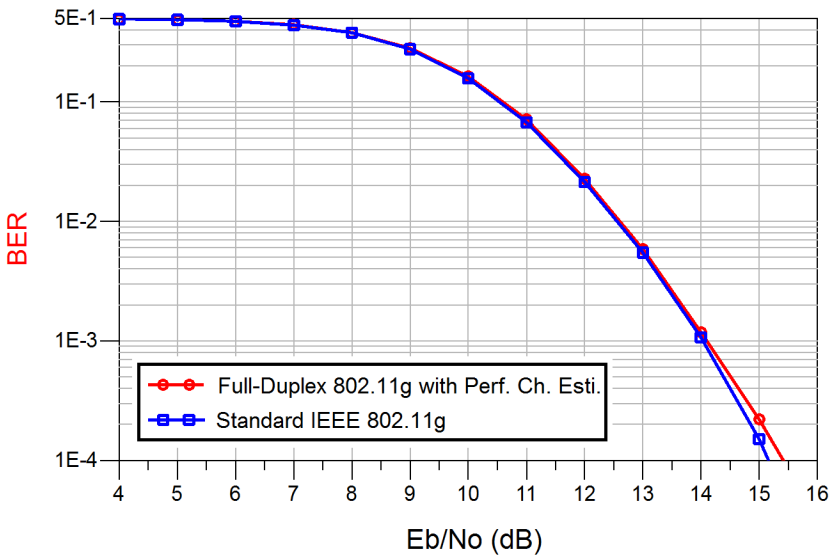

Figure 4.16: **Multi-path SI channel:** The comparison of the BER performance between the Full-Duplex IEEE 802.11g with perfect channel estimation and the standard IEEE 802.11g system.

of $h_{si,1}$, then the m^{th} residual OFDM symbol after the DSICT could be expressed as

$$r^{\text{DSICT}}_{m_0,rsi} = \begin{cases} [x^T_{m_0-1,si}(n-n_1+N+N_{CP})- \\ x^T_{m_0,si}(n-n_1+N)](h_{si,1}-\widetilde{h}_{si,1}), \text{for } n \in [1,n_1]; \\ 0, \text{for } n \in [n_1+1, N+N_{CP}]. \end{cases} \tag{4.37}$$

where we can see that the strong SI in the Full-Duplex OFDM wireless even with a multi-path SI channel can be canceled completely when the perfect CSI of the second path can be obtained.

In order to confirm our theoretical results, we implement a system level design based on the ADS and Matlab software. As shown in Fig. 4.16, the BER curve of the Full-Duplex IEEE 802.11g overlap with that of the Half-Duplex IEEE 802.11g when the perfect SI channel estimation can be obtained, which means the strong multi-path SI can be eliminated completely by the combination of the AARFSIC and DSICT.

As it has been presented above, the perfect CSI of the SI channel can not be obtained exactly. At least, the receiver thermal noise always impacts the received signal. Therefore, in the real SI channel estimation, there is at least the channel estimation error due to the receiver thermal noise, which of course causes the residual SI as well. In Fig. 4.17, there is around 3dB gap between the Full-Duplex IEEE 802.11g and the standard IEEE 802.11g when the SI channel estimation is implemented in the real situation.

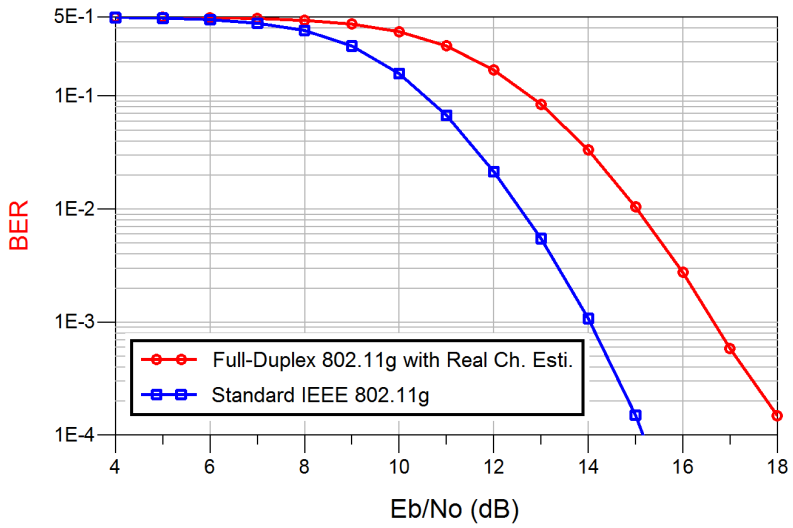

Figure 4.17: **Multi-path SI channel:** The comparison of the BER performance between the Full-Duplex IEEE 802.11g with real channel estimation and the standard IEEE 802.11g system.

However, these results come under the assumption that the transceiver RF front-ends are ideal and the perfect CSI of the SI channel can be obtained. Therefore, the factors “dirtying" the RF front-end and affecting the SI channel estimation need to be taken into account to design a more practical Full-Duplex wireless.

4.5 Residual Self-Interference

Although a lot of efforts [19, 20, 30, 31, 36, 37, 38, 39, 41, 42, 54, 55, 56, 58, 62, 65, 72, 74, 76, 81, 108, 114] are dedicated to cancel the strong SI confronted by the Full-Duplex wireless, the residual SI is still so strong that the concept of Full-Duplex is hard to be putted into practice. In this dissertation, we can cancel the strong SI completely by combining the AARFSIC and DSICT schemes under the assumption that the transceiver RF front-ends are ideal. However, the ideal RF front-end is not available in a practical radio system. The RF impairments, such as ADC [68, 91], phase noise in the local oscillator [8, 93, 94], thermal noise at the transmitter [50] and thermal noise at the receiver [118], I/Q imbalance in the RF front-end [66, 67], non-linearity of the power amplifier [7, 15] and so on, always accompany the radio front-end and cause a big residual SI to the Full-Duplex OFDM wireless systems. Besides, the articles [46, 80] have studied the residual SI and its impact on the Full-Duplex wireless.

4.5.1 Without RF Impairments

If the Full-Duplex OFDM radio system has ideal RF front-ends, only the AARFSIC can bring down the strong single path SI to the thermal noise floor, which can be demonstrated by Fig. 4.3. While for the multi-path SI, a DSICT is required to complement the AARFSIC to mitigate all the SI signals, because the AARFSIC can only eliminate the direct path, which can be confirmed by Fig. 4.11 and Fig. 4.16

4.5.2 With RF Impairments

In the practical Full-Duplex OFDM wireless communications, except for the multiple reflecting paths, the RF impairments are also the key factors limiting the capability of the SIC. The receiver thermal noise brings 3dB residual SI to the Full-Duplex OFDM wireless with a one-path SI channel as shown in Fig. 4.6 and with a multi-path SI channel as shown in Fig. 4.17. With respect to the phase noise, an XdB increase in the power of the phase noise will cause an XdB increase in the power of the residual SI to the Full-Duplex OFDM wireless given the power of the received SI is fixed before SIC, which can be confirmed by Fig. 4.9.

4.6 Full-Duplex OFDM Radio Transceiver Design

In order to decode the useful signal from the distant radio node correctly, a Full-Duplex radio node must have the ability to suppress the interference signal from its own transmitter at the receiver chain. In our design, the AARFSIC and DSICT are cooperatively combined to cancel the strong SI. Fig. 4.18 shows the architecture of a wideband Full-Duplex OFDM radio node based on the physical layer of the IEEE802.11g. The cancellation path is added to the Full-Duplex OFDM radio in order to generate the RF cancellation signal for the implementation of the AARFSIC at the RF component. For the Full-Duplex OFDM wireless with one-path SI channel, the AARFSIC could bring down the strong SI to the thermal noise level. However, for a general Full-Duplex OFDM wireless, the proposed DSICT is required to complement the AARFSIC to eliminate the multi-path SI. Hence, the DSICT following the AARFSIC is optional.

In our developed Full-Duplex OFDM radio system, the additional hardware components required for the AARFSIC at the RF component consist of one RF combiner, one 180^o phase shifter, two DACs and one RF front-end.

In the cancellation path, the component of the SI channel estimation is used for obtaining the coefficient estimation of each subcarrier channel. Further, $\widetilde{H}_{si}[k]$ denotes the magnitude and phase of the k^{th} subcarrier channel. The baseband cancellation

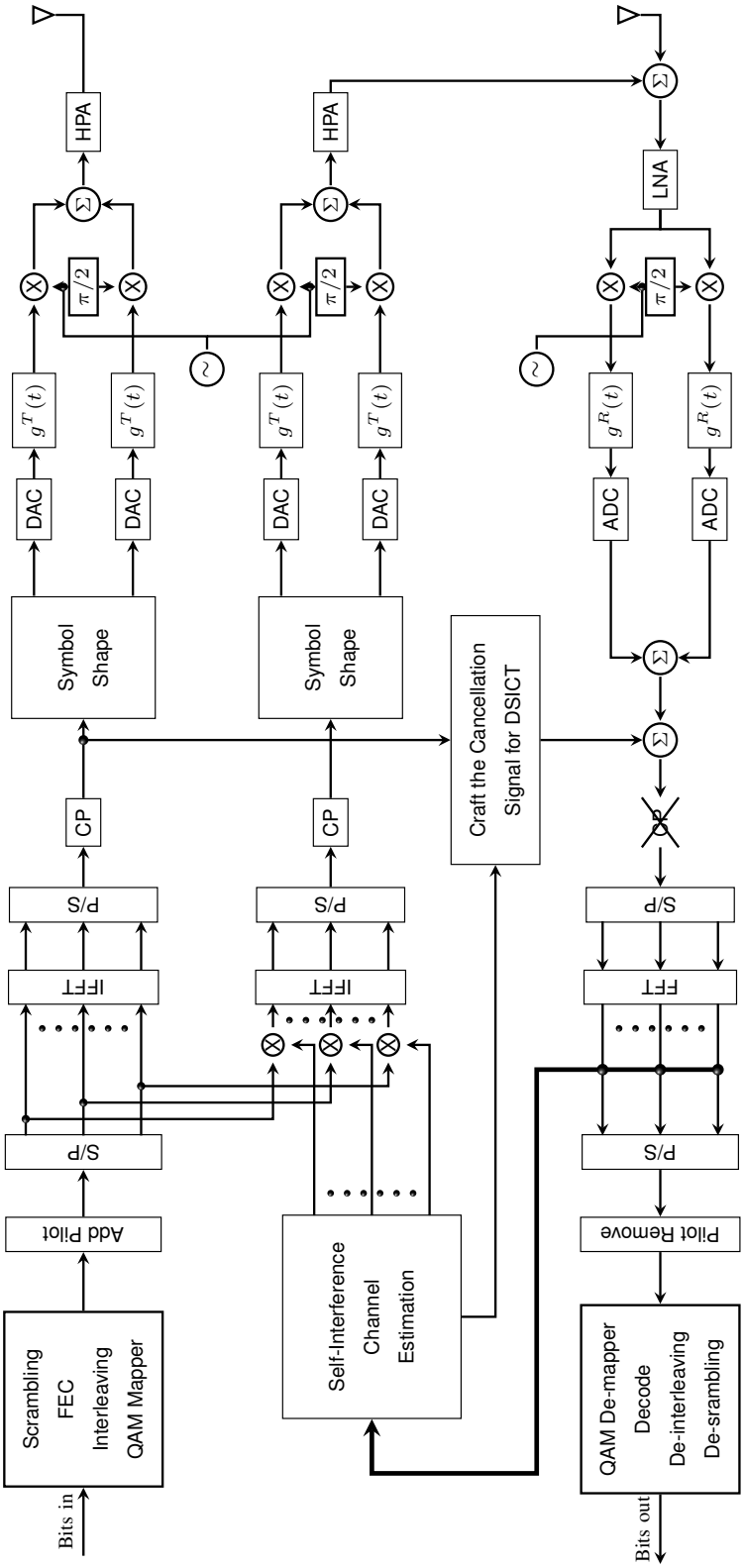

Figure 4.18: Architecture of Full-Duplex OFDM radio node.

signal $x^{C}_{m,c}(t) = \mathsf{DAC}\{\mathsf{CP}\{\mathsf{IDFT}\{X_{m,si}[k]\widetilde{H}_{si}[k]\}\}\}$ is generated by OFDM modulating the new complex symbols sequence $X_{m,si}[k]\widetilde{H}_{si}[k], k \in [1, N]$. Then, another RF front-end is employed to up-convert this baseband cancellation signal to the RF cancellation signal. After the HPA amplifying the RF cancellation signal to match the power of the SI signal, 180^{o} phase shifter is used to get the inverse version. Then, the SIC is carried out at the receiver chain by combining the received signal and the inversed cancellation signal via the RF combiner.

In order to avoid the impact of the phase noise in the local oscillator on the SIC [94], the transmitter and the cancellation path use the same local oscillator. Furthermore, the AARFSIC is implemented by using a RF combiner which combines the received signal and RF cancellation signal between the receiver antenna and the receiver LNA to avoid the influence of the "dirty" RF at the receiver chain on the SIC. After AARFSIC, the signal received including the signal of interest, residual SI and thermal noise will be further processed by the receiver chain performing the inverse operation as the transmitter chain does.

4.7 Conclusion and Discussion

In this Chapter, a single channel 20MHz Full-Duplex OFDM radio system based on the ASIC is developed and elaborated. For the Full-Duplex OFDM wireless with one-path SI channel, just AARFSIC can eliminate the strong SI completely. While with respect to the Full-Duplex OFDM wireless with multi-path SI channel, the residual SI after the AARFSIC is still so strong that the signal of interest is masked completely. Then, a DSICT scheme is required to cancel the residual SI. The strong multi-path SI signals can be canceled completely by the combination scheme of the AARFSIC and DSICT.

However, the RF impairments, such as the thermal noise in the receiver and the phase noise in the local oscillator, significantly limit the capability of the ASIC. In the strength of the residual SI, the receiver thermal noise contributes 3dB. The power-difference-allocation method can reduce this 3dB contribution to 1.5dB. The amount of the residual SI caused by the phase noise in the local oscillator is proportional to the power level of the phase noise and the power level of the received SI. The shared local oscillator between the transmitter link and the cancellation radio link can significantly reduce the impact of the phase noise on the AARFSIC in the Full-Duplex OFDM wireless. However, the phase noise attached to the residual SI can also limit the capability of the DSIC. Therefore, digital estimation and mitigation of the phase noise is highly required in the practical Full-Duplex OFDM radio design. For the Full-Duplex wireless communications, the SI channel is an important research issue. [112] has studied

and measured the SI channel in one-antenna Full-Duplex wireless. The real characteristics of the SI channel in two-antenna Full-Duplex wireless is still an open problem.

Applications: The Full-Duplex radio could be exploited for a lot of applications. Especially, the capability of the simultaneous transmission and reception provided by the Full-Duplex could enhance the spectrum channel sensing in the cognitive radio [2, 3, 4]. Full-Duplex could also greatly improve the efficiency of relay networks [13, 57, 70, 78, 85]. Besides, Full-Duplex could further improve the spectral efficiency of the MIMO system based on the SIC by digital beamforming [52, 51, 96, 98, 122]. The physical layer secrecy can be enhanced by using the Full-Duplex radio [124]. Full-Duplex can also be exploited in the internet-of-things (IoT) network for the device to device communication [63]. In the future millimeter-wave wireless communication, Full-Duplex [73, 89] could also show its advantages. Besides, the Full-Duplex radio can be used for improving the degree of freedom [1], achievable rate region [32, 35, 77] and system capacity [113]. The SIC schemes used in the Full-Duplex could also be employed in the echo cancellation [18].

Part III

Full-Duplex Dual-Band Wireless Radios

5

Full-Duplex Dual-Band OFDM Radio Transceiver

Flexibility is a key feature in 5G wireless networks [12], where there will be a great demand of flexible radio transceivers that can support different wireless standards and meet different service requirements at a time. Besides, there is also a high demand on flexible radio transceivers in cognitive radio networks. For the practical design of flexible radios however, seeking a highly flexible and reconfigurable radio transceiver is always a big challenge. In this Chapter, we first propose a radio architecture: Full-Duplex Dual-Band (FDDB) OFDM radio, which enables the radio transceiver to be much more flexible and also provides viable radio link capacity gain, based on the cooperative combination of Full-Duplex radio and Dual-Band RF front-end. However, the practical implementation of OFDM based wireless systems suffers from the RF impairments such as in-phase and quadrature (I/Q) imbalance in the RF front-end. Especially in FDDB OFDM radio receivers, the mutual leakage signals induced by the I/Q imbalance significantly degrade the performance of the reception. Then, we further develop a digital I/Q imbalance estimation and compensation method based on the behaviors of the frequency-flat-fading of the SI channel for combating this I/Q imbalance. After that, a flexible radio transceiver based on the proposed FDDB OFDM radio is presented.

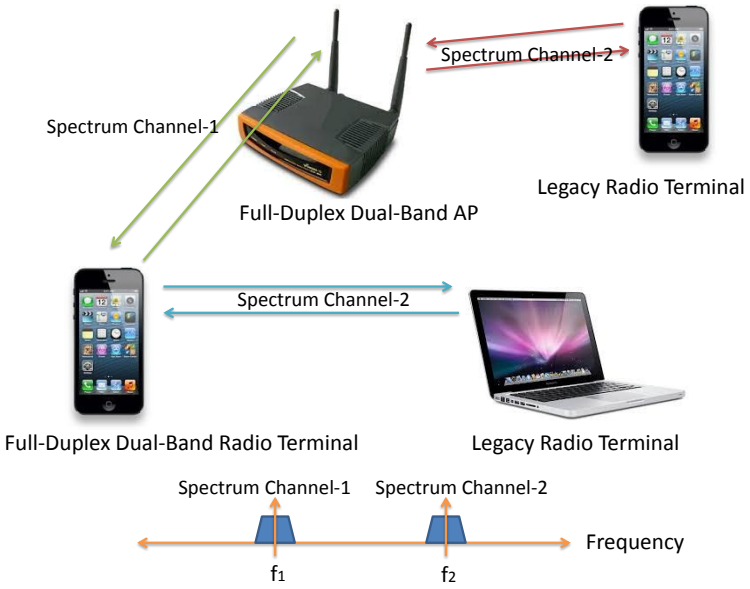

Figure 5.1: One application scenario of FDDB radio.

5.1 Introduction

The growing demand for various multimedia and increasingly pervasive wireless radios calls for the development of advanced and flexible radio transceivers to support high data rate and different wireless standards over limited radio resources in future wireless network. However, seeking a highly flexible and agile radio transceiver is always a big challenge. Fortunately, the noticeable gain of physical layer capacity and the capability of processing two different types of signals on two separate spectrum fragments of the FDDB radio [121] promote it as a flexible radio front-end. Based on this flexible radio, a FDDB OFDM radio is developed.

Full-Duplex is defined as a radio which can simultaneously transmit and receive in the same frequency band [39, 55]. More globally, for any future development of flexible radio system, Full-Duplex radio shows a great potentiality. In the meantime, Dual-Band radio can simultaneously process two different kind of signals, even different physical layer signals, by using one common RF front-end with a double I/Q structure [28]. FDDB radio based on the combination of Full-Duplex radio and Dual-Band radio enables the radio node to simultaneously transmit, simultaneously receive or simultaneously transmit and receive on each separate spectrum fragment. For instance, one FDDB radio terminal can communicate simultaneously with two radio terminals in the Full-Duplex mode as shown in Fig. 5.1.

Such a capability could be exploited to enhance the radio resource sharing and coexistence. Portable radio terminals such as smartphones have to accommodate a

growing list of wireless standards such as WiFi, Bluetooth, 3G, 4G and even future 5G. Current practical implementation is to use separate radio and antenna to meet the different standards requirement, which is costive and also puts high requirements on the space of portable consumer devices. Instead, FDDB radio could enable the radio terminal to accommodate two different wireless standards with one common RF front-end.

Furthermore, OFDM-based capabilities of sensing and spectrum shaping together with its flexibility make it probably the best transmission technology for the flexible radios [79]. Therefore, the FDDB OFDM radio transceivers based on the RF front-end proposed in [121] is the flexible radio transceiver we are exploring.

Although the Full-Duplex radio enables the radio terminal to be much more flexible, the big challenge behind it is the strong SI which could saturate the radio receivers and further break down the proposed radio system. Besides, the proposed FDDB OFDM radio receivers suffer from RF impairments such as I/Q imbalance which causes undesired mutual signal leakage significantly degrading the performance of system reception. In order to implement a high performance FDDB OFDM radio transceiver, it is necessary to reduce the SI to a tolerable level at first and then to estimate and compensate the I/Q imbalance.

In this Chapter, related works on the SIC for Full-Duplex wireless and I/Q imbalance estimation and compensation methods are given at first. Then, the FDDB radio including the SIC for Full-Duplex and Dual-Band RF front-end are presented. Next, the impact of I/Q imbalance on the FDDB is analyzed and studied. After that, a simple but practical I/Q imbalance estimation and compensation method is proposed and elaborated. Finally, the feasibility of FDDB radio is demonstrated and the performance of the proposed I/Q imbalance estimation and compensation method is evaluated by system level simulation conducted with ADS and Matlab software.

5.2 Related Works

5.2.1 State-of-the-Art of the SIC for Full-Duplex Wireless

To handle the strong SI, the researchers at the University of Waterloo [60, 61], Stanford University [30], NEC Lab and Princeton University [17, 83] proposed interference nulling or canceling from the perspective of antennas. The researchers at Rice University [41] proposed PSIS including directional isolation, absorptive shielding and cross polarization. Besides, [30, 39, 55, 95] studied the ASIC. All the details of these method have been summarized in Chapter 2, hence they are dropped here.

5.2.2 Related Works on I/Q Imbalance Estimation and Compensation

Down-converting the radio frequency (RF) signal to baseband signal is a fundamental function of all receiver RF front-ends. Up to date, there are mainly two different RF architectures to convert the RF signals to baseband signals, i.e. through intermediate frequency (IF) or via direct-conversion (zero-IF). Based on this, the radio receivers are classified into zero-IF receivers and superheterodyne (with IF) receivers. With respect to different kinds of radio receivers, there are different approaches for addressing the I/Q imbalance estimation and compensation. Due to the lot of approaches on that topic, we will just point out some significant examples.

- For Zero-IF Receivers
  - Based on Training Symbols

  The authors in [102] proposed an I/Q imbalance estimation technique based on the design of special pilot tones and a Least Mean Squares (LMS) algorithm. This technique requires the modification of the training sequences and suffers from a huge number of OFDM training symbols and low convergence rate. [99] proposed a special training sequence design for the I/Q imbalance parameter estimation. Another I/Q imbalance estimation technique based on the redesign of the preamble proposed by [111] requires the modification of the preamble of IEEE 802.11a. [105] and [115] proposed an I/Q imbalance estimation and compensation method based on the assumption that the adjacent subcarriers are highly correlated.

  - Based on Data Symbols

  Windisch et al. [110] proposed an I/Q imbalance estimation scheme based on the statistical analysis of the data symbols, i.e. blind estimation. This method requires a large number of data symbols to obtain a good I/Q imbalance estimation.

- For Superheterodyne Receiver
  - Based on Training Symbols

  [103] proposed to employ two different long training symbols instead of two identical long training symbols to carry out the channel and I/Q imbalance estimation. However, the two long training symbols are identical in the practical

implementation of IEEE 802.11g. Then, the authors further proposed an iterative algorithm by both using the training and data OFDM symbols.

– Based on Data Symbols

The blind I/Q imbalance estimation based on the two received baseband signals (uncompensated desired and image signal) are presented in [44] and [109]. This approach relies on the assumption that the desired and image signals are zero-mean wide-sense stationary random processes and mutually uncorrelated, which puts high requirements on the design of signals.

5.3 Full-Duplex Dual-Band Radio

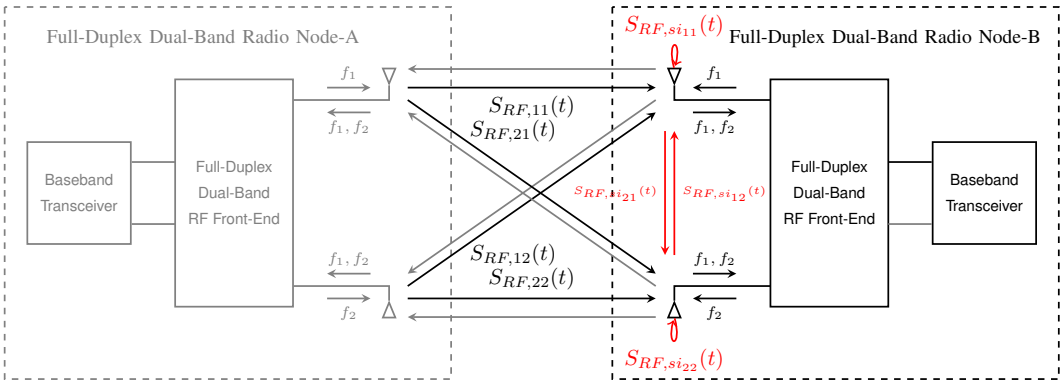

Figure 5.2: Block diagram of a general Full-Duplex Dual-Band wireless radios.

The general system model of the proposed flexible radio is as shown in Fig. 5.2 and the design in details is as shown in Fig. 5.3. Each of the proposed radio nodes employs two antennas which are compatible with future multi-antenna systems. Each antenna is used for simultaneous transmission and reception via a circulator [24, 48, 64] separating the input and output signals. As this is a symmetric problem, the radio node-B, shown in Fig. 5.2, is only studied. At the studied local radio node (FDDB radio node-B), the first antenna transmits the RF signal with carrier frequency f_1 while receives mixed RF signals including the RF signals from the distant radio node (FDDB radio node-A) with carrier frequency f_1 and f_2 as well as the RF signals from the local radio node with carrier frequency f_1 and f_2. Therefore, The signal received by the i^{th} antenna of the local radio node plus the SI signal leaked from the circulator can be expressed as

$$X_{RF,i}(t) = S_{RF,ij}(t) + S_{RF,ii}(t) + S_{RF,si_{ij}}(t) + aS_{RF,si_{ii}}(t), \{i,j\} \in A \tag{5.1}$$

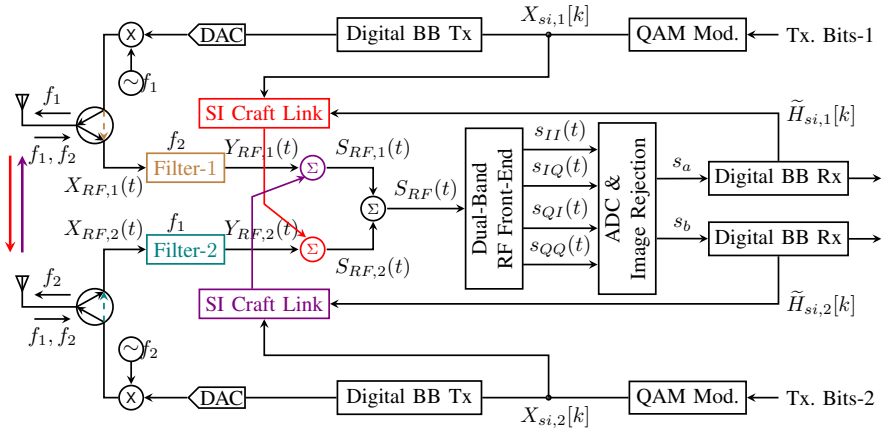

Figure 5.3: Design in details of the Full-Duplex Dual-Band wireless radios.

where $S_{RF,ij}(t)$ and $S_{RF,ii}(t)$ are the RF signals emitted from the j^{th} antenna and the i^{th} antenna of the distant radio node respectively and received by the i^{th} antenna of the local radio node; $S_{RF,si_{ij}}$ denotes the internal RF SI signal transmitted from the j^{th} antenna and received by the i^{th} antenna of the local radio node; $S_{RF,si_{ii}}$ is the inner RF SI signal leaked from its own transmission, a being the inner-SI factor including multi-path reflection factor and inner leakage factor of the circulator and $A \triangleq \{i \in [1,2], j \in [1,2], i+j=3\}$. Due to the short distance between the antennas of the same radio node, the internal SI $S_{RF,si_{ij}}$ is much stronger than the signals from the distant radio node, e.g. $90 \sim 110$dB higher [24, 92]. With respect to the inner SI, it is even stronger than the internal SI which relies on the fact that the circulator has only 15dB of isolation [24]. Therefore, the reception of the desired signal from the distant radio node is challenged by these two strong SI signals.

5.3.1 Full-Duplex Radio

Full-Duplex radio can enhance the flexibility of the spectrum utilization and the link capacity of a radio system, however it also brings strong SI. If no measures are taken, the strong SI could saturate the receiver chain due to the reason that the ADC has a limited dynamic range. Therefore, we need first to suppress or reduce these SI signals to a tolerable level in order to obtain the expected system performance. With respect to the inner and internal SI, we have two different SIC methods. After each of the circulators, the two SIC stages are implemented to eliminate the inner SI leaked from its own transmission and reduce the internal SI from the other antenna of the local radio node. From the other perspective, the inner SI and internal SI can be regarded as SI induced by one-antenna Full-Duplex and two-antenna Full-Duplex respectively.

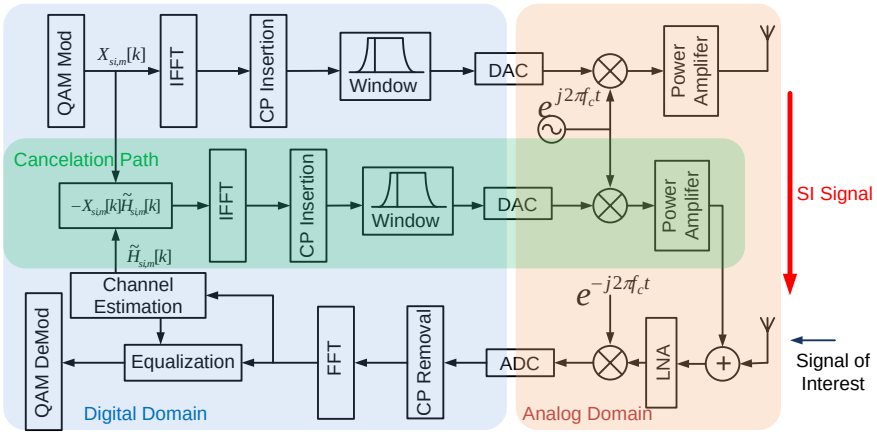

Figure 5.4: Architecture of self-interference cancellation for in-band two-antenna Full-Duplex wireless.

The First Self-Interference Cancellation

The first SIC is carried out by using BPF-i (Band Pass Filter, perfect BPFs are assumed) with center frequency f_j to filter out the inner RF SI signal $aS_{RF,si_{ii}}$ induced by near-field reflection and the imperfect circulator isolation as well as the RF signal $S_{RF,ii}(t)$ with carrier frequency f_i from the i^{th} antenna of the distant radio node. Then, the RF signals with carrier frequency f_j including the signal of interest $S_{RF,ij}(t)$ and the over-the-air SI signal $S_{RF,si_{ij}}(t)$ can be represented by

$$Y_{RF,i}(t) = S_{RF,ij}(t) + S_{RF,si_{ij}}(t), \{i,j\} \in A \tag{5.2}$$

The Second Self-Interference Cancellation

In order to cancel the internal SI signal $S_{RF,si_{ij}}(t)$ expressed in (5.2), [38, 55] proposed an ASIC and [41] studied the PSIS. In this radio design, we craft the RF cancellation signal as presented in [117] and carry out the cancellation at the RF stage as shown in Fig. 5.4. To avoid the impact of the signal from the distant radio node on the SI channel estimation, the frame structure of the FDDB IEEE 802.11g is modified as Fig. 5.5. The crafted RF cancellation signal can be represented by $S_{RF,sic_{ij}}(t)$, which has been presented in details in Chapter 3. Then, the received signal in the i^{th} branch of the receiver after the second SIC (i.e. AARFSIC) would be

$$\begin{aligned} S_{RF,i}(t) &= Y_{RF,i}(t) - S_{RF,sic_{ij}(t)} \\ &= S_{RF,ij}(t) + \underbrace{S_{RF,si_{ij}}(t) - S_{RF,sic_{ij}}(t)}_{\text{residual self-interference}} \end{aligned} \tag{5.3}$$

Therefore, the RF signal $S_{RF,i}(t)$, to be input into the Dual-Band RF front-end, comprises the desired signal $S_{RF,ij}(t)$ from the distant radio node and the residual SI induced by the in-band two-antenna Full-Duplex wireless.

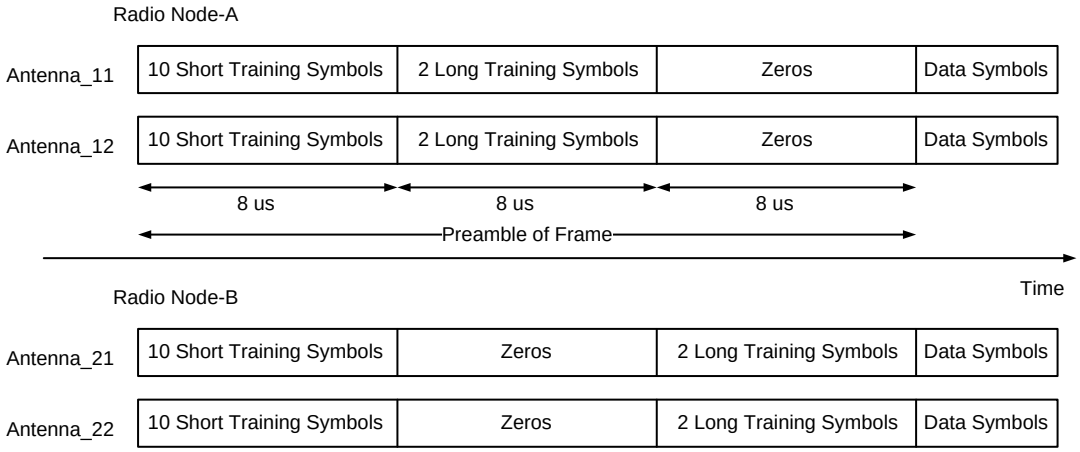

Figure 5.5: The frame structure for the in-band two-antenna Full-Duplex IEEE 802.11g.

5.3.2 Dual-Band RF Front-End

After the two stages of SIC, the received RF signal $S_{RF}(t) = S'_{RF,1}(t) + S'_{RF,2}(t)$, where $S'_{RF,1}(t) \triangleq S_{RF,2}(t)$ with carrier frequency f_1 and $S'_{RF,2}(t) \triangleq S_{RF,1}(t)$ with carrier frequency f_2, will be down-converted to baseband signal by using the double I/Q structure as shown in Fig. 5.6.

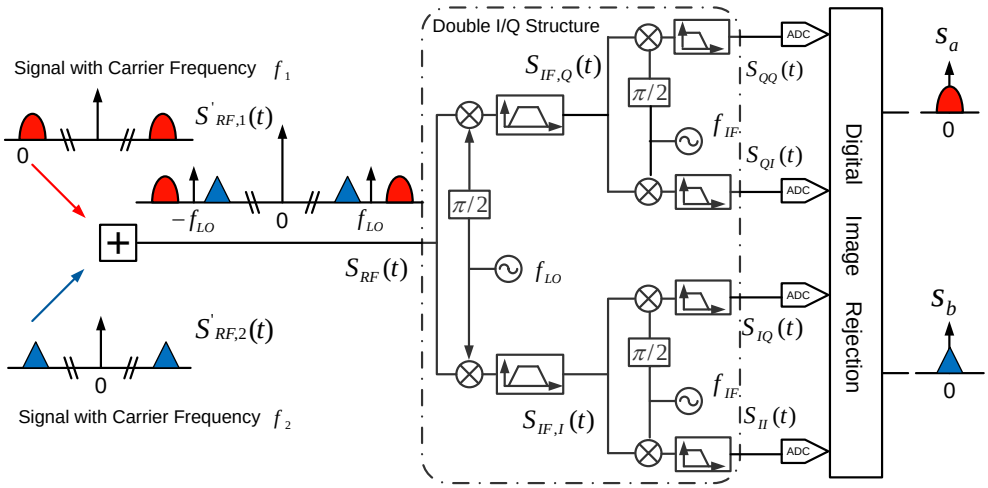

Figure 5.6: Architecture of the Dual-Band RF front-end.

In order to facilitate the theoretical study of the Dual-Band RF front-end, let $s_1 = I_1 + \jmath Q_1$ and $s_2 = I_2 + \jmath Q_2 (\jmath^2 = -1)$ to denote the received equivalent baseband complex symbols carried by the carrier frequencies f_1 and f_2. Then, the RF signals $S'_{RF,1}(t)$ and $S'_{RF,2}(t)$ at the input of the double I/Q structure are

$$S'_{RF,1}(t) = I_1(t)cos(2\pi f_1 t) - Q_1(t)sin(2\pi f_1 t) \tag{5.4}$$

$$S'_{RF,2}(t) = I_2(t)cos(2\pi f_2 t) - Q_2(t)sin(2\pi f_2 t) \tag{5.5}$$

Note that the signal models in Eq. (5.4) (5.5) are reasonably valid even for an interference and noisy environment because $I_i(t)$ can represent the sum of the real part of the received symbol including the desired data and the residual SI data symbol and noise, $Q_i(t)$ can represent the sum of the image part of the received symbol including the desired data and the residual SI data symbol and the receiver thermal noise.

In Fig. 5.6, after the mixed signal, $S_{RF}(t) = S'_{RF,1}(t) + S'_{RF,2}(t)$, going through the first frequency translation stage with carrier frequency $f_{LO} = \frac{f_1+f_2}{2}$, the band pass signals are filtered out. Then, the I/Q branch of the intermediate frequency (IF) signal can be obtained as

$$S_{IF,I}(t) = \frac{I_1(t) + I_2(t)}{2} cos(2\pi f_{IF} t) + \frac{-Q_1(t) + Q_2(t)}{2} sin(2\pi f_{IF} t) \tag{5.6}$$

$$S_{IF,Q}(t) = \frac{I_1(t) - I_2(t)}{2} sin(2\pi f_{IF} t) + \frac{Q_1(t) + Q_2(t)}{2} cos(2\pi f_{IF} t) \tag{5.7}$$

where $f_{IF} = \frac{f_1-f_2}{2} = f_1 - f_{LO} = f_{LO} - f_2$.

Then, the baseband signals $s_{II}(t)$, $s_{IQ}(t)$, $s_{QI}(t)$ and $s_{QQ}(t)$ obtained by down-converting the IF signals $S_{IF,I}(t)$ and $S_{IF,Q}(t)$ with the carrier frequency f_{IF} can be expressed as

$$s_{II}(t) = \frac{I_1(t) + I_2(t)}{4} \tag{5.8}$$

$$s_{IQ}(t) = \frac{Q_1(t) - Q_2(t)}{4} \tag{5.9}$$

$$s_{QI}(t) = \frac{Q_1(t) + Q_2(t)}{4} \tag{5.10}$$

$$s_{QQ}(t) = \frac{-I_1(t) + I_2(t)}{4} \tag{5.11}$$

After the analog-to-digital converter (ADC), we can obtain $s_{II} = \frac{I_1+I_2}{4}, s_{IQ} = \frac{Q_1-Q_2}{4}, s_{QI} = \frac{Q_1+Q_2}{4}, s_{QQ} = \frac{-I_1+I_2}{4}$. By using the digital-image-rejection, the received

baseband complex symbols s_a and s_b corresponding to symbols s_1 and s_2 are given by

$$\begin{aligned} s_a &= s_{II} - s_{QQ} + \jmath(s_{IQ} + s_{QI}) \\ &= \frac{I_1 + \jmath Q_1}{2} \\ &= \frac{s_1}{2} \end{aligned} \tag{5.12}$$

$$\begin{aligned} s_b &= s_{II} + s_{QQ} + \jmath(-s_{IQ} + s_{QI}) \\ &= \frac{I_2 + \jmath Q_2}{2} \\ &= \frac{s_2}{2} \end{aligned} \tag{5.13}$$

From Eq. (5.12) (5.13), the two different kinds of signals (even with different physical layer technologies) are perfectly separated by using this double I/Q structure. That means the Dual-Band radio receiver can simultaneously process two different kind of signals with different carrier frequencies by using a relatively simple RF front-end compared to the conventional multiband radios.

Therefore, the FDDB radio could simultaneously transmit as well as receive two different types of signals with different carrier frequencies which yields a four times increase in the radio link capacity. Besides, this radio architecture could also show its flexibility in the spectrum utilization. This is because the FDDB radio receiver not only can simultaneously receive two different types of signals with two different carrier frequencies but also can receive one signal with carrier frequency f_1 or f_2.

5.4 Impact of I/Q Imbalance on the Full-Duplex Dual-Band OFDM Radios

However, the noticeable gain in the radio link capacity and the flexibility in the spectrum channel utilization can be obtained only when the transceiver RF front-ends are theoretically ideal. In the practical implementation of wireless system, any part of the I/Q imbalance of the RF front-end may contribute to degrade the radio receiver performance and no exception for the FDDB OFDM radio. In the following, the I/Q imbalance model and its impact on the FDDB OFDM radio receiver will be studied.

The purpose of a radio front-end is to down-convert the RF signal to the baseband analog signal. However, all of the analog components (such as mixers, filters and ADC) at the radio front-end lead to deviations from the desired 90^o phase shift and the desired equal gain in the I and Q branches as shown in Fig. 5.7. Here, ΔA and $\Delta\phi$

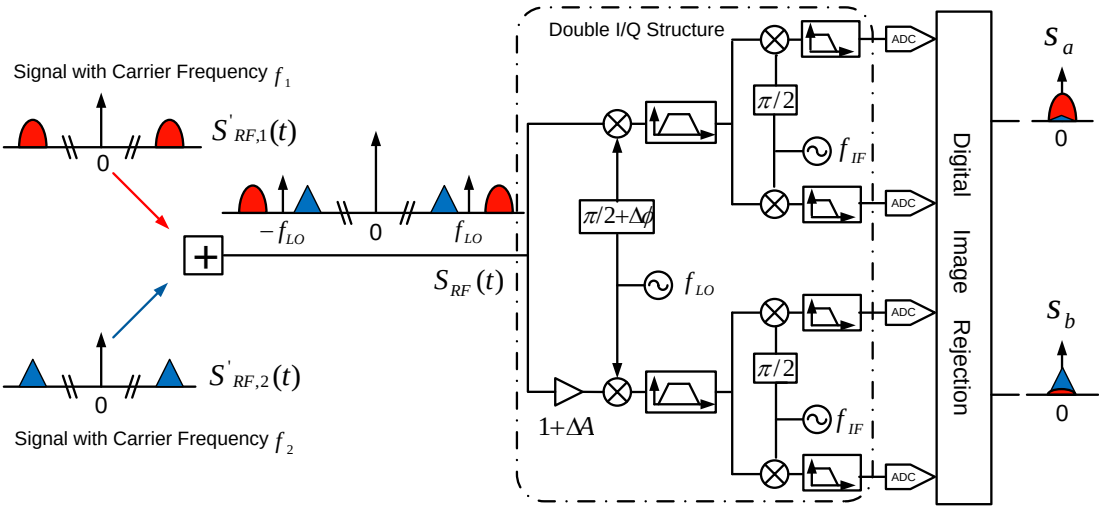

Figure 5.7: Architecture of Dual-Band RF front-end with I/Q imbalance.

are used to denote the amplitude imbalance and the phase imbalance respectively.[1] In the Dual-Band radio receivers, this I/Q imbalance causes undesirable mutual signal leakage. After double I/Q frequency translation with I/Q imbalance, the two base-band analog signals can be expressed as [28]

$$s_a = \alpha s_1 + \beta s_2^* \tag{5.14}$$

$$s_b = \alpha s_2 + \beta s_1^* \tag{5.15}$$

where s_a and s_b are the two output signals from the double I/Q structure with I/Q imbalance, $(\cdot)^*$ denotes complex conjugation, and the I/Q imbalance coefficients α and β [28] are represented by

$$\alpha = \frac{1 + (1 + \Delta A)e^{-\jmath\Delta\phi}}{2} \tag{5.16}$$

$$\beta = \frac{1 - (1 + \Delta A)e^{+\jmath\Delta\phi}}{2} \tag{5.17}$$

According to the definition (5.16) (5.17), we can get

$$\alpha + \beta^* = \alpha^* + \beta = 1 \tag{5.18}$$

Especially, with an ideal I/Q, i.e. $\Delta A = 0$ and $\Delta\phi = 0$, therefore $\alpha = 1$ and $\beta = 0$, which means the received two different carrier frequency signals are separated

[1] Here, we model the I/Q imbalance just in the first IQ demodulator due to the fact that the I/Q imbalance in the second IQ demodulator has negligible effect compared to that of the first demodulator does [28].

completely by using the double I/Q structure just as the study case in Sec. 5.3.

From the Eq. (5.14) (5.15), we can see that the I/Q imbalance makes the image of the other signal superimpose on the desired signal. This mutual leakage of the signals will be regarded as interference to degrade the performance of the radio reception. However, if we can obtain the I/Q imbalance parameters (α and β), s_1 and s_2 can be calculated as

$$s_1 = \frac{\alpha^* s_a - \beta s_b^*}{|\alpha|^2 - |\beta|^2} \tag{5.19}$$

$$s_2 = \frac{\alpha^* s_b - \beta s_a^*}{|\alpha|^2 - |\beta|^2} \tag{5.20}$$

That means, even with I/Q imbalance, the two received signals can be separated completely just like the RF front-end without I/Q imbalance does if the values of α and β are known. Unfortunately, the exact values of α and β are difficult to obtain. However, α and β are quite stable due to the reason that the values of ΔA and $\Delta\phi$ are largely dependent on the performance of analog devices in the RF front-end. Therefore, the values can be estimated by using a training sequence.

5.5 Digital Estimation and Compensation of I/Q Imbalance

In order to mitigate the impact of the I/Q imbalance on the FDDB OFDM radio, a simple but practical digital estimation and compensation of I/Q imbalance scheme will be presented in this Section.

5.5.1 Digital Estimation of I/Q Imbalance

In the system design, the I/Q imbalance estimation is carried out during the SI channel estimation. Therefore, the received symbols s_1 and s_2 in Eq. (5.14) (5.15) just include the long training symbols from its own transmitter and the receiver thermal noise during the I/Q imbalance estimation as the different radio nodes take different time slots for transmitting the long training signals. Therefore, these two equations during the time of SI channel estimation can be rewrote as

$$s_{LTS,a} = \alpha s_{LTS_{si},12} + \beta s^*_{LTS_{si},21} \tag{5.21}$$

$$s_{LTS,b} = \alpha s_{LTS_{si},21} + \beta s^*_{LTS_{si},12} \tag{5.22}$$

where $s_{LTS_{si},12}$ is the long training symbols transmitted from the 2^{nd} antenna and received by the 1^{st} antenna of the local radio node, and $s_{LTS_{si},21}$ is the long training symbols from the 1^{st} antenna and received by the 2^{nd} antenna of the local radio node.

According to Eq. (5.21) (5.22) and using the Least Squares (LS) channel estimation algorithm in the frequency domain, the estimated coefficients of the SI channel-1 $H_{si,a}$ and channel-2 $H_{si,b}$ can be expressed as

$$H_{si,a}[k] = \alpha \widetilde{H}_{si,12}[k] + \beta T'[k] \widetilde{H}^*_{si,21}[N_{nz} - k + 1] \tag{5.23}$$

$$H_{si,b}[k] = \alpha \widetilde{H}_{si,21}[k] + \beta T'[k] \widetilde{H}^*_{si,12}[N_{nz} - k + 1] \tag{5.24}$$

where $\widetilde{H}_{si,12}[k]$ denotes the coefficient of the k^{th} subcarrier channel of the SI channel from the 2^{nd} antenna to the 1^{st} antenna of the local radio node; $\widetilde{H}_{si,21}[k]$ denotes the coefficient of the k^{th} subcarrier channel of the SI channel from the 1^{st} antenna to the 2^{nd} antenna of the local radio node. $\widetilde{H}_{si,21}[N_{nz} - k + 1]$ and $\widetilde{H}_{si,12}[N_{nz} - k + 1]$ are the mirror images of the channel $\widetilde{H}_{si,21}[k]$ and $\widetilde{H}_{si,12}[k]$, $T'[k] \triangleq T[k]T[N_{nz} - k + 1]$. Eq. (5.23) (5.24) show that each channel estimation consists of two components: one is the SI channel which is scaled by a complex factor $\alpha \approx 1$ and the other one is the mirror image of the other SI channel scaled by a factor $\beta T'[k] \approx 0$. As a consequence, the I/Q imbalance in the double frequency structure makes the mirror image of the SI channel superimpose on the desired SI channel. This channel estimation error induced by I/Q imbalance will affect the equalization at the receiver.

In the FDDB OFDM wireless system, the distance between the antennas of the same radio node is quite short, so the power of the line-of-sight path dominates the SI channel. As a consequence, the SI channel is much more close to a frequency flat fading channel [41]. From Eq. (5.23) (5.24), if α and β are known exactly, the SI channel $\widetilde{H}_{si,12}[k]$ and $\widetilde{H}_{si,21}[k]$ can be obtained as

$$\begin{aligned} \widetilde{H}_{si,12}[k] &= \frac{\alpha^* H_{si,a}[k] - \beta T'[k] \cdot H^*_{si,b}[N_{nz} - k + 1]}{|\alpha|^2 - |\beta|^2} \\ \widetilde{H}_{si,21}[k] &= \frac{\alpha^* H_{si,b}[k] - \beta T'[k] \cdot H^*_{si,a}[N_{nz} - k + 1]}{|\alpha|^2 - |\beta|^2} \end{aligned} \tag{5.25}$$

The SI channel $\widetilde{H}_{si,12}[k]$ and $\widetilde{H}_{si,21}[k]$ are frequency flat fading channel which can be shown as in Fig. 5.8, while the estimated SI channel $H_{si,a}[k]$ and $H_{si,b}[k]$ with I/Q imbalance are more likely a frequency selective fading channel. With the estimated $\widetilde{\alpha}$ and $\widetilde{\beta}$ under the I/Q imbalance condition, we can obtain the virtual SI channel

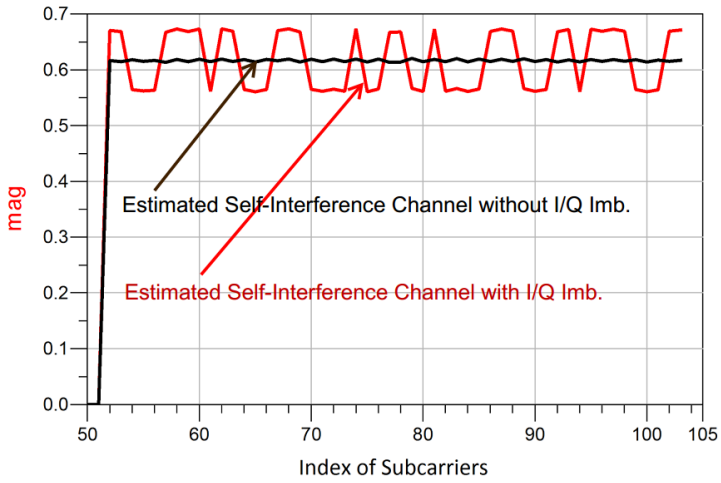

Figure 5.8: **The estimated magnitude of each subcarrier channel of the over-the-air SI channel with or without I/Q Imbalance**. Without I/Q imbalance, the over-the-air SI channel is almost a frequency flat fading channel, while the SI channel will be a frequency selective fading channel when I/Q imbalance ($\Delta A = 0.2, \Delta\phi = 10^o$) exists in the FDDB radio front-end.

$\widehat{H}_{si,12}[k]$ and $\widehat{H}_{si,21}[k]$ as

$$\begin{aligned}\widehat{H}_{si,12}[k] &= \frac{\widetilde{\alpha}^* H_{si,a}[k] - \widetilde{\beta} T'[k] \cdot H^*_{si,b}[N_{nz} - k + 1]}{|\widetilde{\alpha}|^2 - |\widetilde{\beta}|^2} \\ \widehat{H}_{si,21}[k] &= \frac{\widetilde{\alpha}^* H_{si,b}[k] - \widetilde{\beta} T'[k] \cdot H^*_{si,a}[N_{nz} - k + 1]}{|\widetilde{\alpha}|^2 - |\widetilde{\beta}|^2}\end{aligned} \tag{5.26}$$

The more accurate the estimated $\widetilde{\alpha}$ and $\widetilde{\beta}$, the more closely the virtual SI channels $\widehat{H}_{si,12}[k]$ and $\widehat{H}_{si,21}[k]$ are to the SI channel $\widetilde{H}_{si,12}[k]$ and $\widetilde{H}_{si,21}[k]$. Therefore, the I/Q imbalance parameters $(\widetilde{\alpha}, \widetilde{\beta})$ that make the virtual SI channel $\widehat{H}_{si,1}[k]$ and $\widehat{H}_{si,2}[k]$ as flat as possible like the SI channels do are what we are searching. We define the mean square error (MSE) of the consecutive subcarrier channels as the criteria to measure how flat the virtual SI channel is as following

$$MSE_1 = \sum_k |\widehat{H}_{si,12}[k+1] - \widehat{H}_{si,12}[k]|^2 \tag{5.27}$$

$$MSE_2 = \sum_k |\widehat{H}_{si,21}[k+1] - \widehat{H}_{si,21}[k]|^2 \tag{5.28}$$

As this is a symmetric problem, the case MSE_1 will be studied first. According to

Eq. (5.26), we can obtain

$$
\begin{aligned}
&|\widehat{H}_{si,12}[k+1] - \widehat{H}_{si,12}[k]|^2 \\
&= \frac{|\widetilde{\alpha}^* H_{si,a}[k+1] - \widetilde{\beta} T'[k+1] H^*_{si,b}[N_{nz}-k] - \widetilde{\alpha}^* H_{si,a}[k] + \widetilde{\beta} T'[k] H^*_{si,b}[N_{nz}-k+1]|^2}{(|\widetilde{\alpha}|^2 - |\widetilde{\beta}|^2)^2} \\
&= \frac{|\widetilde{\alpha}^* (H_{si,a}[k+1] - H_{si,a}[k]) - \widetilde{\beta} (T'[k+1] H^*_{si,b}[N_{nz}-k] - T'[k] H^*_{si,b}[N_{nz}-k+1])|^2}{(|\widetilde{\alpha}|^2 - |\widetilde{\beta}|^2)^2}
\end{aligned}
\tag{5.29}
$$

In order to simplify the Eq. (5.29), we define

$$
\begin{aligned}
\Delta H_{si,a}[k] &= H_{si,a}[k+1] - H_{si,a}[k] && (5.30)\\
\Delta H'_{si,b}[k] &= T'[k+1] \cdot H^*_{si,b}[N_{nz}-k] - T'[k] \cdot H^*_{si,b}[N_{nz}-k+1] && (5.31)
\end{aligned}
$$

After combining Eq. (5.30) (5.31) with Eq. (5.29), the Eq. (5.29) can be rewrote as

$$
|\widehat{H}_{si,12}[k+1] - \widehat{H}_{si,12}[k]|^2 = \frac{|\widetilde{\alpha}^* \cdot \Delta H_{si,a}[k] - \widetilde{\beta} \cdot \Delta H'_{si,b}[k]|^2}{(|\widetilde{\alpha}|^2 - |\widetilde{\beta}|^2)^2} \tag{5.32}
$$

As the SI channel is a frequency flat fading channel, so the adjacent subcarrier channel should be very close to each other. However, the I/Q imbalance ($\widetilde{\alpha}$ and $\widetilde{\beta}$) makes the frequency flat fading SI channel $\widehat{H}_{si,12}[k]$ and $\widehat{H}_{si,21}[k]$ much more fluctuating. Then, the parameters ($\widetilde{\alpha}$ and $\widetilde{\beta}$) which make the $|\widehat{H}_{si,12}[k+1] - \widehat{H}_{si,12}[k]|$ as small as possible are the values we are exploring. Therefore, the optimization problem can be formulated as

$$
\begin{aligned}
(\widetilde{\alpha}_{o,1}, \widetilde{\beta}_{o,1}) &= \arg \min_{\widetilde{\alpha} \in \mathcal{C}, \widetilde{\beta} \in \mathcal{C}} \left\{ \sum_k \left\| \widehat{H}_{si,12}[k+1] - \widehat{H}_{si,12}[k] \right\|^2 \right\} \\
&= \arg \min_{\widetilde{\alpha} \in \mathcal{C}, \widetilde{\beta} \in \mathcal{C}} \left\{ \frac{\sum_k \left\| \widetilde{\alpha}^* \cdot \Delta H_{si,a}[k] - \widetilde{\beta} \cdot \Delta H'_{si,b}[k] \right\|^2}{(|\widetilde{\alpha}|^2 - |\widetilde{\beta}|^2)^2} \right\}
\end{aligned}
\tag{5.33}
$$

where $\mathcal{C}$ denotes the set of complex numbers.

In order to obtain the optimal estimated values $(\widetilde{\alpha}_{o,1}, \widetilde{\beta}_{o,1})$, we take the partial

derivative of the MSE_1 with respect to $\widetilde{\beta}$ as

$$\begin{aligned}\frac{\partial MSE_1}{\partial \widetilde{\beta}} &= \frac{\partial \left\{ \sum_k \left\| \widehat{H}_{si,12}[k+1] - \widehat{H}_{si,12}[k] \right\|^2 \right\}}{\partial \widetilde{\beta}} \\ &= \sum_k \frac{\partial \left\{ \frac{\left\| \widetilde{\alpha}^* \cdot \Delta H_{si,a}[k] - \widetilde{\beta} \cdot \Delta H'_{si,b}[k] \right\|^2}{(|\widetilde{\alpha}|^2 - |\widetilde{\beta}|^2)^2} \right\}}{\partial \widetilde{\beta}}\end{aligned} \tag{5.34}$$

Because of $(|\widetilde{\alpha}|^2 - |\widetilde{\beta}|^2)^2 \approx 1$, even valid for high gain imbalance and phase imbalance, e.g. ($\Delta A = 0.2$ and $\Delta\phi = 10$), then Eq. (5.34) can be simplified as

$$\frac{\partial MSE_1}{\partial \widetilde{\beta}} \approx \sum_k \frac{\partial \left\| \widetilde{\alpha}^* \cdot \Delta H_{si,a}[k] - \widetilde{\beta} \cdot \Delta H'_{si,b}[k] \right\|^2}{\partial \widetilde{\beta}} = \sum_k \frac{\partial z_k}{\partial \widetilde{\beta}} \tag{5.35}$$

where we define $z_k \triangleq \left\| \widetilde{\alpha}^* \cdot \Delta H_{si,a}[k] - \widetilde{\beta} \cdot \Delta H'_{si,b}[k] \right\|^2$ which is function of $\widetilde{\beta} = \Re(\widetilde{\beta}) + \jmath\Im(\widetilde{\beta})$. Eq. (5.23) (5.24) show that the complex value $\widetilde{\beta}$ is the key factor that makes the originally flat fading SI channel much more fluctuating. Therefore, the problem of calculating the optimal $\widetilde{\beta}$ in Eq. (5.35) becomes solving the Cauchy-Riemann equations as following

$$\sum_k \frac{\partial \Re(z_k)}{\partial \Re(\widetilde{\beta})} = \sum_k \frac{\partial \Im(z_k)}{\partial \Im(\widetilde{\beta})} \tag{5.36}$$

$$\sum_k -\frac{\partial \Re(z_k)}{\partial \Im(\widetilde{\beta})} = \sum_k \frac{\partial \Im(z_k)}{\partial \Re(\widetilde{\beta})} \tag{5.37}$$

The definition z_k is function of $\widetilde{\beta}$, which can be expressed as

$$\begin{aligned} z_k &= |\widetilde{\alpha}|^2 |\Delta H_{si,a}[k]|^2 + |\widetilde{\beta}|^2 |\Delta H'_{si,b}[k]|^2 - \widetilde{\alpha}\widetilde{\beta} \cdot \Delta H^*_{si,a}[k] \cdot \Delta H'_{si,b}[k] \\ &\quad -\widetilde{\alpha}^*\widetilde{\beta}^* \cdot \Delta H_{si,a}[k] \cdot \Delta H'^*_{si,b}[k] \end{aligned} \tag{5.38}$$

Then, the real part and image part of z_k can be obtained as

$$\begin{aligned} \Re(z_k) &= |\widetilde{\alpha}|^2 |\Delta H_{si,a}[k]|^2 + (\Re(\widetilde{\beta})^2 + \Im(\widetilde{\beta})^2) |\Delta H'_{si,b}[k]|^2 \\ &\quad -2\Re(\widetilde{\alpha} \cdot \Delta H^*_{si,a}[k] \cdot \Delta H'_{si,b}[k]) \Re(\widetilde{\beta}) + 2\Im(\widetilde{\alpha} \cdot \Delta H^*_{si,a}[k] \cdot \Delta H'_{si,b}[k]) \Im(\widetilde{\beta}) \\ \Im(z_k) &= 0 \end{aligned} \tag{5.39}$$

According to Eq. (5.39) (5.39), Eq. (5.36) (5.37) can be rewritten as

$$\sum_k \frac{\partial \Re(z_k)}{\partial \Re(\widetilde{\beta})} = 0 \tag{5.40}$$

$$\sum_k -\frac{\partial \Re(z_k)}{\partial \Im(\widetilde{\beta})} = 0 \tag{5.41}$$

Based on Eq. (5.40) (5.41), the real and image part of the optimal estimated $\widetilde{\beta}$ can be obtained as

$$\Re(\widetilde{\beta}_{o,1}) = \frac{\sum_k \Re(\widetilde{\alpha}_{o,1} \cdot \Delta H^*_{si,a}[k] \cdot \Delta H'_{si,b}[k])}{\sum_k |\Delta H'_{si,b}[k]|^2} \tag{5.42}$$

$$\Im(\widetilde{\beta}_{o,1}) = \frac{-\sum_k \Im(\widetilde{\alpha}_{o,1} \cdot \Delta H^*_{si,a}[k] \cdot \Delta H'_{si,b}[k])}{\sum_k |\Delta H'_{si,b}[k]|^2} \tag{5.43}$$

Therefore, the optimal value $\widetilde{\beta}_{o,1}$ of the estimated $\widetilde{\beta}$ is expressed as

$$\begin{aligned} \widetilde{\beta}_{o,1} &= \Re(\widetilde{\beta}_{o,1}) + \jmath\Im(\widetilde{\beta}_{o,1}) \\ &= \frac{\sum_k \alpha^* \cdot \Delta H_{si,a}[k] \cdot \Delta H'^*_{si,b}[k]}{\sum_k |\Delta H'_{si,b}[k]|^2} \\ &= \widetilde{\alpha}^*_{0,1}\widetilde{\beta_1} \end{aligned} \tag{5.44}$$

Here, we define $\widetilde{\beta}_1$

$$\begin{aligned} \widetilde{\beta}_1 &= \frac{\sum_k \Delta H_{si,a}[k] \cdot \Delta H'^*_{si,b}[k]}{\sum_k |\Delta H'_{si,b}[k]|^2} \\ &= \frac{\sum_k (H_{si,a}[k+1] - H_{si,a}[k])(T'[k+1] \cdot H_{si,b}[N_{nz}-k] - T'[k] \cdot H_{si,b}[N_{nz}-k+1])}{\sum_k |T'[k+1] \cdot H_{si,b}[N_{nz}-k] - T'[k] \cdot H_{si,b}[N_{nz}-k+1]|^2} \end{aligned} \tag{5.45}$$

which means that $\widetilde{\beta}_1$ can be estimated by using the estimated SI channel coefficients $H_{si,a}[k]$ and $H_{si,b}[k]$ which are corrupted by the I/Q imbalance parameters (α and β). After getting the estimated $\widetilde{\beta}_1$, the optimal estimated value $\widetilde{\beta}_{o,1}$ can be obtained by

$$\widetilde{\beta}_{o,1} = \widetilde{\alpha}^*_{o,1} \cdot \widetilde{\beta}_1 \tag{5.46}$$

According to the characterization of $\widetilde{\alpha}_{o,1}$ and $\widetilde{\beta}_{o,1}$ as in (5.16) (5.17), hence

$$\widetilde{\alpha}_{o,1} + \widetilde{\beta}^*_{o,1} = 1 \tag{5.47}$$

Then, the optimal estimated I/Q imbalance parameters $\widetilde{\alpha}_o$ and $\widetilde{\beta}_o$ can be solved as

$$\widetilde{\alpha}_{o,1} = \frac{1}{1+\widetilde{\beta}} \tag{5.48}$$

$$\widetilde{\beta}_{o,1} = 1-\widetilde{\alpha}^*_{o,1} \tag{5.49}$$

The same method can be used to obtain another pair of optimal I/Q imbalance parameters $\widetilde{\alpha}_{o,2}$ and $\widetilde{\beta}_{o,2}$ by solving the optimization problem

$$(\widetilde{\alpha}_{o,2},\widetilde{\beta}_{o,2}) = \arg \min_{\widetilde{\alpha}\in\mathcal{C},\widetilde{\beta}\in\mathcal{C}} \left\{ \sum_k \left\| \widehat{H}_{si,21}[k+1] - \widehat{H}_{si,21}[k] \right\|^2 \right\} \tag{5.50}$$

Then, the optimal estimated values $\widetilde{\alpha}_o$ and $\widetilde{\beta}_o$ which are employed to compensate the receiver I/Q imbalance are

$$\alpha_o = \frac{\widetilde{\alpha}_{o,1}+\widetilde{\alpha}_{o,2}}{2} \tag{5.51}$$

$$\beta_o = \frac{\widetilde{\beta}_{o,1}+\widetilde{\beta}_{o,2}}{2} \tag{5.52}$$

5.5.2 Digital Compensation of I/Q Imbalance

With the estimated I/Q imbalance parameters α_o and β_o available, we can compensate the I/Q imbalance existing in the FDDB RF front-end and separate the two different symbol sequences carried by the two different carrier frequencies by solving Eq. (5.14) (5.15) as

$$\begin{aligned} \widetilde{s}_1 &= \frac{\alpha^*_o s_a - \beta_o s^*_b}{|\alpha_o|^2 - |\beta_o|^2} \\ \widetilde{s}_2 &= \frac{\alpha^*_o s_b - \beta_o s^*_a}{|\alpha_o|^2 - |\beta_o|^2} \end{aligned} \tag{5.53}$$

The proposed I/Q imbalance estimation and compensation for the FDDB OFDM radio receiver is as shown in Fig. 5.9. The two baseband symbol sequences $\widetilde{s}_1$ and $\widetilde{s}_2$ after I/Q imbalance compensation will be processed by two baseband WLAN receivers as shown in Fig. 5.10. After that, the two data sequences from the distant radio node can be recovered.

The procedure of the I/Q imbalance estimation and compensation is described in the Algorithm 1. The received two baseband long training signals ($s_{LTS,a}, s_{LTS,b}$) are used to obtain the channel estimates ($H_{si,a}[k], H_{si,b}[k]$) by the LS algorithm. Then, the optimal estimates of the I/Q imbalance parameters (α_o, β_o) are calculated by cooperatively utilize ($H_{si,a}[k], H_{si,b}[k]$). Finally, we can use (α_o, β_o) to eliminate the image part

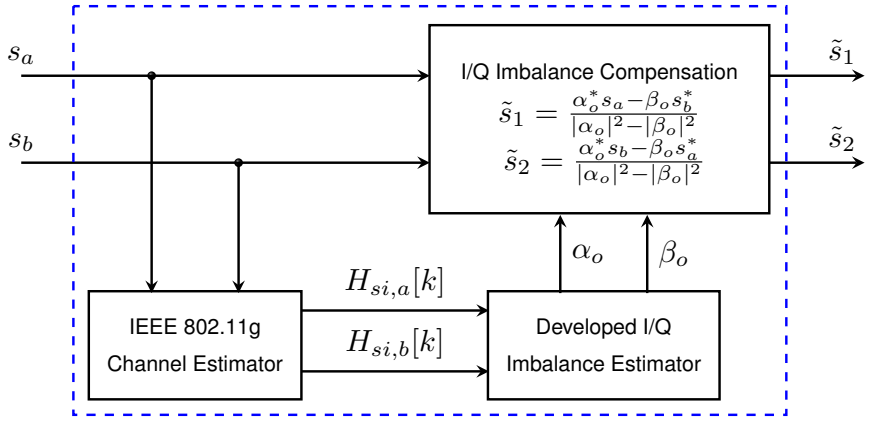

Figure 5.9: Compensation block for the I/Q imbalance.

in (s_a, s_b) and obtain the pured signal $(\tilde{s}_1, \tilde{s}_2)$.

Algorithm 1 I/Q imbalance estimation and compensation algorithm

procedure ESTIMATE(α_o, β_o) for each frame of IEEE 802.11g

1. $s_{lts,a}, s_{lts,b} \rightarrow H_{si,a}[k], H_{si,b}[k]$
2. $H_{si,a}[k], H_{si,b}[k] \rightarrow \alpha_o, \beta_o$
3. $s_a, s_b, \alpha_o, \beta_o \rightarrow \tilde{s}_1, \tilde{s}_2$

end procedure

5.6 Full-Duplex Dual-Band OFDM Radio Transceiver

From the studies above, FDDB radio could enable a radio terminal to simultaneously work on two spectrum fragments. In each spectrum fragment, it enables a radio transceiver to simultaneously transmit and receive signals. Therefore, FDDB radio could provide the users much more flexible radio connection and higher aggregate throughput than the current radio terminals operating on Half-Duplex model in a single spectrum channel at a time.

In this Section, the system level design of a more practical FDDB OFDM radio transceiver as shown in Fig. 5.10 is presented and the capacity of this radio link will be analyzed.

In each of the two spectrum fragments, the radio link capacity

$$\begin{aligned} C_i &= W \log_2(1 + SINR_i) \\ &= W \log_2 \left(1 + \frac{SNR_i}{INR_i \mathsf{A}_{\mathsf{SIC}}(INR_i) + 1} \right) \end{aligned} \tag{5.54}$$

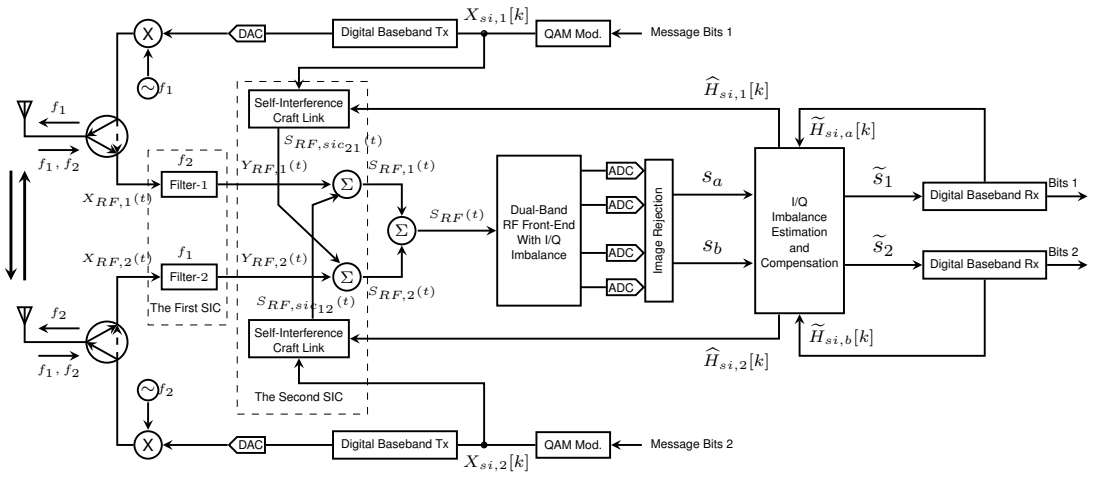

Figure 5.10: Full-Duplex Dual-Band OFDM radio transceiver with I/Q imbalance compensation.

where W_i denotes the bandwidth, $SINR_i$ represents the power ratio of the signal to interference plus noise, SNR_i denotes the power ratio of signal to thermal noise, INR_i represents the power ratio of the SI to noise, and $\mathsf{A}_{\mathsf{SIC}}(INR_i)$, depending on INR_i, denotes the amount of SIC the scheme can achieve.

Apparently, the residual SI, $INR_i\mathsf{A}_{\mathsf{SIC}}(INR_i)$, depends on INR_i and $\mathsf{A}_{\mathsf{SIC}}(INR_i)$. Given INR_i is fixed, the higher $\mathsf{A}_{\mathsf{SIC}}(INR_i)$ is, the less the residual SI occurs, which means a more advanced SIC scheme. The ideal scheme is the one that can make $INR_i\mathsf{A}_{\mathsf{SIC}}(INR_i) = 0$. As it has been studied in Chapter 4, the strong SI can be canceled completely only when the transceiver front-ends are ideal and the CSI of the SI channel can be obtained perfectly. In practical system design, it is hard to achieve so much SIC. Even the receiver thermal noise could make $INR_i\mathsf{A}_{\mathsf{SIC}}(INR_i) = 1 \gg 0$, others elements, such as phase noise, non-linearity of power amplifier and so on, will even make $INR_i\mathsf{A}_{\mathsf{SIC}}(INR_i) \gg 1$. Therefore, the performance and the practical prototype of the FDDB OFDM radio more depends on the practical implementation of Full-Duplex OFDM wireless.

5.7 Performance Evaluation and Discussion

In this section, the radio architecture proposed in this dissertation is demonstrated and validated by ADS-Matlab co-simulations. Additionally, the performance of the FDDB OFDM radio transceiver with or without I/Q imbalance are presented and analyzed. The performance of the proposed radio transceiver with I/Q imbalance is significantly reduced by the mutual signal leakages. However, the loss of the performance caused

by the I/Q imbalance can be compensated by the developed I/Q imbalance compensation method.

A typical OFDM based 36Mbps 802.11g physical layer is employed to construct a FDDB OFDM radio link. The parameters used in the simulation are as shown in Tab. 5.1 according to the IEEE 802.11g WLAN standard.

Table 5.1: System Parameters

Parameter	Value
Bandwidth	20MHz
Total number of subcarriers	52
Number of data subcarriers	48
Number of pilot subcarriers	4
Bit rate	36Mbps
IFFT/FFT period	3.2us
GI duration	0.8us

Generally, the signal emitted from each of the antennas has the same power level and the signals of interest with different carrier frequencies go through almost the same propagation loss L and the SI signals also experience almost the same propagation loss L_{si}, based on which we assume that each receiver has the same power ratio of signal-to-noise ratio (SNR) and the same power ratio of SI-to-noise ratio (INR).

5.7.1 Performance Evaluation

The BER (bit error rate) versus Eb/No for the proposed radio link is calculated by ADS-Matlab co-simulation and as shown in Fig. 5.11-5.14. In all these figures, “FDDB WiFi-1" and “FDDB WiFi-2" refer to the Full-Duplex Dual-Band IEEE 802.11g signals with carrier frequency $f_1 = 2.4$GHz and $f_2 = 2.2$GHz respectively; “Ideal IQ" refers to the radio receiver without I/Q imbalance; “Conventional WiFi Link" refers to the standard IEEE 802.11g wireless link which is used as the reference; “with IQ Imb./No Comp." refers to the proposed radio receiver with I/Q imbalance but without I/Q imbalance compensation; “with I/Q Imb./Comp." refers to the proposed radio receiver with I/Q imbalance and with the I/Q imbalance compensation algorithm.

FDDB OFDM Radio Transceiver without I/Q Imbalance

As shown in Fig. 5.11, the BER curve of the FDDB WiFi-1 overlap with that of the FDDB WiFi-2. This is because these two signals have the same signal-to-interference-and-noise ratio (SINR) which relies on a reasonable assumption that each signal of

interest has the same SNR and INR. However, there is around 3 dB performance loss for the FDDB WiFi compared to the conventional WiFi link. This can be explained by the noise-level residual SI induced by the Full-Duplex OFDM radio as presented in Chapter 4.

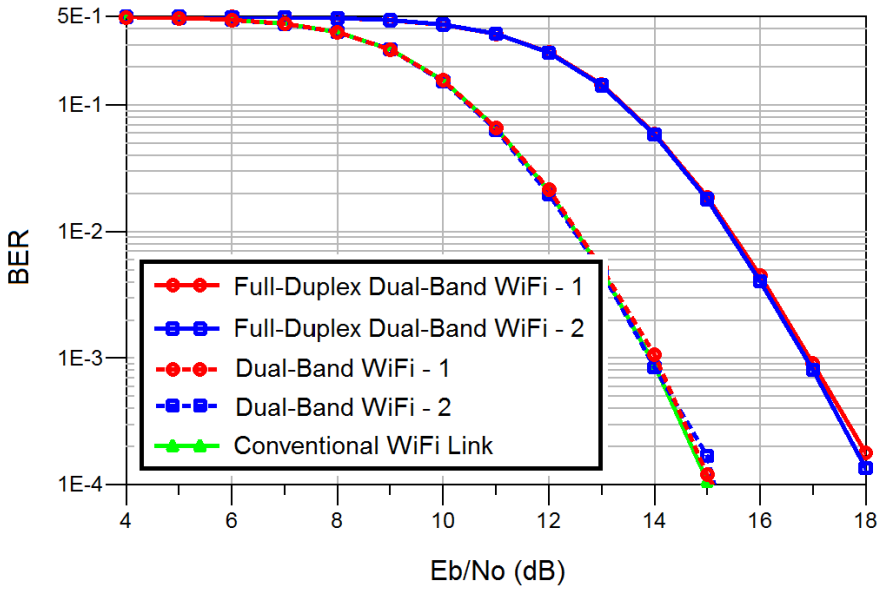

Figure 5.11: The BER of Full-Duplex Dual-Band 802.11g wireless system, with ideal I/Q.

FDDB OFDM Radio Transceiver with I/Q Imbalance

The I/Q imbalance in the FDDB RF front-end causes undesired signal leakage as studied in Sec. 5.4. The leaked image signal superimposed on the signal of interest degrades the performance of reception.

As it can be seen in Fig. 5.12, the high level I/Q imbalance ($\Delta A = 0.2, \Delta\phi = 10^o$) seriously degrades the proposed FDDB WiFi system. However, the proposed system performs very close to the ideal I/Q scenario after using the I/Q imbalance mitigation algorithm as presented in Sec. 5.5. Specifically, there is about 1 dB residual leaked image signal caused by the I/Q imbalance estimation error when $BER = 10^{-4}$.

As shown in Fig. 5.13, even with a medial level I/Q imbalance ($\Delta A = 0.1, \Delta\phi = 5^o$), there is around 5.5 dB gap induced by the leaked image signal when $BER = 10^{-4}$. While after the I/Q imbalance compensation, the performance loss is negligible.

In order to show that the developed compensation method can also be applied to combat the low I/Q imbalance, we have simulated the scenario ($\Delta A = 0.05, \Delta\phi = 1^o$) as shown in Fig. 5.14. Note that the BER curve of FDDB WiFi system with low I/Q

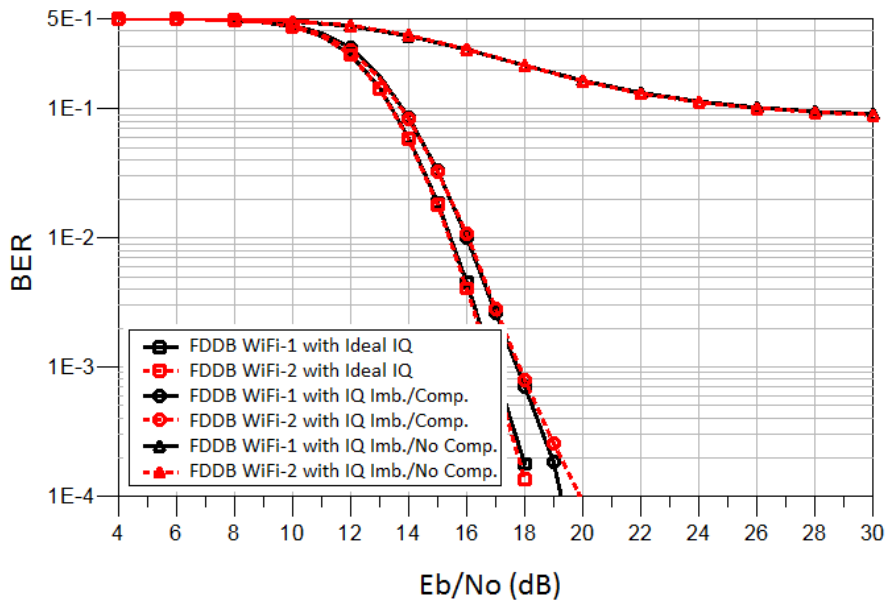

Figure 5.12: The BER of Full-Duplex Dual-Band 802.11g wireless system, with I/Q imbalance ($\Delta A = 0.2, \Delta\phi = 10^o$).

imbalance is very close to that of the ideal case. This is because the low I/Q imbalance causes low leaked image signal to the signal of interest. It can also be shown that the BER curve of the I/Q imbalance corrupted FDDB WiFi system with compensation scheme almost overlap with the ideal scenario.

Additionally, Fig. 5.11 shows that the proposed FDDB OFDM radio transceiver can simultaneously receive two different RF signals with carrier frequency f_1 and f_2 correctly while transmitting another two different RF signals. Besides, comparing the BER performance of the proposed FDDB OFDM radio transceiver without or with different level of I/Q mismatch shows that the I/Q imbalance in the FDDB RF front-end indeed affect the performance of the receiver. However, the developed I/Q imbalance combating method can compensate the RF impaired front-end and make it very close to the ideal scenario.

5.7.2 Discussion

In this paper, we assume that the two signals of interest carried by the frequency f_1 and f_2 arrive at the FDDB RF front-end with equal power level, so the two WiFi signals operating on two separate spectrum channel have the same reception performance even with I/Q imbalance. However, this assumption does not hold all the time. For example, when the radio terminal receives two different RF signals transmitted from different radio nodes, these two signals should have unequal power levels even if

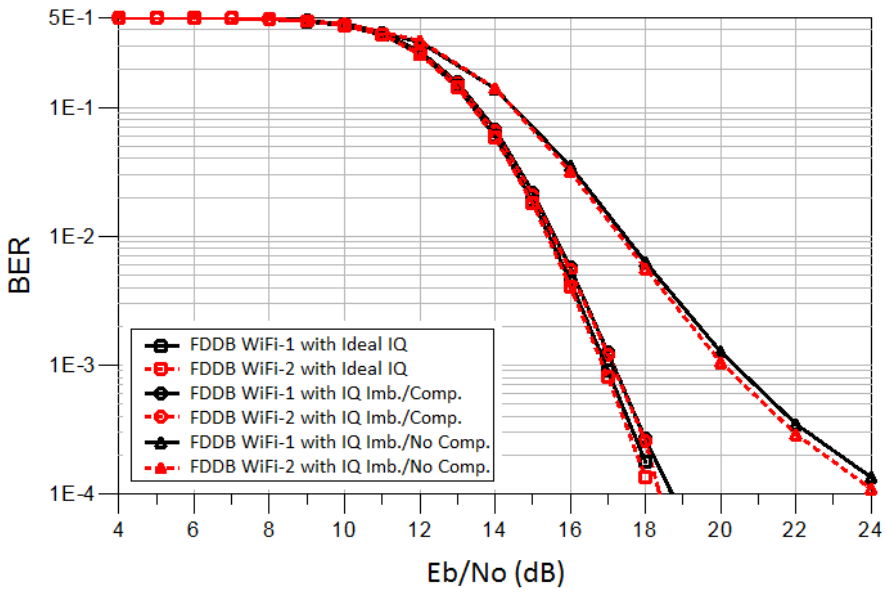

Figure 5.13: The BER of Full-Duplex Dual-Band 802.11g wireless system, with I/Q imbalance ($\Delta A = 0.1, \Delta\phi = 5^o$).

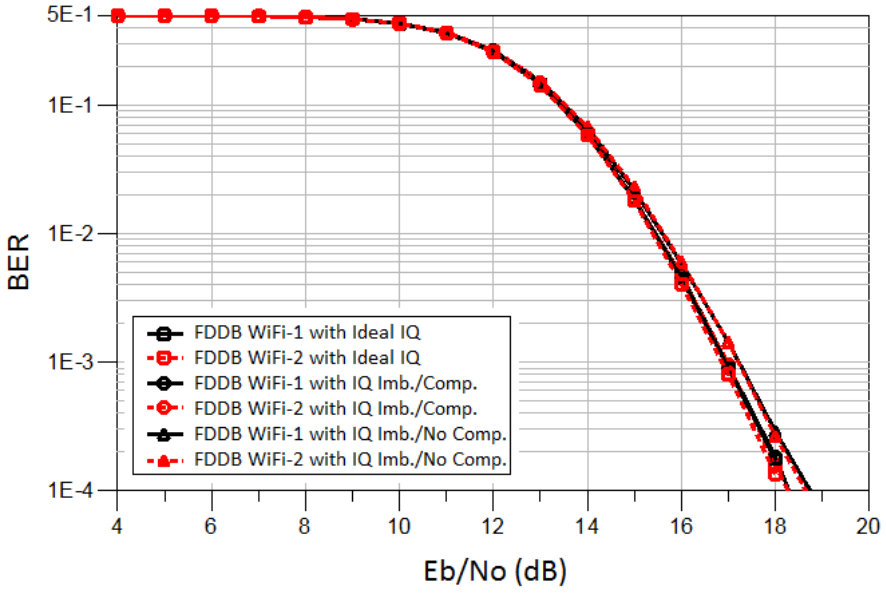

Figure 5.14: The BER of Full-Duplex Dual-Band 802.11g wireless system, with I/Q imbalance ($\Delta A = 0.05, \Delta\phi = 1^o$).

they are transmitted with the same power level, because they experience different fading and propagation loss. In this case, the signal with low power level will be significantly degraded by the undesired signal leakage induced by the I/Q imbalance. In this scenario, the I/Q imbalance mitigation is much more important to make sure that the weak signal can also be recovered correctly.

The FDDB radio could be exploited for a lot of applications, but we particularly emphasize on the Cognitive Radio. In fact, cognitive radio can be defined as intelligent radio systems which have the both abilities to sense the surrounding spectrum environment and flexibly adapt its transceiver parameters accordingly to optimize the radio link while coexisting with primary users [29]. It could greatly improve the efficiency of spectrum utilization. However, cognitive radios put high requirements on the RF front-end which is required to be highly flexible and reconfigurable and to realize wideband and agile transceiver. For example, the secondary user in cognitive radio systems can only use the spectrum channel unused or released by the primary user. Once the primary user starts to utilize this spectrum channel again, the secondary user should sense it and release this spectrum channel as soon as possible, and handover to another spectrum channel immediately. Therefore, the cognitive radio transceiver should be capable of spectrum channel sensing and provide candidate spectrum channel for handover. The proposed FDDB radio could meet these requirements. Full-Duplex wireless is defined as simultaneous wireless transmit and receive in the same frequency band [30, 95], so the Full-Duplex enables the radio terminals to sense spectrum channel while it is transmitting and receiving [31]. Dual-Band radio can simultaneously receive two different carrier frequency signals via using one RF front-end with double I/Q structure [28], so it can realize multiband radio with a relative simple RF front-end. Besides, OFDM's capabilities of spectrum sensing and shaping and its flexibility and adaptivity render it probably the best physical technique for cognitive radio systems [79]. Therefore, we also propose FDDB OFDM radio transceiver as a candidate radio transceiver for the cognitive radios.

5.8 Conclusion

In this Chapter, a flexible radio: FDDB radio is presented. In order to study and demonstrate the potentiality of this flexible radio, we build the system level simulation framework by combining the FDDB radio and WiFi OFDM PHY and make it operate on two separate spectrum fragments. The SI including the inner SI caused by the one-antenna Full-Duplex and the internal SI induced by the two-antenna Full-Duplex have been suppressed or canceled to noise level by creatively using the available SIC

methods. The ADS-Matlab co-simulation results show that the studied flexible radio transceiver based on the proposed flexible radio could simultaneously receive two different types of signals with a relatively simple RF front-end at the cost of 3 dB loss in BER, which is tolerable when the system capacity has almost 4 times enhancement. However, the noticeable gain in radio link capacity disappears when I/Q imbalance exists in the FDDB RF front-end. In order to mitigate the I/Q imbalance, an advanced and suitable I/Q imbalance estimation and compensation method dedicated to the FDDB OFDM radio is developed based on the frequency-flat-fading characteristic of the SI channel.

We can bring down the SI to noise level and obtain the viable system performance based on the assumption that the over-the-air SI channel is one-path channel relying on the fact that the power of the line-of-sight path dominates the SI channel. However, in practical consideration, the over-the-air SI channel should be a multi-path fading wireless channel with higher Ricean factor K which denotes the relative strength of the direct and scattered components of the received signals. Therefore, as a perspective of this work, designing or developing a more robust SIC algorithm is an important future task.

Besides, the phase noise in the local oscillator would be another important factor affecting the FDDB OFDM radio transceivers. Especially, it will affect the SIC in two-antenna Full-Duplex OFDM wireless. Hence, studying and eliminating the impact of phase noise on the proposed radio system is also our future work.

Furthermore, it was mentioned that the FDDB OFDM radio could be a good radio transceiver candidate for the cognitive radios, because this radio could enable the radio terminal to carry out the spectrum channel sensing while it is working and provide the candidate spectrum channel for hand-over. However, this viable radio performance has not been demonstrated experimentally. Therefore, prototyping the proposed radio system on hardware and demonstrating the actual performance are also considered as future works.

Part IV

Conclusion and Future Outlook

6

Conclusion and Future Outlook

In this Chapter, we conclude the dissertation with a summary of our contributions and discuss the directions for future research.

6.1 Conclusion

In conclusion, this dissertation is about the flexible radio transceiver designs: Full-Duplex OFDM radio design and FDDB OFDM radio design. Traditional systems have worked on Half-Duplex mode, i.e. the radio node uses orthogonal radio resource to transmit and receive signals, like Frequency Division Duplex (FDD) and Time Division Duplex (TDD). In this dissertation, we take an alternate mode, i.e. Full-Duplex, which enables a radio node to support simultaneous transmission and reception over the licensed entire frequency band. Besides, the traditional systems can only process one frequency band signal with one RF front-end. In this dissertation, we design a radio system which could simultaneously process two different frequency band signals with one common RF front-end. Specifically, we make the following contributions:

- *Self-Interference Cancellation:* Exploiting Full-Duplex requires to cancel the strong SI which is a big challenge behind the Full-Duplex to a tolerable level in advance. This dissertation presents the design of various analog and digital SIC

schemes to eliminate the strong SI. The developed SIC scheme based on the AARFSIC and DSICT could mitigate all the SI signals even for the Full-Duplex OFDM wireless with multi-path SI channel when the transceiver RF front-ends are ideal.

- *Full-Duplex OFDM Radio:* We design and evaluate a Full-Duplex OFDM wireless with both one-path SI channel and multi-path SI channel. We find that the AARFSIC can efficiently eliminate the strong SI completely for the Full-Duplex OFDM wireless with one-path SI channel. With respect to the Full-Duplex OFDM wireless with multi-path SI channel, AARFSIC can only mitigate the direct path and part of the remaining paths. Therefore, we propose an ADSICT to cancel the residual SI after the AARFSIC.

- *Full-Duplex Dual-Band OFDM Radio:* We design a flexible radio transceiver which can simultaneously transmit, simultaneously receive or simultaneously transmit and receive in the same or different spectrum fragments with one common RF front-end. The I/Q imbalance in the radio front-end significantly degrades the performance of one or both of the two spectrum fragment radio links. To mitigate the impact of the I/Q imbalance, a simple but practical I/Q imbalance estimation and compensation method, which can compensate both high and low I/Q imbalance level, is proposed.

6.2 Future Outlook

It can be envisioned that the flexible utilization of spectrum fragment will be a key technology for future 5G wireless. Duplex mode is an important factor determining the way of using spectrum fragment. FDD requires paired spectrum for downlink and uplink, making it extremely difficult to allocate the FDD spectrum. FDD also requires spectrum space for downlink and uplink isolation, which is not efficiency in spectrum utilization. TDD allows to use a single unpaired frequency, which is a big advantage of the TDD over the FDD. While TDD requires disparate time slots for downlink and uplink, which potentially increases the latency. In 5G wireless network, specifically driverless cars wireless system, latency is unacceptable. An alternate duplex mode, Full-Duplex is identical to the TDD in terms of spectrum allocation. Full-Duplex, allowing unpaired spectrum allocation, dramatically simplifies the spectrum management and vastly enhance the flexibility of spectrum utilizations. Besides, Full-Duplex supports simultaneous transmission and reception, which significantly reduces the latency. Therefore, Full-Duplex could be a good candidate duplex mode for future 5G

wireless network. Parts of this dissertation devote to Full-Duplex OFDM wireless. However, there are still lots of works needed to be done before the deployment of Full-Duplex in 5G wireless network.

- *Robust Self-Interference Cancellation:* This thesis has discussed a single channel Full-Duplex OFDM wireless without taking the impact of transmitter noise on the SIC into consideration. Although we have studied and qualified the impact of the phase noise on the SIC, a practical method to mitigate the residual SI due to the phase noise have not been proposed. Robust SIC schemes to completely eliminate the SI including direct path, multiple reflecting paths, non-linearity distortion and transmitter noise induced by RF impairments can be proposed.

- *Prototype Full-Duplex OFDM Radio:* Prototyping a Full-Duplex OFDM radio based on hardware and software to demonstrate our studies and analysis would be very rewarding works.

FDDB radio can work on two spectrum fragments with one common RF front-end. In each spectrum fragment, it enables a wireless device to transmit and receive data simultaneously over the entire frequency band. That means FDDB radio can sense the spectrum environment when it is working and it can provide a candidate spectrum channel for handover. Therefore, we think it is a promising physical layer technology for the cognitive radio network. However, there are still some works needed to be done at first.

- *Self-Interference Cancellation:* In FDDB radio, there are inner SI induced by one-antenna Full-Duplex and internal SI caused by two-antenna Full-Duplex. How to cooperatively and creatively cancel these two SIs in practical wireless environment would be important future works.

- *Prototype Full-Duplex Dual-Band OFDM Radio:* We have presented the advances of the FDDB radio in the level of theoretical study. Experimental results based on the over-the-air test would confirm the studies and analysis. The performance of the digital I/Q imbalance estimation and compensation scheme proposed in this dissertation also need to be experimentally demonstrated. Therefore, prototyping the FDDB radio would be my following works.

Part V

References

Bibliography

[1] M.J. Abdoli, A. Ghasemi, and A.K. Khandani. Full-Duplex transmitter cooperation, feedback, and the degrees of freedom of SISO gaussian interference and X channels. In *Proc. IEEE International Symposium on Information Theory (ISIT)*, 2012.

[2] W. Afifi and M. Krunz. Exploiting self-interference suppression for improved spectrum awareness/efficiency in cognitive radio systems. In *Proc. IEEE INFOCOM*, 2013.

[3] W. Afifi and M. Krunz. Adaptive transmission-reception-sensing strategy for cognitive radios with Full-Duplex capabilities. In *Proc. IEEE International Symposium on Dynamic Spectrum Access Networks (DYSPAN)*, 2014.

[4] E. Ahmed, A. Eltawil, and A. Sabharwal. Simultaneous transmit and sense for cognitive radios using Full-Duplex: A first study. In *Proc. IEEE Antenna and Propagation Society International Symposium (APSURSI)*, 2012.

[5] E. Ahmed and A.M. Eltawil. All-digital self-interference cancellation for Full-Duplex systems. In *online: http://arxiv.org/pdf/1406.5555v1.pdf*, 2014.

[6] E. Ahmed and A.M. Eltawil. On phase noise suppression in Full-Duplex systems. In *online: http://arxiv.org/abs/1401.6437*, 2014.

[7] E. Ahmed, A.M. Eltawil, and A. Sabharwal. Self-interference with nonlinear suppression for Full-Duplex. In *Proc. GlobeCom*, 2013.

[8] E. Ahmed, A.M. Eltawil, and A. Sabharwal. Self-interference with phase noise induced ici suppression for Full-Duplex. In *Proc. GlobeCom*, 2013.

[9] I.F. Akyildiz, W.Y. Lee, M.C. Vuran, and S. Mohanty. A survey on spectrum management in cognitive radio networks. *IEEE Communications Magazine*, 46(4):40–48, 2008.

[10] S. Alamouti. A simple transmit diversity technique for wireless communications. *IEEE Journal on Selected Areas in Communications*, 16(8):1451–1458, 1998.

[11] K. Alexandris, A. Balatsoukas-Stimming, and A. Burg. Measurement-based characterization of residual self-interference on a Full-Duplex MIMO testbed. In *Proc. IEEE 8th Sensor Array and Multichannel Signal Processing Workshop (SAM)*, 2014.

[12] J.G. Andrews, S. Buzzi, W. Choi, S.V. Hanly, A. Lozano, A.C.K. Soong, and J.C. Zhang. What will 5G be? *IEEE Journal on Selected Areas in Communications*, 32(6):1065–1082, 2014.

[13] E. Antonio-Rodriguez and R. Lopez-Valcarce. Cancelling self-interference in Full-Duplex relays without angle-of-arrival information. In *Proc. IEEE International Conference on Acoustics, Speech and Signal Processing (ICASSP)*, 2013.

[14] L. Anttila, D. Korpi, E. Antonio-Rodriguez, R. Wichman, and M. Valkama. Modeling and efficient cancellation of nonlinear self-interference in MIMO Full-Duplex transceivers. In *online: http://arxiv.org/pdf/1406.0671v1.pdf*, 2014.

[15] L. Anttila, D. Korpi, V. Syrjala, and M. Valkama. Cancellation of power amplifier induced nonlinear self-interference in Full Duplex transceivers. In *Proc. 2013 Asilomar Conference on Signals, Systems and Computers (ASILOMAR)*, 2013.

[16] E.H. Armstrong. A new system of short wave amplification. In *Proc. of the Institute of Radio Engineers*, 1921.

[17] E. Aryafar, M.A. Khojastepour, K. Sundaresan, S. Rangarajan, and M. Chiang. MIDU: Enabling MIMO Full-Duplex. In *Proc. ACM MobiCom*, 2012.

[18] F. Asharif, S. Tamaki, M.R. Alsharif, and H.-G. Ryu. Application of Full-Duplex wireless communication system on echo cancellation. In *Proc. IEEE Wireless Communications and Networking Conference (WCNC)*, 2013.

[19] R. Askar, T. Kaiser, B. Schubert, T. Haustein, and W. Keusgen. Active self-interference cancellation mechanism for Full-Duplex wireless transceivers. In *Proc. 9th International Conference on Cognitive Radio Oriented Wireless Networks and Communications (CROWNCOM)*, 2014.

[20] P. Bahl, A. Adya, and J. Padhye. Reconsidering wireless systems with multiple radios. In *Proc. ACM SIGCOMM CCR*, 2004.

[21] A. Balatsoukas-Stimming, P. Belanovic, K. Alexandris, and A. Burg. On self-interference suppression methods for low-complexity Full-Duplex MIMO. In *Proc. Asilomar Conference on Signals, Systems and Computers (ASILOMAR)*, 2013.

[22] P. Belanovic, A. Balatsoukas-Stimming, and A. Burg. A multipurpose testbed for Full-Duplex wireless communications. In *Proc. IEEE 20th International Conference on Electronics, Circuits, and Systems (ICECS)*, 2013.

[23] D. Bharadia and S. Katti. Full Duplex MIMO radios. In *Proc. 11th USENIX Symposium on Networked Systems Design and Implementation*, 2014.

[24] D. Bharadia, E. McMilin, and S. Katti. Full Duplex radios. In *Proc. ACM SIGCOM*, 2013.

[25] E. Biglieri, A. Calderbank, A. Goldsmith, H. Paulraj, and H.V. Poor. *MIMO Wireless Communications*. Cambridge University Press, 2007.

[26] D.W. Bliss, T.M. Hancock, and P. Schniter. Hardware phenomenological effects on cochannel Full-Duplex MIMO relay performance. In *Proc. Asilomar Conference on Signals, Systems and Computers (ASILOMAR)*, 2012.

[27] D.W. Bliss and Y. Rong. Effects of channel estimation errors on in-band Full-Duplex MIMO radios using adaptive transmit spatial mitigation. In *Proc. Asilomar Conference on Signals, Systems and Computers (ASILOMAR)*, 2013.

[28] I. Burciu, G. Villemaud, J. Verdier, and M. Gautier. Low power front-end architecture dedicated to the multistandard simultaneous reception. *Cambridge International Journal of Microwave and Wireless Technologies*, 2(6):505–514, 2010.

[29] D. Cabric, S.M. Mishra, and R.W. Brodersen. Implementation issues in spectrum sensing for cognitive radios. In *Proc. Asilomar Conference on Signals, Systems and Computers (ASILOMAR)*, 2004.

[30] J. I. Choi, M. Jain, k. Srinivasan, P. Levis, and S. Katti. Achieving single channel, Full Duplex wireless communications. In *Proc. ACM MOBICOM*, 2010.

[31] Y.S. Choi and S.M. Hooman. Simultaneous transmission and reception: Algorithm, design and system level performance. *IEEE Transactions on Wireless Communications*, 12(12):5992–6010, 2013.

[32] A.C. Cirik, Y. Rong, and Y. Hua. Achievable rates of Full-Duplex MIMO radios in fast fading channels with imperfect channel estimation. *IEEE Transactions on Signal Processing*, 62(15):3874–3886, 2014.

[33] C. Cox and E. Ackerman. Demonstration of a single-aperture Full-Duplex communication system. In *Proc. IEEE Radio and Wireless Symposium (RWS)*, 2013.

[34] W.B. Daniel, W.F. Keith, and M.C Amanda. MIMO wireless communication. *Lincoln Laboratory Journal*, 15(1):97–126, 2005.

[35] B.P. Day, A.R. Margetts, D.W. Bliss, and P. Schniter. Full-Duplex MIMO relaying: Achievable rates under limited dynamic range. *IEEE Journal on Selected Areas in Communications*, 30(8):1541–1553, 2012.

[36] B. Debaillie, D. Van den Broek, and B. Van Liempd. Analog/RF solutions enabling compact Full-Duplex radios. *IEEE Journal on Selected Areas in Communications*, PP(99):?–?, 2014.

[37] M. Duarte. *Full-Duplex Wireless: Design, Implementation and Characterization*. PhD thesis, Rice University, 2012.

[38] M. Duarte, C. Dick, and A. Sabharwal. Experiment driven characterization of Full-Duplex wireless communications. *IEEE Transactions on Wireless Communications*, 11(12):505–514, 2012.

[39] M. Duarte and A. Sabharwal. Full-Duplex wireless communications using off-the-shelf radios: Feasibility and first results. In *Proc. Asilomar Conference on Signals, Systems and Computers (ASILOMAR)*, 2009.

[40] M. Duarte, A. Sabharwal, V. Aggarwal, R. Jana, K.K. Ramakrishnan, and N.K. Shankaranaryanan. Design and characterization of a Full-Duplex multiantenna system for WiFi networks. *IEEE Transactions on Vehicular Technology*, 63(3):1160–1177, 2014.

[41] E. Everett, A. Sahai, and A. Sabharwal. Passive self-interference suppression for Full-Duplex infrastructure nodes. *IEEE Transactions on Wireless Communications*, 13(2):680–694, 2014.

[42] E. Foroozanfard, O. Franek, A. Tatomirescu, and E. Tsakalaki. Full-Duplex MIMO system based on antenna cancellation technique. *IET Electronics Letters*, 50(16):1116–1117, 2014.

[43] A. Gholian, Y. Ma, and Y. Hua. A numerical inverstigation of all-analog radio self-interference cancellation. In *Proc. IEEE 15th International Workshop on Signal Processing Advances in Wireless Communications (SPAWC)*, 2014.

[44] G. Gil, Y. Kim, and Y. Lee. Non-data-aided approach to I/Q mismatch compensation in low-IF receivers. *IEEE Transactions on Signal Processing*, 55(7):3360–3365, 2007.

[45] Z. He, S. Shao, Y. Shen, and C. Qing. Performance analysis of RF self-interference cancellation in Full-Duplex wireless communications. *IEEE Wireless Communications Letters*, 3(4):405–408, 2014.

[46] Z. He, S. Shao, Y. Shen, C. Qing, and Y. Tang. Impact of analog cancellation error on Full-Duplex wireless communications system over rayleigh fading channel. In *Proc. International Conference on Communications, Circuits and Systems (ICCCAS)*, 2013.

[47] S. Hong, J. Brand, J. Choi, M. Jain, J. Mehlman, S. Katti, and P. Levis. Applications of self-interference cancellation in 5G and beyond. *IEEE Communications Magazine*, 52(2):114–121, 2014.

[48] S.S. Hong, E. McMilin, and S. Katti. Picasso: flexible RF and spectrum slicing. In *Proc. ACM SIGCOM*, 2012.

[49] Y. Hua, P. Liang, Y. Ma, A.C. Cirik, and Q. Gao. A method for broadband Full-Duplex MIMO radio. *IEEE Signal Processing Letter*, 19(12):793–796, 2012.

[50] Y. Hua, Y. Ma, P. Liang, and A. Cirik. Breaking the barrier of transmission noise in Full-Duplex radio. In *Proc. IEEE Military Communications Conference (MILCOM)*, 2013.

[51] S. Huberman and T. Le-Ngoc. Self-interference pricing-based MIMO Full-Duplex precoding. *IEEE Wireless Communications Letters*, PP(99), 2014.

[52] S. Huberman and Tho Le-Ngoc. Sequential convex programming for Full-Duplex single-user MIMO systems. In *Proc. IEEE International Conference on Communications (ICC)*, 2014.

[53] G. Hueber and R.B. Staszewski. *Multi-mode/mulit-band RF Transceivers for Wireless Communications*. John Wiley Sons, INC, Hoboken, New Jersey, USA, 2011.

[54] M. Jain. *Single Channel Full-Duplex Wireless: Radios*. PhD thesis, Stanford University, 2011.

[55] M. Jain, J. Choi, T. Kim, D. Bharadia, K. Srinivasan, P. Levis, S. Katti, P. Sinha, and S Seth. Practical real-time Full Duplex wireless. In *Proc. ACM MOBICOM*, 2011.

[56] S.E. Johnston and P.D. Fiore. Full-Duplex MIMO via adaptive nulling. In *Proc. Asilomar Conference on Signals, Systems and Computers (ASILOMAR)*, 2013.

[57] H. Ju, E. Oh, and D. Hong. Improving efficiency of resource usage in two-hop Full Duplex relay systems based on resource sharing and interference cancellation. *IEEE Transactions on Wireless Communications*, 8(8):3933–3938, 2009.

[58] B. Kaufman, J. Lilleberg, and B. Aazhang. An analog baseband approach for designing Full-Duplex radios. In *Proc. Asilomar Conference on Signals, Systems and Computers (ASILOMAR)*, 2013.

[59] B. Kaufman, J. Lilleberg, and B. Aazhang. Analog baseband cancellation for Full-Duplex: An experiment driven analysis. *online: http://arxiv.org/pdf/1312.0522.pdf*, 2014.

[60] A.K. Khandani. Methods for spatial multiplexing of wireless two-way channels. In *US Patent*, 2010.

[61] A.K. Khandani. Two-way (true full-duplex) wireless. In *Proc. 13th Canadian Workshop on Information Theory (CWIT)*, 2013.

[62] M.A. Khojastepour and S. Rangarajan. Wideband digital cancellation for Full-Duplex communications. In *Proc. Asilomar Conference on Signals, Systems and Computers (ASILOMAR)*, 2012.

[63] S. Kim and W. Stark. Full-Duplex device to device communication in cellular networks. In *Proc. International Conference on Computing, Networking and Communications (ICNC)*, 2014.

[64] M.E. Knox. Single antenna Full Duplex communications using a common carrier. In *Proc. IEEE 13th Annual Wireless and Microwave Technology Conference (WAMICON)*, 2012.

[65] K.E. Kolodziej, J.G. McMichael, and B.T. Perry. Adaptive RF canceller for transmit-receive isolation improvement. In *Proc. IEEE Radio and Wireless Symposium (RWS)*, 2014.

[66] D. Korpi, L. Anttila, V. Syrjala, and M. Valkama. Widely-linear digital self-interference cancellation in direct-conversion Full-Duplex transceiver. *IEEE Journal on Selected Areas in Communications*, PP(99):?–?, 2014.

[67] D. Korpi, L. Anttila, and M. Valkama. Feasibility of in-band Full-Duplex radio transceivers with imperfect RF components: Analysis and enhanced cancellation algorithms. In *Proc. 9th Cognitive Radio Oriented Wireless Networks and Communications (CROWNCOM)*, 2014.

[68] D. Korpi, T. Riihonen, V. Syrjala, L. Anttila, M. Valkama, and R. Wichman. Full-Duplex transceiver system calculations: Analysis of ADC and linearity challenges. *IEEE Transactions on Wireless Communications*, 13(7):3821–3836, 2014.

[69] J.R. Krier and I.F. Akyildiz. Active self-interference cancellation of passband signals using gradient descent. In *Proc. IEEE 24th Annual International Symposium on Personal, Indoor and Mobile Radio Communications (PIMRC)*, 2013.

[70] P. Larsson and M. Prytz. MIMO on-frequency repeater with self-interference cancellation and mitigation. In *Proc. IEEE 69th Vehicular Technology Conference (VTC Spring)*, 2009.

[71] G. Lebrun, J. Gao, and M. Faulkner. MIMO transmission over a time-varying channel using SVD. *IEEE Transactions on Wireless Communications*, 4(2):757–764, 2005.

[72] J.H. Lee. Self-interference cancelation using phase rotation in Full-Duplex wireless. *IEEE Transactions on Vehicular Technology*, 62(9):4421–4429, 2013.

[73] L. Li, K. Josiam, and R. Taori. Feasibility study on Full-Duplex wireless millimeter-wave systems. In *Proc. IEEE International Conference on Acoustics, Speech and Signal Processing (ICASSP)*, 2014.

[74] N. Li, W. Zhu, and H. Han. Digital interference cancellation in single channel, Full-Duplex wireless communication. In *Proc. 8th International Conference on Wireless Communications, Networking and Mobile Computiing (WiCOM)*, 2012.

[75] S. Li and R.D. Murch. Full-Duplex wireless communication using transmitter output based echo cancellation. In *Proc. GlobeCom*, 2011.

[76] S. Li and R.D. Murch. An investigation into baseband techniques for single-channel Full-Duplex wireless communication systems. *IEEE Transactions on Wireless Communications*, 13(9):4794–4806, 2014.

[77] W. Li, J. Lilleberg, and K. Rikkinen. On rate region analysis of Half- and Full-Duplex OFDM communication links. *IEEE Journal on Selected Areas in Communications*, PP(99):?–?, 2014.

[78] P. Lioliou, M. Viberg, M. Coldrey, and F. Athley. Self-interference suppression in Full-Duplex MIMO relays. In *Proc. Asilomar Conference on Signals, Systems and Computers (ASILOMAR)*, 2010.

[79] H. Mahmoud, T. Yucek, and H. Arslan. OFDM for cognitive radio: merits and challenges. *IEEE Wireless Communications*, 16(2):6–15, 2009.

[80] A. Masmoudi and Tho Le-Ngoc. Residual self-interference after cancellation in Full-Duplex systems. In *Proc. IEEE International Conference on Communications (ICC)*, 2014.

[81] J.G. McMichael and K.E. Kolodziej. Optimal tuning of analog self-interference cancellers for Full-Duplex wireless communication. In *Proc. 50th Annual Allerton Conference on Communication, Control, and Computing (Allerton)*, 2012.

[82] J. Mitola III. *Cognitive Radio - An Integrated Agent Architecture for Software Defined Radio*. PhD thesis, Royal Institute of Technology (KTH), 2000.

[83] A. Mohammad, K. Sundaresan, S. Rangarajan, X. Zhang, and S. Barghi. The case for antenna cancellation for scalable Full-Duplex wireless communications. In *Proc. ACM Hotnet*, 2011.

[84] R.V. Nee and R. Prasad. *OFDM for Wireless Multimedia Communications*. Artech House, Boston, 2000.

[85] D.W.K. Ng, E.S. Lo, and R. Schober. Dynamic resource allocation in MIMO-OFDMA systems with Full-Duplex and hybrid relaying. *IEEE Transactions on Communications*, 60(5):1291–1304, 2012.

[86] A. Oppenheim and R. Schafer. *Discrete Time Signal Processing: 3rd Edition*. Prentice Hall Inc, 2009.

[87] A.J. Paulraj, D.A. Gorce, R.U. Nabar, and H. Bolcskei. An overview of MIMO communications - a key to gigabit wireless. *Proceeding of the IEEE*, 92(2):198–218, 2004.

[88] B. Radunovic, D. Gunawardena, P. Key, A. Proutiere, N. Singh, V. Balan, and G. Dejean. Rethinking indoor wireless: Low power, low frequency, Full-Duplex. In *Microsoft Technical Report, MSR-TR-2009-148*, 2009.

[89] S. Rajagopal, R. Taori, and S. Abu-Suura. Self-interference mitigation for in-band mmWave wireless backhaul. In *Proc. IEEE 11th Consumer Communications and Networking Conference (CCNC)*, 2014.

[90] T. Riihonen, P. Mathechen, and R. Wichman. Effect of oscillator phase noise and processing delay in Full-Duplex OFDM repeaters. In *Proc. Asilomar Conference on Signals, Systems and Computers (ASILOMAR)*, 2012.

[91] T. Riihonen and R. Wichman. Analog and digital self-interference cancellation in Full-Duplex MIMO-OFDM transceivers with limited resolution in A/D conversion. In *Proc. Asilomar Conference on Signals, Systems and Computers (ASILOMAR)*, 2012.

[92] A. Sabharwal, P. Schniter, D. Guo, D.W. Bliss, S. Rangarajan, and R. Wichman. In-band Full-Duplex wireless: Challenges and opportunities. *IEEE Journal on Selected Areas in Communications*, PP(99):?–?, 2014.

[93] A. Sahai, G. Patel, C. Dick, and A. Sabharwal. Understanding the impact of phase noise on active cancellation in Full-Duplex. In *Proc. Asilomar Conference on Signals, Systems and Computers (ASILOMAR)*, 2012.

[94] A. Sahai, G. Patel, C. Dick, and A. Sabharwal. On the impact of phase noise on active cancelation in wireless Full-Duplex. *IEEE Transactions on Vehicular Technology*, 62(9):4494–4510, 2013.

[95] A. Sahai, G. Patel, and A. Sabharwal. Pushing the limits of Full-Duplex: Design and real-time implementation. Technical report, Rice University, June 2011.

[96] D. Senaratne and C. Tellambura. Beamforming for space division duplexing. In *Proc. IEEE International Conference on Communications (ICC)*, 2009.

[97] S. Shao, X. Quan, Y. Shen, and Y. Tang. Effect of phase noise on digital self-interference cancellation in wireless Full Duplex. In *Proc. IEEE International Conference on Acoustic, Speech and Signal Processing (ICASSP)*, 2014.

[98] T. Snow, C. Fulton, and W.J. Chappell. Transmit-receive duplexing using digital beamforming system to cancel self-interference. *IEEE Transactions on Microwave Theory and Techniques*, 59(12):3494–3503, 2011.

[99] I. Sohn, E. Jeong, and Y. Lee. Data-aided approach to I/Q mismatch and DC offset compensation in communication receivers. *IEEE Communications Letters*, 6(12):547–549, 2002.

[100] G.L. Stuber, J.R. Barry, S.W. Mclaughlin, Y. Li, M.A. Ingram, and T.G. Pratt. Broadband MIMO-OFDM wireless communications. *Proceeding of IEEE*, 92(2):271–294, 2004.

[101] V. Syrjala, M. Valkama, L. Anttila, T. Riihonen, and D. Korpi. Analysis of oscillator phase-noise effects on self-interference cancellation in Full-Duplex OFDM radio transceivers. *IEEE Transactions on Wireless Communications*, 13(6):2977–2990, 2014.

[102] H. Tarighat, R. Bagheri, and A.H. Sayed. Compensation schemes and performance analysis of iq imbalance in OFDM receivers. *IEEE Transactions on Signal Processing*, 53(8):3257–3268, 2005.

[103] S. Traverso, M. Ariaudo, I. Fijalkow, J. Gautier, and C. Lereau. Decision-directed channel estimation and high I/Q imbalance compensation in OFDM receivers. *IEEE Transactions on Communications*, 57(5):1246–1249, 2009.

[104] E. Tsakalaki, E. Foroozanfard, E. de Carvalho, and G.F. Pedersen. A 2-order MIMO Full-Duplex antenna design. In *Proc. The 8th European Conference on Antenna and Propagation (EuCAP)*, 2012.

[105] J. Tubbax, B. Come, L.D. Perre, S. Donnay, H. Engels, H. Man, and M. Moonen. Compensation of IQ imbalance and phase noise in OFDM systems. *IEEE Transactions on Wireless Communications*, 4(3):872–877, 2005.

[106] B. van Liempd, B. Debaillie, J. Craninckx, C. Lavin, C. Palacios, S. Malotaux, J.R. Long, and D.J. van den Broek. RF self-interference cancellation for Full-Duplex. In *Proc. 9th International Conference on Cognitive Radio Oriented Wireless Networks and Communications (CROWNCOM)*, 2014.

[107] M. Vu and A. Paulraj. MIMO wireless linear precoding. *IEEE Signal Processing Magazine*, 24(5):86–105, 2007.

[108] J. Wang, H. Zhao, and Y. Tang. A RF adaptive least mean square algorithm for self-interference cancellation in co-frequency co-time Full-Duplex systems. In *Proc. IEEE International Conference on Communications (ICC)*, 2014.

[109] M. Windisch and G. Fettweis. Blind I/Q imbalance parameter estimation and compensation in low-IF receivers. In *Proc. First International Symposium on Control, Communications and Signal Processing (ISCCSP)*, 2004.

[110] M. Windisch and G. Fettweis. Standard-independent I/Q imbalance compensation in OFDM direct-conversion receivers. In *Proc. 9th International OFDM workshop*, 2004.

[111] M. Windisch and G. Fettweis. Preamble design for an efficient I/Q compensation in OFDM direct-conversion receivers. In *Proc. 10th International OFDM workshop*, 2005.

[112] X. Wu, Y. Shen, and Y. Tang. The power delay profile of the single-antenna Full-Duplex self-interference channel in indoor environments at 2.6GHz. *IEEE Antennas and Wireless Propagation Letters*, 13:1561–1564, 2014.

[113] X. Xie and X. Zhang. Does Full-Duplex double the capacity of wireless networks? In *Proc. IEEE INFOCOM*, 2014.

[114] B. Yang, Y. Dong, Z. Yu, and J. Zhou. An RF self-interference cancellation circuit for the Full-Duplex wireless communications. In *Proc. International Symposium on Antenna and Propagation (ISAP)*, 2013.

[115] J. Yu, M. Sun, T. Hus, and C. Lee. A novel technique for I/Q imbalance and CFO compensation in OFDM systems. In *Proc. IEEE International Symposium on Circuit and Systems (ISCAS)*, 2005.

[116] Z. Zhan and G. Villemaud. Combination of digital self-interference cancellation and AARFSIC for Full-Duplex OFDM wireless. In *Proc. IEEE/CIC International Conference on Communications in China (ICCC)*, 2014.

[117] Z. Zhan, G. Villemaud, and J.-M. Gorce. Design and evaluation of a wideband Full-Duplex OFDM system based on AASIC. In *Proc. IEEE 24th Annual International Symposium on Personal, Indoor and Mobile Radio Communications (PIMRC)*, 2013.

[118] Z. Zhan, G. Villemaud, and J.-M. Gorce. Analysis and reduction of the impact of thermal noise on the Full-Duplex OFDM radio. In *Proc. IEEE Radio and Wireless Symposium (RWS)*, 2014.

[119] Z. Zhan, G. Villemaud, F. Hutu, and J.-M. Gorce. Digital estimation and compensation of I/Q imbalance for Full-Duplex Dual-Band OFDM radio. In *Proc. IEEE 25th Annual International Symposium on Personal, Indoor and Mobile Radio Communications (PIMRC)*, 2014.

[120] Z. Zhan, G. Villemaud, F. Hutu, and J.-M. Gorce. Full-Duplex Dual-Band OFDM radio transceiver dedicated to flexible radio communications. *submitted to Cambridge International Journal of Microwave and Wireless Technologies*, 2014.

[121] Z. Zhan, G. Villemaud, F. Hutu, and J.-M. Gorce. Full-Duplex Dual-Band radio dedicated to flexible radio systems. *submitted to IET Electronics Letters*, 2014.

[122] J. Zhang, O. Taghizadeh, and M. Haardt. Robust transmit beamforming design for Full-Duplex point-to-point MIMO systems. In *Proc. The 10th International Symposium on Wireless Communication Systems (ISWCS)*, 2013.

[123] P. Zhang, T. Nguyen, C. Lam, and D Gambetta. A 5-GHz direct-conversion CMOS transceiver. *IEEE Journal of Solid-State Circuits*, 38(12):2232–2238, 2003.

[124] G. Zheng, I. Krikidis, J. Li, A.P. Petropulu, and B. Ottersten. Improving physical layer secrecy using Full-Duplex jamming receivers. *IEEE Transactions on Signal Processing*, 61(20):4962–4974, 2014.

[125] W. Zhou, G. Villemaud, and T. Risset. Full-Duplex prototype of OFDM on GNU-Radio and USRPs. In *Proc. IEEE Radio and Wireless Symposium (RWS)*, 2014.

List of publications

Journal Papers

[1] **Z. Zhan**, G. Villemaud and F. Hutu and J-M. Gorce. "Full-Duplex Dual-Band OFDM Radio Transceivers Dedicated to Flexible Radio Communications," (submitted to) *International Journal of Microwave and Wireless Technologies*, May 2014. (under revision)

International Conference Papers

[2] **Z. Zhan** and G. Villemaud, "Combination of Digital Self-Interference Cancellation and AARFSIC for Full-Duplex OFDM Wireless," *IEEE/CIC International Conference on Communications in China (ICCC)*, Shanghai, China, 13-15 Oct. 2014.

[3] **Z. Zhan**, G. Villemaud, F. Hutu and J-M. Gorce, "Digital Estimation and compensation of I/Q imbalance in Full-Duplex Dual-Band OFDM Radio," *The 25th IEEE International Symposium on Personal, Indoor and Mobile Radio Communications* (PIMRC), Washington, DC, USA, 2-5 Sep. 2014.

[4] **Z. Zhan**, G. Villemaud and J-M. Gorce, "Analysis and Reduction of the Impact of Thermal Noise on the Full-Duplex OFDM Radio," *IEEE Radio and Wireless Symposium* (RWS), Newport Beach, CA, USA, 19-22 Jan. 2014.

[5] **Z. Zhan**, G. Villemaud and J-M. Gorce, "Design and evaluation of a wideband Full-Duplex OFDM system based on AASIC," *The 24th IEEE International Symposium on Personal, Indoor and Mobile Radio Communications* (PIMRC), London, UK, 8-11 Sep. 2013.

Research Reports

[6] **Z. Zhan**, G. Villemaud, F. Hutu and J-M. Gorce, "Full-Duplex Dual-Band Radio Dedicated to Flexible Radio Communications," *INRIA Research Report, RR-8558*, Jul. 2014.